

Risk assessment of pollution at Hvorup barracks

Master of Water &
Environmental Engineering
1st semester



Rupa Chand
Tiberiu Tulucan
Charles Pesch

Matthias Oursin
Emil Nielsen

Master in Water and Environment and

Environmental Engineering

Sofiendalsvej 9-11

9200 Aalborg SV

Title:

Soil & Groundwater

Project:

1. semester of Master

Project duration:

October 2015 - December 2015

Project group:

F3-22

Group members:

Rupa Chand

Tiberiu Tulucan

Charles Pesch

Matthias Oursin

Emil Nielsen

Supervisors:

Per Møldrup

Jacob Birk Jensen

Kaj Henriksen

Copies: 10

Amount of pages: 103

Finished: 21-12-2015

Synopsis:

This project is regarding a risk assessment of a pollution that has occurred in Hvorup barracks.

Four pollution hotspots have been found where oil compounds have been detected in the ground. A risk assessment is done on two of these hotspots to investigate whether the pollution can constitute a risk for indoor climate and the regional drinking water resource.

The risk assessment consists of three elements: An analytical gas diffusion model to analyze the transport of the contaminant benzene to nearby buildings. An analytical advection-dispersion model and a numerical groundwater and transport model to analyze the transport of the contaminant benzene to the water abstractions of the municipality, including a hypothetical relocation of Lindholm well field.

It is concluded that the pollutant diffuses into nearby buildings to the extent that the concentration of benzene exceeds the limit for working areas.

It is possible that the pollution is transported to the water abstractions to the extent that the concentration of benzene exceeds the limit for drinking water. However due to uncertainties of parameters it can not be concluded with absolute certainty that this is the case.

Authors

Rupa Chand

Tiberiu Tulucan

Charles Pesch

Matthias Oursin

Emil Nielsen

Contents

	Page
1 Introduction	1
1.1 Danish water resource	1
1.1.1 Protection of the resource	1
1.2 Pollution at Hvorup barracks	2
1.3 Problem Statement	3
I Site parameters	5
2 Pollution site	7
2.1 Hvorup Barracks	7
2.2 Previous and ongoing investigations of soil pollution	7
2.2.1 Pollution hotspots	7
2.3 Dangerous chemical compounds expected at the pollution site	9
2.4 Concentration of pollutants	9
2.4.1 Concentration in groundwater	9
2.4.2 Concentration in air	10
3 Regional drinking water resource	13
3.1 Quality of current abstractions	14
3.2 Location of new abstractions	15
3.3 Threat of the pollution in Hvorup barracks for water abstractions	16
4 Soil and hydrological parameters for risk assessments	17
4.1 Physical soil properties	17
4.2 Particle size distribution	18
4.3 Water retention	19
4.4 Saturated hydraulic conductivity	22
4.5 Diffusion coefficient of benzene in the air phase	22
4.6 Retardation of benzene	23
4.6.1 Retardation of benzene in the air phase	23
4.6.2 Retardation of benzene in the liquid phase	24
4.6.3 Retardation in fractured limestone	25
4.7 Biodegradation potential at pollution site	26
4.7.1 Biodegradation in environment	26
4.7.2 Biodegradation model	27
4.7.3 Samples	28

4.7.4	Biodegradation results	29
4.8	Groundwater Recharge	30
II	Risk to indoor climate	33
5	Risk to indoor climate in Hvorup barracks	35
5.1	Analytical Model	36
5.2	Input parameters	38
5.3	Results	38
5.4	Stochastic model	40
5.5	Parameter sensitivity	45
5.6	Discussion	46
III	Risk to regional drinking water resource	47
6	Risk to regional drinking water resource	49
	Analytical model	
6.1	Vertical transport	49
6.1.1	Analytical method	50
6.1.2	Input parameters	51
6.1.3	Results	54
6.1.4	Stochastic model on vertical transport	54
6.2	Horizontal transport	59
6.2.1	Analytical method	59
6.2.2	Input parameters	61
6.2.3	Results	63
6.2.4	Stochastic model on horizontal transport	64
6.3	Parameter sensitivity	67
6.4	Discussion	68
7	Risk to regional drinking water resource	71
	Numerical model	
7.1	Groundwater model	71
7.1.1	Input parameters	71
7.1.2	Calibration	81
7.1.3	Conclusion	86
7.2	Transport model	87
7.2.1	Input parameters	87
7.2.2	Calibration of longitudinal dispersion	88
7.2.3	Results	89
7.2.4	Parameter sensitivity	90
7.2.5	Discussion	91

IV Conclusion	95
 8 Conclusion	97
Bibliography	99
V Appendix	103
A Soil and hydrological properties	
A.1 Hydraulic conductivity	105
A.2 Soil properties of soils from Tylstrup, Roskilde and Golfparken	108
B Methods	
B.1 Collecting Soil Samples	113
B.2 Sieving analysis	114
B.2.1 Setup	114
B.3 Suction Box	117
B.4 Constant head	121
C Statistical Analysis on Soil Parameters	
D Penman-Monteith evapotranspiration	
E Determining BTEX-concentration with other samples as reference	
E.1 Method 1: Same fraction BTEX	129
E.2 Method 2: PID	130
F Biodegradation Appendix	
F.1 Physicochemical factors	133
F.2 Description of experiment	134
F.2.1 Preparations of samples	134
F.2.2 Measurement of benzene concentration	136
F.2.3 Description of the Gas chromatography	137
F.3 Presentation of different models of kinetics	137
F.4 Biodegradation results and data	139
F.4.1 First order biodegradation rate:	139
F.4.2 Zero order biodegradation rate	144
F.5 Discussion	149
F.5.1 Autoclaved samples	149
F.5.2 Lag-phase and fluctuation	149
F.5.3 First-order versus zeroth-order	150
F.5.4 Nutriment and inhibitions	151
G Abstraction amount	

H Observed head compared to calculated head before calibration

1. Introduction

1.1 Danish water resource

Groundwater is a major source of water supply for drinking purposes and it has been monitored since 1990 primarily in the Danish Groundwater Monitoring Network (LOOP and GRUMO) as a part of National Action Plan Program for Water Environment and Nature.

Denmark has a good and clean source of water and the majority of the water supply is from groundwater. The groundwater is very clean and can often be consumed directly only by having simple treatment such as aeration, filtration, and pH adjustment. Regarding the history of water supply, in 1970s it has been reported by GEUS (Geological Survey of Denmark and Greenland) that there was drying of the water resources especially in the summer months of the 1975 and 1976. It resulted in a problem for the big cities and they were forced to gather water from outside the city. The water resource planning and administration has regulated the abstraction of surface and groundwater [Stockmarr, 2005].

1.1.1 Protection of the resource

In overall, nitrate from farming, chemicals from old waste dumps and oil tanks, toxic materials from enterprises and pesticides from urban areas and farmland are the major polluters for groundwater in Denmark. Shallow water aquifers suffer even more from these pollutions. Bearing in mind the protection of the groundwater and water supply, in 1994 the Danish Government presented ten points of interest:

- Removal of pesticides dangerous to health and environment
- Pesticide tax
- Reduction of nitrate pollution
- Encouragement of organic farming
- OSD area protection
- New Soil Contamination Act (cleaning of waste deposits)
- Protection of groundwater by afforestation and restoration of nature
- EU achievements strengthening
- Increased groundwater and drinking water quality
- Dialog with farmers and their organization

These ten points are the foundation of groundwater protection besides various efforts taken locally and national to make a more effective water supply sector. Monitoring of water supply wells, groundwater monitoring networks and agricultural watershed monitoring are

important in supplementary groundwater condition and implementation of the necessary step to control. GEUS is managing the collected database related to all water supply which is mandated according to the Danish Water Supply Act. [Stockmarr, 2005]

1.2 Pollution at Hvorup barracks

Pollution has been detected inside Hvorup barracks, located in the northern part of Aalborg municipality, as seen in figure 1.1. Pollution poses a risk for the groundwater resource as well as the residents and workers within the barracks. The pollution can also constitute a risk for the quality of nearby surface water and aquatic life.

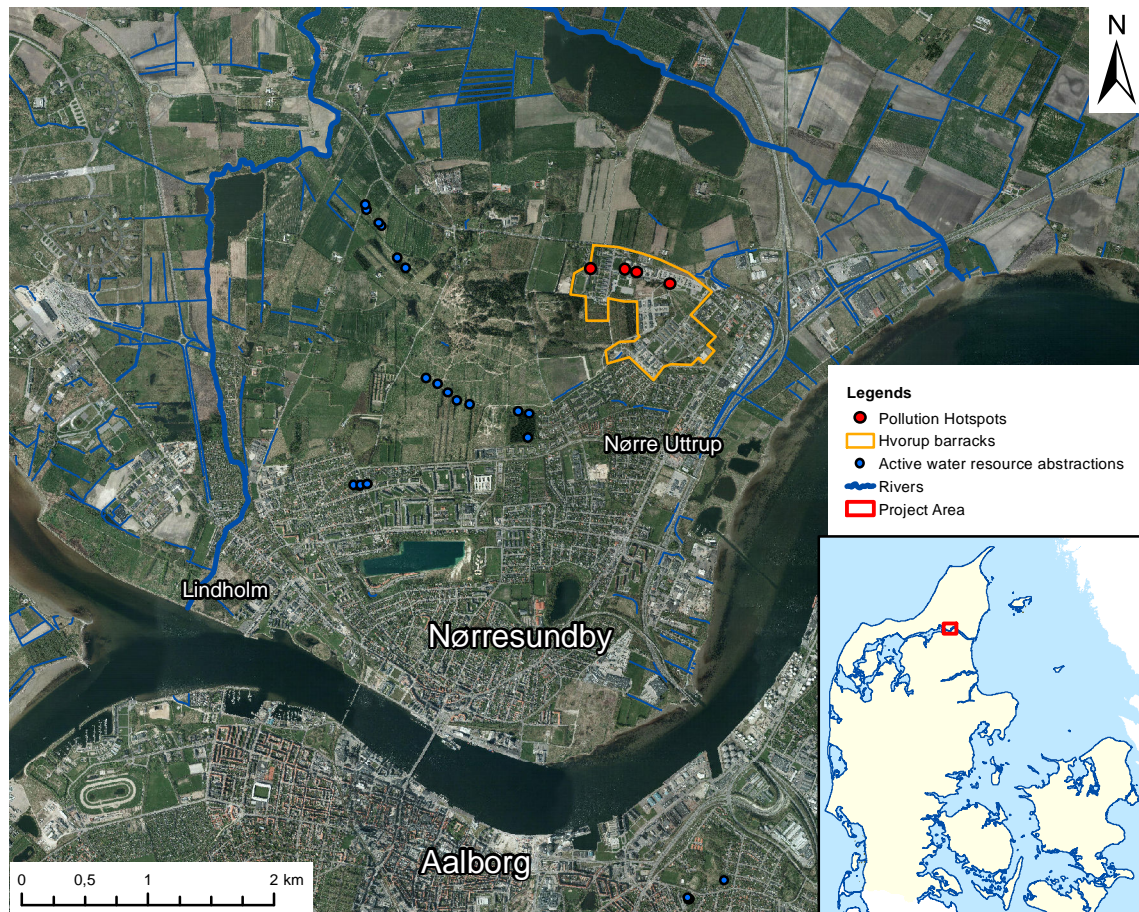


Figure 1.1. The project location.

A simple conceptual model for the potential issues regarding the pollution site is shown in figure 1.2. Pollution can constitute a problem for air and soil quality. Pollution can diffuse in the upper, unsaturated zone, and thereby enter the buildings in close proximity to the pollution spill and hence constitute a risk to indoor air quality.

It seems to be unlikely that the pollution is a risk to outdoor air quality because of the high dilution. As no activities take place at the barracks where humans are exposed directly

to the possibly polluted soil, the risk to soil quality can also be disregarded.

It is believed that the groundwater in Hvorup barracks consists of two aquifers, separated by a low-permeable clay layer. Currently no water abstractions are located inside the upper of the two aquifers, however all abstractions of the municipality are located in the deeper aquifer in the limestone. The contaminants can potentially penetrate the clay layer, and be transported to nearby water abstractions.

Although all current water abstractions are located far from the pollution site, this project will consider a possible relocation of one of the well fields for Lindholm water plant, thereby bringing it closer to the pollution site.

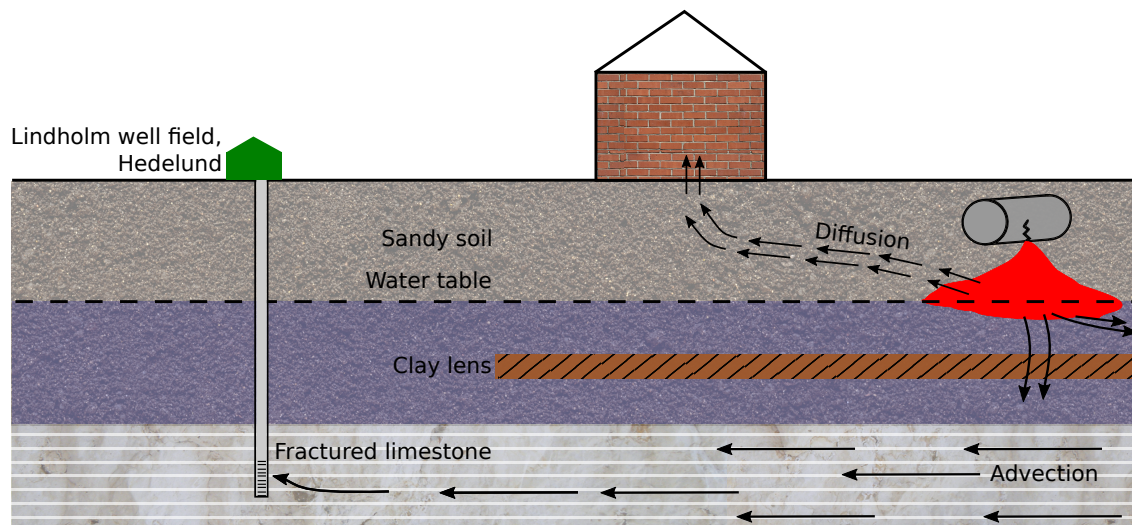


Figure 1.2. Conceptual model for the pollution site.

1.3 Problem Statement

The problem statement is based on the close proximity of the pollution site to both residential and working area as well as current abstractions and the possible new location of the abstractions of Aalborg municipality. The main objective of this study is then to answer the following two-part question:

- Will the pollutions in Hvorup barracks enter the buildings to an extent above the legal amount?
- Will the pollution in Hvorup barracks reach the abstraction wells of the municipality to an extent above the legal amount?

To answer this a risk assessment for the pollution site in Hvorup barracks is done. The risk assessment consists of the following:

- Assessment of risk to indoor climate at Hvorup barracks
- Assessment of risk to regional drinking water resource

Prior to the risk assessment the relevant site specific parameters are investigated.

Investigation of site parameters

The site specific parameters are the foundation for the risk assessments. It consists of three parts:

- Pollution site: A description of the pollution at Hvorup barracks as well as the expected pollutants in the soil
- Regional drinking water resource: A description of the abstractions of the municipality and a suggestion for relocation of Lindholm well field
- Soil and hydrological parameters: A description of the physical, chemical and biological properties of the soil in Hvorup barracks as well as recharge of the regional groundwater aquifer

The two risk assessments are described below

Assessment of risk to indoor climate at Hvorup barracks

The diffusion process from pollution site to nearby indoor working area is investigated to determine whether the concentration of pollutant in indoor air exceeds the limit for working area.

Assessment of risk to regional drinking water resource

The transport process from pollution site to regional drinking water abstractions is investigated to determine whether the concentration of pollutant in the abstraction wells exceeds the limit for drinking water.

The assessment of risk to regional drinking water resource is split into two different parts:

- Analytical model
- Numerical model using GMS

The analytical model is a fast way to model a transport process from pollution site to abstraction well. Because of its simplicity it is suitable for a stochastic analysis. It is however one-dimensional and thus not sensitive to the heterogeneity of the subsurface.

The commercial software GMS is used to perform the numerical model simulation. The numerical model can implement a quite detailed geological model and thus accounts for the heterogeneity of the subsurface. It is however a time-consuming process that requires calibration and is not suitable for a stochastic analysis.

Part I

Site parameters

2. Pollution site

2.1 Hvorup Barracks

Founded in 1950, Hvorup barracks is a danish military facility located northeast of Aalborg, Denmark. It is a part of Aalborg barracks with Nørre Uttrup barracks, and covers an area of 285 ha. Currently it serves as a training and working place for about 1500 conscripts and employees [Aalborg Kaserner, 2011].

2.2 Previous and ongoing investigations of soil pollution

In 2005, Hvorup barracks was classified as a potential source of contamination. In 2008, the Danish Defense Of Construction and Establishment services (FBE) analyzed the risk of contamination of the groundwater, the air quality and the soil pollution in Hvorup barracks. Based on the investigations FBE prepared three reports in 2009, 2010, and 2012:

In 2009:

Pollution (mainly consisting of oil products and chlorinated solvents) has been found in air, soil and water samples, however not all the pollutants necessarily are from the workshop area. That lead FBE to conclude that more investigations are needed [FBE, 2009].

In 2010:

In this report FBE has mentioned new hot-spots of chemical pollution originating from the workshop area. Chemicals such as oil products and chlorinated solvents were found in air and water, however the report concluded that this was not a threat for the groundwater. They also planned a decontamination of the workshop area by removing the source of pollution [FBE, 2010a].

In 2012:

The last report from FBE found another spot of pollution in Hvorup barracks, close to the central heating system. Pollution (consisting of mainly oil compounds) were detected in the monitoring well. Regarding the distance between the contamination spot and the well, the report concluded that pollutants were not a threat for groundwater resources [FBE, 2012].

2.2.1 Pollution hotspots

Pollution of air, soil and groundwater has been detected in multiple locations within Hvorup barracks. The four locations where the amount of pollution is expected to be the

greatest are labeled as A, B, C, D, as shown in figure 2.1.



Figure 2.1. Location of the four pollution hot-spots.

The pollution at site A originates from a heating central, where a spill occurred in 1985/1986. Oil pollution including free-phase oil has been detected in one location, but no pollution has been detected in drillings further away from the oil tanks. Thus it is believed that the pollution is delineated horizontally.

The pollution at site B originates from an oil separator in the area. Pollution has been detected, but it's delineated horizontally and vertically.

The pollution at site C originates from two underground storage tanks. Pollution has been detected and the measured concentration of total carbohydrates in this location is the highest of the entire barracks area. The underground tanks have since been removed, although the time of excavation is unknown.

The pollution at site D originates from a gas station. Free-phase oil pollution has been detected. The source of the pollution has been excavated and drained.

As both chlorinated solvents and oil compounds have been detected, the pollution site is at risk of contaminating the groundwater resource and indoor air quality for the nearby residential and working areas.

The chemicals expected to be at the pollution site are analyzed. Data that makes up foundation for this analysis is from the previous and ongoing pollution studies for Hvorup barracks done by NIRAS (a private consultancy company).

2.3 Dangerous chemical compounds expected at the pollution site

Both oil products and chlorinated solvents have been detected at the pollution site. An important part of the oil products are BTEXs, which is the technical term used for benzene, toluene, ethyl-benzene, and xylene-volatile aromatic compounds. According to table 2.1 BTEX only make up a small part of gasoline, heating oil and diesel. However, because of their relatively high solubility in water, they often constitute a risk for groundwater quality.

Table 2.1. The approximate part of oil that consists of BTEXs [Loll and Moldrup, 2000]

BTEX compound	Gasoline	Heating oil / diesel
Benzene [% g · g ⁻¹]	0.15-6	0.02-0.1
Toluene [% g · g ⁻¹]	0.7-18	0.07
Ethylbenzene and Xylene [% g · g ⁻¹]	9 – 18	0.15
Total [% g · g ⁻¹]	9.85-42	0.24-0.32

Oil products and chlorinated solvents are known to be a threat to human health, as they are carcinogens. Limits exist for the concentration of these chemicals in air at work places. As these chemicals easily reach the groundwater, limits also exist for the maximum permitted concentration of both, aromatic hydrocarbons as well as chlorides in groundwater and drinking water.

2.4 Concentration of pollutants

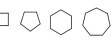
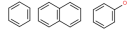
Benzene is the most soluble and diffusive of the BTEXs [Loll and Moldrup, 2000]. It is thus picked as the model chemical, which the risk assessment will be done for.

2.4.1 Concentration in groundwater

The highest concentration of total hydrocarbons measured in the water phase in Hvorup barracks is at location C with a concentration of 44 mg · L⁻¹ in 2014 at a depth of 5 m.

The hydrocarbons consist of aromatic, aliphatic and alicyclic compounds, see table 2.2. The mono-aromatic, which is a part of the aromatic compounds, is the BTEXs. As the pollution is believed to originate from two 20 m³ tanks containing diesel/gasoline [FBE, 2010b], it is expected that the original BTEX content would be a mix between the two columns in table 2.1. However, in the analysis of solute transport by water, it is necessary to know the concentration in the water phase. The concentration of the BTEXs in the water phase is expected to be different from the concentration in the plume, because of solubility as well as different conditions for biodegradations, among these a limitation in oxygen.

Table 2.2. Aromatic, aliphatic and alicyclic compounds

Name	Chemical structure	Particularity	Physical state
aliphatic		Non-aromatic compound	liquid
alicyclic		Non-aromatic compound with a ring	liquid and solid
aromatic		One or more aromatic rings	gas, liquid, solid

As the exact distribution between the types of hydrocarbons in the water phase are unknown for the drilling at location C, the concentration of BTEX, among these benzene, is also unknown. However other, similar drillings in Hvorup Barracks can be used as a reference for the distribution between the hydrocarbons. Two different attempts have been done and are documented in appendix E page 129, but both are evaluated to be a poor estimate of the concentration of BTEXs.

Instead of using the other samples as a reference, a conservative estimate is made. The maximum percentage of benzene in gasoline, heating oil and diesel is 6 % by weight, according to table 2.1. As the two tanks that caused the pollution contained both, diesel and gasoline, the benzene in the spill is assumed to be 6 % of the gasoline. Furthermore, since benzene is more soluble than most hydrocarbons, the percentage of benzene is expected to be higher in the groundwater. It is assumed that the benzene fraction makes up 50 % of the total hydrocarbons at the pollution site as a conservative estimate. The highest concentration of benzene in the groundwater is estimated at $22 \text{ mg} \cdot \text{L}^{-1}$.

2.4.2 Concentration in air

Near the heating central, at location A, non-aqueous phase liquids (NAPL) of oil have been detected in at least one drilling. It is to be expected that this pollution creates the greatest concentration of volatile compounds in the air through the vadose zone. The spill is expected to be from a leakage of the three tanks, which contained heating oil. It is noted that the NAPLs then consist of a mixture of all the compounds that make up heating oil. The distribution between compounds in the air phase and NAPL can then be calculated with Raoult's law:

$$C_{a,i} = \frac{P_i \cdot MW_i \cdot x_i}{R \cdot T} \quad (2.1)$$

Where

$C_{a,i}$	Concentration of contaminant i [$\text{mg} \cdot \text{cm}^{-3}$]
P_i	Vapour pressure of contaminant i [Pa]
MW_i	Molar weight of contaminant i [$\text{g} \cdot \text{mol}^{-1}$]
x_i	Mole fraction of contaminant i [$\text{mol} \cdot \text{mol}^{-1}$]
R	Ideal gas constant, $R = 8.314 \cdot 10^6 \cdot \text{cm}^3 \cdot \text{Pa} \cdot \text{mol}^{-1} \cdot \text{K}^{-1}$
T	Temperature [K]

Because of its high volatility and impact on human health, Benzene will be the model compound for which the risk assessment will be done for. Its vapour pressure and molar weight are shown in table 2.3. The temperature is assumed to be 10°C for the interface between air and NAPL.

Table 2.3. Data for benzene at groundwater temperature, P : Vapour pressure, MW : Molar weight, S : Solubility, K_H : Henry's constant, K_{OW} [Loll and Moldrup, 2000]

	P [Pa]	MW [$\text{g} \cdot \text{mol}^{-1}$]	S [$\text{mg} \cdot \text{L}^{-1}$]	K_H [-]	$\log(K_{OW})$ [-]
Benzene	6733	78.1	1760	0.14	2.1

The mole fraction of benzene in relation to the NAPL, can be calculated by assuming that the NAPL is identical in terms of compound composition to the oil found in the tanks. It is thus assumed that 0.1% of the NAPL consist of benzene by weight. The mole fraction can be calculated with the following equation:

$$x_{\text{benzene}} = \frac{n_{\text{benzene}}}{n_{\text{NAPL}}} = \frac{m_{\text{benzene}}}{MW_{\text{benzene}}} / \frac{m_{\text{NAPL}}}{MW_{\text{NAPL}}} \quad (2.2)$$

$$= \frac{0.1\%}{MW_{\text{benzene}}} / \frac{100\%}{MW_{\text{NAPL}}} \quad (2.3)$$

Where

n_{benzene}	Number of moles of benzene [mol]
n_{NAPL}	Number of moles of gasoline [mol]
m_{benzene}	Mass of benzene [g]
m_{NAPL}	Mass of gasoline [g]
MW_{benzene}	Molar mass of benzene [$\text{g} \cdot \text{mol}^{-1}$]
MW_{NAPL}	Molar mass of gasoline [$\text{g} \cdot \text{mol}^{-1}$]

As the gasoline is a mixture of many different hydrocarbon groups, getting the average molar weight of the gasoline can be difficult. According to American Petroleum Institute [2001] the molar weight of gasoline is $100 \text{ g} \cdot \text{mol}^{-1}$ to $105 \text{ g} \cdot \text{mol}^{-1}$. The mole fraction can be calculated with equation (2.3) and the concentration of the contaminant in the air phase can be calculated with equation (2.1). The values are shown in table 2.4.

No report is available for the drilling at location C that shows the highest hydrocarbon content in the area, so it is uncertain whether free-phase oil has been detected in this drilling. Because this tank has contained both, diesel and gasoline, the benzene content is expected to be higher than at location A, and it is thus assumed that it also contains NAPL. The concentration of benzene, assuming that this location contains NAPL of gasoline, is shown in table 2.4.

Table 2.4. Mole fraction and concentration of benzene in the air phase

	x_i [mol · mol ⁻¹]	$C_{a,i}$ [mg · L ⁻¹]
Location A (heating central)	0.0013-0.0013	0.54-0.57
Location C	0.077-0.081	32.6-34.3

The assumption that the composition of the free phase is identical to the oil in the tanks, is not necessarily correct, as the compounds in hydrocarbons have different physical/chemical properties.

	$C_{a,i}$ [mg · L ⁻¹]
Pollution in soil air	
Location A (heating central)	0.54-0.57
Location C	32.6-34.3
Pollution in groundwater	
Location C	22

3. Regional drinking water resource

In figure 3.1 the northern part of Aalborg municipality is shown. The Hvorup barracks surroundings are labeled as an area of drinking water interest (OSD).

The OSD areas are classifications of aquifers according to degree of drinking water interest, which started in 1997 in order to protect groundwater. This classification was based on the size and the quality of groundwater resources [Thomsen et al., 2004]. The three categories are:

- Particularly valuable areas for drinking water interests (OSD)
- Valuable areas for drinking water interests (OS)
- Less valuable areas for drinking water interests.

Several water abstractions are located west and southwest of the barracks which supply the part of Aalborg municipality north of Limfjorden with clean drinking water. The water resource abstractions inside the OSD-area are grouped in three well fields: Lindholm, Nørre Uttrup and Hvorup Syd. The three well fields make up Hvorup supply group and supply most of Nørresundby with clean drinking water. The permitted abstraction amount as well as amount abstracted in 2011 are shown in table 3.1. [Aalborg Kommune, 2013, p. 142]

Table 3.1. The abstraction from the three water plants

Water plant	Permitted abstraction amount [m ³ · year ⁻¹]	Abstraction amount in 2011 [m ³ · year ⁻¹]
Lindholm	600 000	540 908
Nørre Uttrup	308 000	225 331
Hvorup Syd	750 000	504 326
Total	1 658 000	1 270 565

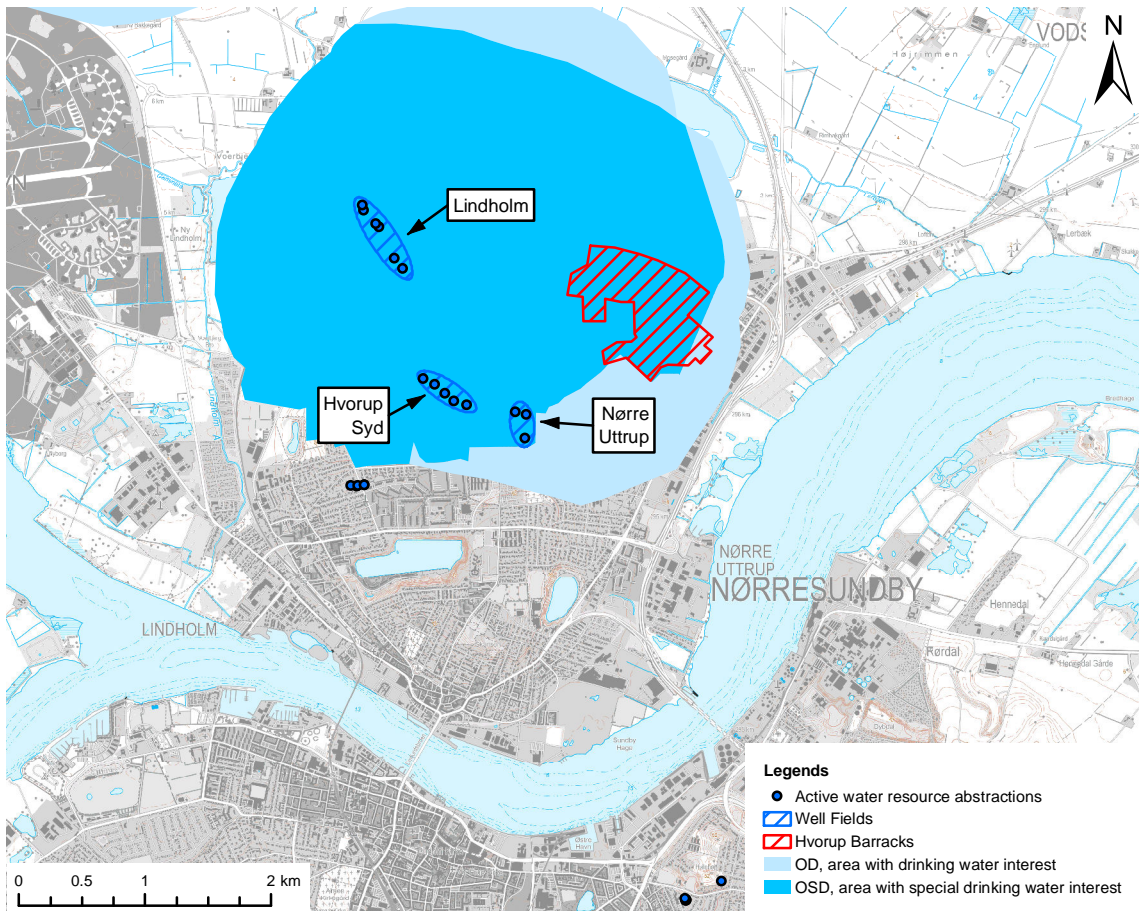


Figure 3.1. Water resource abstractions, OD and OSD areas in relation to Hvorup barracks.

3.1 Quality of current abstractions

Figure 3.2 shows the close proximity of Lindholm well field to the freeway connected to the third Limfjord connection. It is possible that the reduction in water table during construction can constitute a significant risk for the water abstractions. This risk was investigated in the environmental assessment for the third Limfjord connection. The report evaluated that the water abstractions in Lindholm well field will suffer no significant impact during construction. [Vejdirektoratet, 2011]

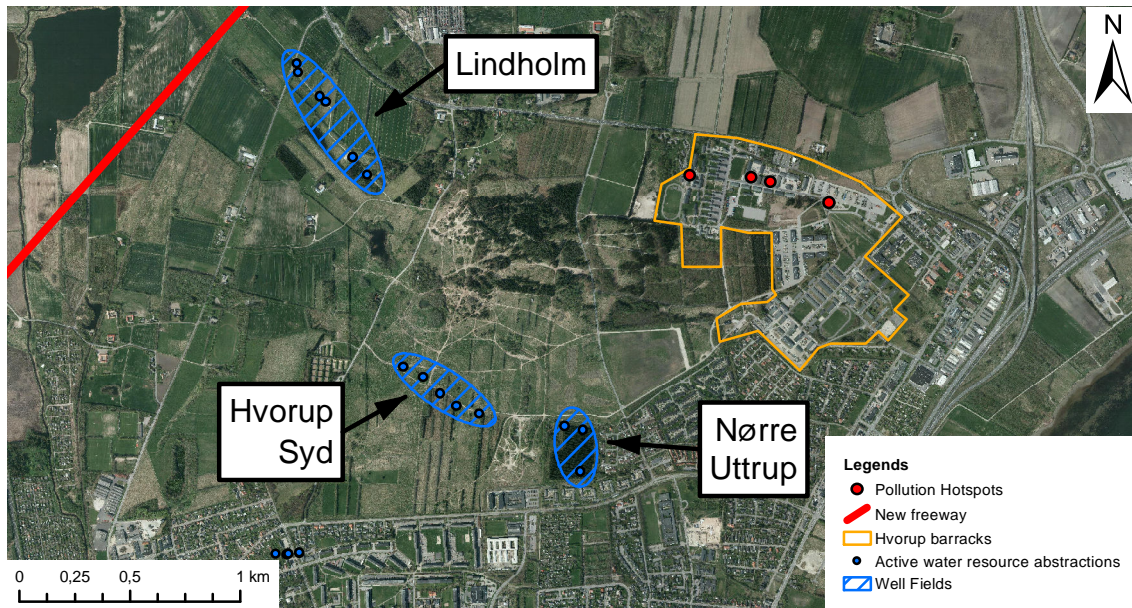


Figure 3.2. Location of the current well fields and the planned third Limfjord connection.

The highest nitrate levels measured in the three well fields are shown in table 3.2. This is still well below the limit of $50 \text{ mg} \cdot \text{L}^{-1}$ [Miljøministeriet, 2014]. The nitrate concentrations in the three well fields are also far lower than the average nitrate content in the water abstractions of Aalborg Forsyning, which was $29.5 \text{ mg} \cdot \text{L}^{-1}$ in 2013 [Aalborg Forsyning, 2013].

Table 3.2. The highest measured nitrate concentrations in three well fields close to Hvorup barracks

Well field	Highest $[\text{NO}_3^-]$ $[\text{mg} \cdot \text{L}^{-1}]$
Lindholm	11
Hvorup Syd	5,4
Nørre Uttrup	7

Because all three well fields are located close to either agriculture or residential areas, it is possible that abstractions can get contaminated with pesticides or an increase in concentrations of nitrate. So even if the current water abstractions show good water quality now, the quality can decrease in the future.

3.2 Location of new abstractions

Although no significant issues with water quality have been found for the three well fields, it is still possible that the abstractions will be moved in the future. For the purpose of this study it is assumed that Lindholm well field is relocated. This well field is chosen

due to its close proximity to the track of the third Limfjord bridge and because it has the highest measured nitrate concentration.

The suggested sites for relocation of Lindholm well field is shown in figure 3.3. It is located inside Hvorup and Hedelund Plantage. This is likely to offer greater protection against contamination, since the area is neither used for agriculture nor residential use. The distance to the new freeway is also increased, which decreases the risk of influence during construction. The major disadvantage about this new location is however that it is significantly closer to the pollution site in Hvorup Barracks.

It is considered that the two other well fields will not be relocated to the forest. They can then function as a backup resource if Lindholm well field becomes contaminated.

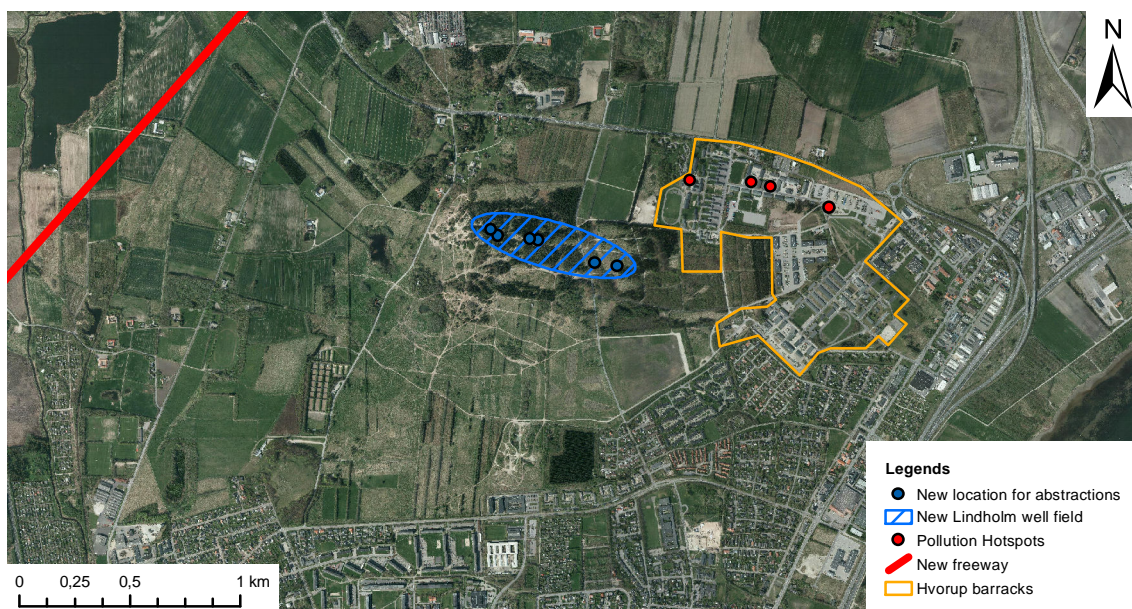


Figure 3.3. The new location of Lindholm well field.

3.3 Threat of the pollution in Hvorup barracks for water abstractions

The new location of the abstractions is very close to the pollution site. It is therefore possible that the pollution in Hvorup reaches the groundwater and thereby contaminates the water resource for these abstractions. The limit for benzene in drinking water is $1 \mu\text{g} \cdot \text{L}^{-1}$ [Miljøministeriet, 2014]. As such it should be assessed whether the pollution in Hvorup barracks will cause the concentration of benzene in the water abstraction to exceed this limit.

4. Soil and hydrological parameters for risk assessments

Soil and hydrological parameters that are used in following risk assessments are analyzed. The relation between parameters and the risk assessment they pertain to are shown in table 4.1. The parameters appear in chapter are in the same order as in table.

Table 4.1. What risk assessment the following parameters pertain to

		Risk to indoor climate	Risk to regional drinking water resource	
			Analytical	Numeric
Physical properties	soil	X	X	X
Particle size distribution				
Water retention		X		
Saturated hydraulic conductivity			X	X
Diffusion coefficient of benzene in the air phase		X		
Retardation		X	X	X
Biodegradation potential at pollution site		X	X	X
Groundwater recharge				X

4.1 Physical soil properties

As the flow of fluids through a porous medium is highly complex, and a large part of it is based on assumptions and averages, it is crucial to estimate the properties of the porous medium the flow occurs in as precise as possible. In order to be able to reduce the

error, the estimation should be based on complete datasets of measurements. Because no complete datasets for Hvorup are available, the assessment is based on comparable soils from Denmark, collected by [Hansen, 1976]. The soils are a sandy soil from Tylstrup and a clayey soil from Roskilde. They are denoted sand a) and clay b). The basic physical soil properties are shown in table 4.2.

Whenever the discussion is about the particle size fraction, it will be clarified by the addition of the word *content*, e.g clay content.

Table 4.2. Physical soil properties [Hansen, 1976], ρ_s : Particle density, ρ_b : Bulk density, ϕ_{tot} : Total porosity, f_{oc} : Organic carbon content

	ρ_s [g · cm ⁻³]	ρ_b [g · cm ⁻³]	ϕ_{tot} [cm ³ · cm ⁻³]	f_{oc} [g · g ⁻¹]
Sand a)	2.66	1.40	0.44	0.0076
Clay b)	2.65	1.53	0.45	0.0061

4.2 Particle size distribution

The properties of a porous medium are controlled to a large extend by the size and shape of the composing particles, especially when the fluid flow is investigated. The pore size distribution gives a first overview of the expected flow properties. The particle size and the compaction of the sediment define the pore size available for the flow. The relation (4.1) associates the particle size and the pore size for spherical particles.

$$D_{max} = 0.28 \cdot d_{90} \quad (4.1)$$

Where

D_{max}	Size of the largest pores [μm]
d_{90}	Size of pore [μm]

The fraction of the total water content in a saturated soil that can be drained only by gravitation is associated to the largest pore size fraction, represented by D_{max} formed by the largest particles, i.e. the fraction for which 90% of the particles are smaller than the indicated d_{90} particle size. Plotting the cumulated weight fraction against its particle size, the value for d_{90} can easily be retrieved. This is shown in figure 4.1.

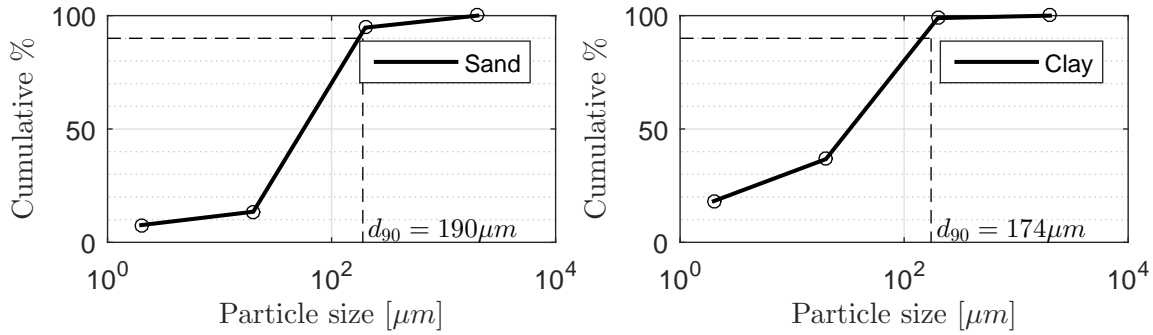


Figure 4.1. Particle Size Distributions, data from Hansen [1976]

The biggest pore size for sand and clay are shown in table 4.3.

Table 4.3. Estimated largest pore sizes

	d_{90} [μm]	D_{max} [μm]
Sand a)	190	50.3
Clay b)	174	48.7

4.3 Water retention

The *Campbell model* of the water retention for its limit ($pF < 3.2$, see equation (4.5) for a definition of pF) expressed as a function of the matrix potential is given by:

$$\theta = \theta_s \left(\frac{\psi_e}{\psi} \right)^{1/b} \quad (4.2)$$

Where

θ	Volumetric water content [$\text{cm}^3 \cdot \text{cm}^{-3}$]
θ_s	Saturated volumetric water content [$\text{cm}^3 \cdot \text{cm}^{-3}$]
ψ_e	Matrix suction at air entry [$\text{cm H}_2\text{O}$]
ψ	Matrix suction [$\text{cm H}_2\text{O}$]
b	Campbell pore connectivity parameter [-]

The saturated water content θ_s is assumed to be equal to the total porosity, hysteresis is assumed to be negligible. It can be measured or calculated by the relation (4.3).

$$\phi_{tot} = \theta_s = 1 - \frac{\rho_b}{\rho_s} \quad (4.3)$$

Where

ρ_b	Bulk density [$\text{g} \cdot \text{cm}^{-3}$]
ρ_s	Particle density [$\text{g} \cdot \text{cm}^{-3}$]

The air entry matrix potential is the suction that has to be applied to the soil water in order to drain the largest pores. From the particle size distribution and the capillary law, the air entry suction can be calculated with equation (4.4).

$$\psi_e = \frac{3000}{D_{max}} = \frac{3000}{0.28 \cdot d_{90}} \quad (4.4)$$

The air entry suctions are pF equal to 1.79 and 1.86 for the sand and clay layer respectively, where pF is defined by equation (4.5).

$$pF = \log(-\psi) \quad (4.5)$$

The negative slope of the water retention curve in the validity range of the Campbell model plotted in a log - log plot is the parameter b , or *Campbell pore connectivity factor*. Figure 4.2 shows the retention values in a log – log plot, the fitted line and the confidence bounds for the estimation of the parameter b .

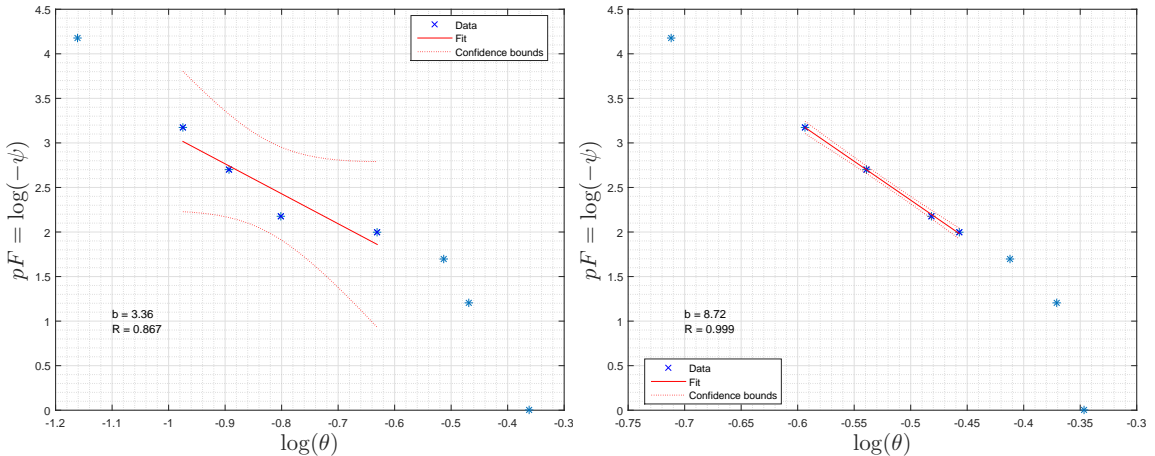


Figure 4.2. Retention curves, data from Hansen [1976]

In order to get a predictive range for the parameter b , a statistical analysis on the linear regression is performed. Bootstrapping gives a 95% prediction interval for the parameter b . Mean, standard deviation of the distribution and prediction range are given in table 4.4.

Table 4.4. Statistical result of predicting parameters b . b first guess is by using no bootstrapping, as shown in figure 4.2

	b first guess	b mean [-]	b stdev [-]	b range	Distribution
Sand a)	3.36	3.46	1.05	2.57 - 4.29	normal
Clay b)	8.72	8.84	1.01	8.63 - 9.03	not determined

From the knowledge of the retention curve, a lot of other relevant information can be obtained. The fraction of the water content that can not be drained by gravity alone is the fraction occupied by pores above $30 \mu\text{m}$. Applying the capillary law, the necessary suction potential to drain these pores yields $-100 \text{ cm H}_2\text{O}$ or $pF = 2$. The retention curve gives average values of 0.22 for sand a) and 0.35 for clay b) for water content at $pF = 2$, which is commonly referred to as the field capacity of the soil. The air content ε in unsaturated conditions for a given matrix suction is obtained by simply subtracting the water content at the specified matrix potential from the saturated water content.

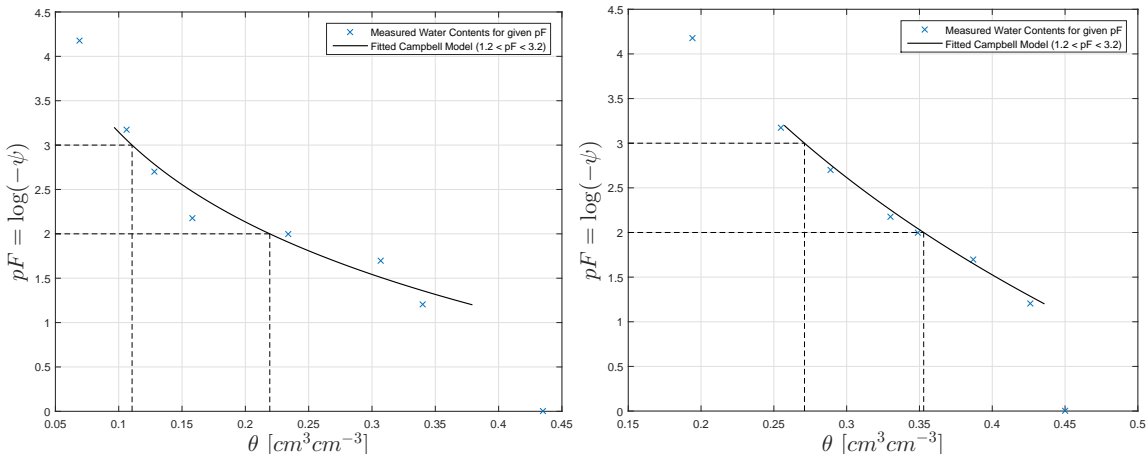


Figure 4.3. Measured water contents and fitted Campbell model, data from Hansen [1976]

Figures 4.3 show the measured water contents for different negative potentials and the fitted Campbell model for its validity range ($1.2 < pF < 3.2$). The dashed lines indicate the locations of the important suction potentials and their respective water contents. Table 4.5 displays the values as well as the saturated water content.

Table 4.5. Water and air contents for important suction potentials, data from [Hansen, 1976]

	θ_s	$\theta_{pF=2}$	$\theta_{pF=3}$	$\varepsilon_{pF=2}$	$\varepsilon_{pF=3}$	Unit
Sand a)	0.44	0.22	0.11	0.22	0.33	$[\text{cm}^3 \cdot \text{cm}^{-3}]$
Clay b)	0.45	0.35	0.27	0.10	0.18	$[\text{cm}^3 \cdot \text{cm}^{-3}]$

4.4 Saturated hydraulic conductivity

Measurements of saturated horizontal hydraulic conductivity are retrieved from multiple sources. The data set is shown in appendix A.1 page 105. A figure of all the values is shown in figure 4.4. It is evident that the measurements for clay are above the range and are roughly equivalent to that for sand. It is evaluated that these measurements are not representative for the clay in Hvorup barracks and are thus excluded from the risk assessments.

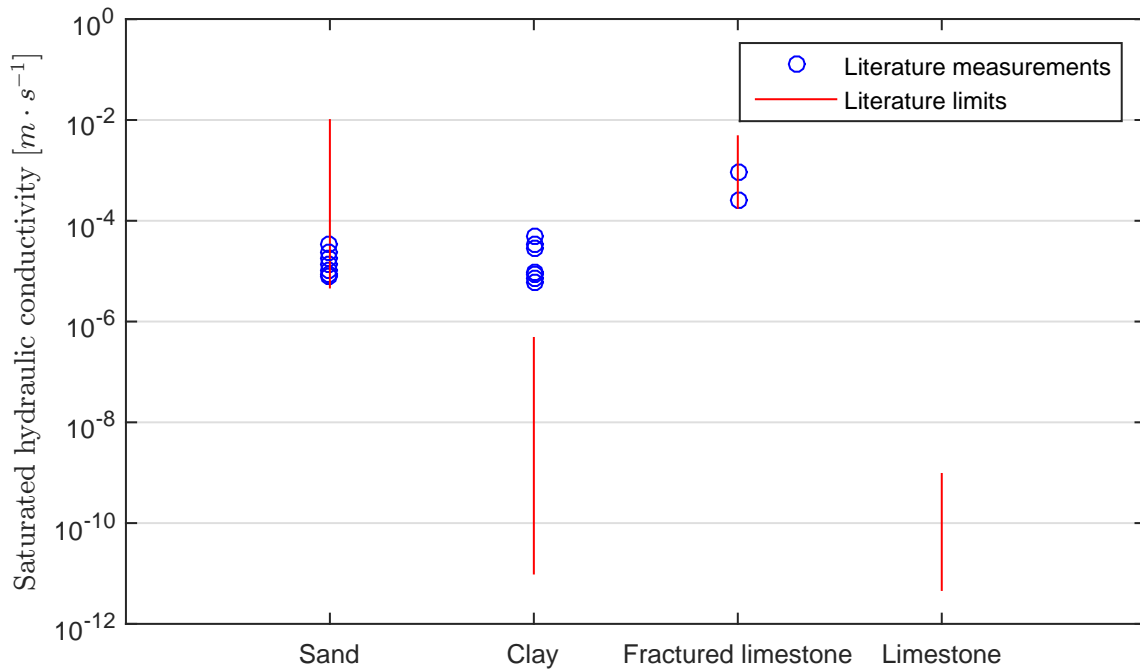


Figure 4.4. Values of horizontal saturated hydraulic conductivity from literature and experiments close to or inside Hvorup barracks. Sources are shown in appendix A.1 page 105

4.5 Diffusion coefficient of benzene in the air phase

The effective gas diffusion coefficient in a porous medium is given by

$$D = \frac{\lambda_a \cdot D_{o,a}}{\varepsilon} \quad (4.6)$$

Where

D	Effective gas diffusion coefficient in a porous medium [$m^2 \cdot s^{-1}$]
λ_a	Air phase tortuosity [-]
$D_{o,a}$	Gas diffusion coefficient in free air [$m^2 \cdot s^{-1}$]
ε	Air content [$cm^3 \cdot cm^{-3}$]

According to Loll and Moldrup [2000], the air phase tortuosity can be estimated by:

$$\lambda_a = \left(2 \cdot \varepsilon_{100}^3 + 0.04 \cdot \varepsilon_{100} \right) \cdot \left(\frac{\varepsilon}{\varepsilon_{100}} \right)^{2+3/b} \quad (4.7)$$

Where

ε	Air content $[\text{cm}^3 \cdot \text{cm}^{-3}]$
ε_{100}	Air content at field capacity $[\text{cm}^3 \cdot \text{cm}^{-3}]$

The water content θ is obtained by applying equation (4.2). The corresponding air content is:

$$\begin{aligned}\varepsilon_{100} &= \phi_{tot} - \theta_{pF=2} \\ \varepsilon &= \phi_{tot} - \theta\end{aligned}$$

The diffusion coefficient in free air, $D_{o,a}$, can be obtained by the *Einstein-Stokes equation*, based on thermodynamic kinetics theory. It depends on pressure and temperature of the environment. An estimation of the diffusion coefficient of benzene in air is given by Fuller et al., (1966) in Hsieh [1994] assuming atmospheric pressure:

$$D_{o,a} = 8.6 \cdot 10^{-3} \cdot T^{1.75} \cdot \frac{\sqrt{(29 + M_x)/(29 \cdot M_x)}}{\left(2.7 + V_x^{1/3}\right)^2} \quad (4.8)$$

Where

M_x	Molecular mass $[\text{g} \cdot \text{mol}^{-1}]$
V_x	Molar volume $[\text{cm}^3 \cdot \text{mol}^{-1}]$
T	Temperature [K]

For the assumed temperature (10°C), the diffusion coefficient in free air is $0.684 \text{ m}^2 \cdot \text{d}^{-1}$ or $7.917 \cdot 10^{-6} \text{ m}^2 \cdot \text{s}^{-1}$.

4.6 Retardation of benzene

4.6.1 Retardation of benzene in the air phase

In order to account for retardation in the air phase, a retardation coefficient for the gas phase will be introduced [Majid, 2006]:

$$R_a = 1 + \frac{\rho_b \cdot K_d}{\varepsilon \cdot H} + \frac{\theta}{\varepsilon \cdot H} \quad (4.9)$$

Where

R_a	Retardation in air [−]
K_d	Sorption coefficient [$\text{L} \cdot \text{kg}^{-1}$]
ρ_b	Bulk density [$\text{g} \cdot \text{cm}^{-3}$]
ε	Air content [$\text{cm}^3 \cdot \text{cm}^{-3}$]
H	Henry's constant [$\text{mol} \cdot \text{L}^{-1} \cdot \text{Pa}^{-1}$]
θ	Water content [$\text{cm}^3 \cdot \text{cm}^{-3}$]

The Henry's constant is the ratio between the concentration of compound in aqueous phase and the partial pressure of that compound in gas phase, see equation (4.10).

$$H = \frac{C}{P} \quad (4.10)$$

Where

C	Concentration on the aqueous phase [$\text{mg} \cdot \text{L}^{-1}$]
P	Partial pressure [Pa]

Sander [1999] reports a value for H at 20 °C of $0.18 \text{ M} \cdot \text{atm}^{-1}$ and a temperature dependence factor:

$$-\frac{\Delta \ln(H)}{\Delta \ln(1/T)} = \frac{\Delta E_{sol}}{R} = 3200$$

Where

$\Delta \ln(H)$	Normal log of Henry constant difference
$\Delta \ln(1/T)$	Temperature-difference
ΔE_{sol}	Enthalpy of the solution [J]
R	Gas constant [$\text{J} \cdot \text{K}^{-1} \cdot \text{mol}^{-1}$]

Inserting the values and calculating the dependence gives the value $0.1224 \text{ M} \cdot \text{atm}^{-1}$ for the Henry's constant at 10 °C.

4.6.2 Retardation of benzene in the liquid phase

The retardation factor depends on the soil and on the chemical compound. It can be calculated by equation (4.11):

$$R = 1 + \frac{\rho_b \cdot K_d}{\theta} \quad (4.11)$$

Where the distribution coefficient K_d is given by equation (4.12):

$$K_d = f_{oc} \cdot K_{oc} \quad (4.12)$$

Where

K_d	Sorption coefficient [$\text{L} \cdot \text{kg}^{-1}$]
R	Retardation factor [-]
K_{oc}	Partitioning coefficient between organic carbon and water [-]
f_{oc}	Organic carbon content [$\text{g} \cdot \text{g}^{-1}$]

K_{oc} is the *soil organic carbon-water partitioning coefficient* which can be in turn estimated from the K_{ow} value, reported for many chemical compounds. The model used for estimating the K_{oc} value depends on the content of organic matter and the chemical compound investigated. This empirical relation is used to estimate K_{oc} of benzene from its K_{ow} for the given soil properties [Loll and Moldrup, 2000]:

$$\log(K_{oc}) = 1.04 \cdot \log(K_{ow}) - 0.88 \quad (4.13)$$

Where

K_{ow}	Octanol-Water partitioning coefficient [-]
----------	--

For benzene, $\log(K_{ow})$ is equal to 2.13 as shown in table 2.3. The $\log(K_{oc})$ value then equals to 1.335. The estimated sorption coefficient and retardation for the sand and clay layer are displayed in table 4.6 for a fully saturated soil.

Table 4.6. Retardation of benzene at full water saturation [Hansen, 1976]

	ρ_b [$\text{g} \cdot \text{cm}^{-3}$]	$\phi_{tot} = \theta_{sat}$ [$\text{cm}^3 \cdot \text{cm}^{-3}$]	f_{oc} [$\text{g} \cdot \text{g}^{-1}$]	K_d [$\text{L} \cdot \text{kg}^{-1}$]	R [-]
Sand a)	1.40	0.45	0.0076	0.164	1.51
Clay b)	1.53	0.44	0.0061	0.132	1.45

4.6.3 Retardation in fractured limestone

Water and contaminant flow in fractured porous medium can be divided into two separate processes. First, there is the usual convective flow occurring in the fractures. At high water velocities, there will be no or little exchange between the fractures and the matrix, thus, the contaminant will not likely enter the matrix and the spread of the contaminant can be described by the usual convection dispersion equation.

At low water velocities however, there will be an exchange between the fractures and the matrix. To describe these processes, the porous medium is divided into two zones, one, covering the flow in the fractures and another, covering the flow in the matrix. The flow differences are a result of the highly heterogeneous hydraulic conductivities occurring on

a very small scale. In order to separate the two regions, the porous medium is separated into zones with high hydraulic conductivity and mobile water and on the other hand, a zone with immobile water and low hydraulic conductivity.

Because of the above mentioned properties of the fractured limestone aquifer, two mechanisms take place which influence the retardation of a dissolved compound. First, there is the sorption and desorption of the contaminant to the solid phase and second, there is the diffusion of the solute from the mobile region (fractures) into the immobile/stagnant region (matrix).

The retardation due to diffusion between immobile and mobile pores can be calculated by the following equation:

$$R = 1 + \frac{\phi_{im}}{\phi_m} \quad (4.14)$$

R	Retardation [-]
ϕ_{im}	Porosity of the immobile phase [$\text{cm}^3 \cdot \text{cm}^{-3}$]
ϕ_m	Porosity of the mobile phase [$\text{cm}^3 \cdot \text{cm}^{-3}$]

By assuming that the mobile volume is the effective porosity and the immobile volume is the microporosity, the retardation in fractured limestone can then be calculated. The retardation by sorption is assumed to be negligible. The values of total porosity for fractured limestone are described in appendix A.2 page 110. The values of secondary or fissure porosity which make up the mobile volume in fractured limestone are also described in appendix A.2 page 110.

The retardation for fractured limestone is shown in table 4.7, calculated with equation 4.14 where immobile volume is $\phi_{im} = \phi_{total} - \phi_m$.

Table 4.7. Retardation in fractured limestone [Hansen, 1976]

ϕ_{total} [$\text{cm}^3 \cdot \text{cm}^{-3}$]	0.42
ϕ_m [$\text{cm}^3 \cdot \text{cm}^{-3}$]	$1 \cdot 10^{-5} - 1 \cdot 10^{-2}$
ϕ_{im} [$\text{cm}^3 \cdot \text{cm}^{-3}$]	≈ 0.42
R [-]	43 - 42 001

4.7 Biodegradation potential at pollution site

This section analyzes biodegradation in the soil at Hvorup Barracks. Biodegradation is an important part of evaluating the spread of contamination, as it decreases the concentration of pollution. The kinetics of biodegradation are analyzed as well as how it can be interpolated to a large scale.

4.7.1 Biodegradation in environment

Biodegradation is a biochemical process, involving bacteria and fungi that cause the decomposition of materials. The IUPAC (International Union of Pure and Applied Chemistry) gives the following definition:

“Degradation caused by enzymatic process resulting from the action of cells.
[Vert et al., 2012]”

The biodegradation can be quantified as a decrease in the concentration of pollutants. Aromatic hydrocarbons can be degraded by several types of bacteria and microorganisms. Each type of bacteria grows in specific conditions, this is why biodegradation depends on several physical and chemical parameter. A short review of the different parameters can be found in appendix F.1.

For determining the degradation rate of benzene, a previous group has made a biodegradation experiment in 2014 using the soil and groundwater from Hvorup barracks [Nielsen et al., 2013].

4.7.2 Biodegradation model

For the soil in Hvorup barracks it is assumed that the biodegradation follows a first order biodegradation rate. A short description of the different kinetic models can be found in appendix F.3.

However, it is evident from the data, that there is a concentration variation from day to day, probably due to uncertainties in the measurement procedure, wrong calibration and not acquiring the equilibrium between benzene in water and air phases. Biodegradation does not seem to follow a strict first order law. In order to obtain more information, a comparative study has been done by using a zero-order biodegradation model.

For each set of data, the zero- and first-order degradation rates are calculated, then the *root mean square error (RMSE)* is calculated to see which model fits the best.

4.7.2.1 Extension to groundwater

The experiment was conducted at 20°C, but the soil and groundwater temperatures are much lower (between 8 and 4°C). To account for that temperature differences, the temperature coefficient Q_{10} is introduced. It is a measure of the rate of change of a biological system after an increase in temperature of 10°C. The Q_{10} coefficient is calculated as following:

$$Q_{10} = \left(\frac{R_{T_2}}{R_{T_1}} \right)^{\left(\frac{10}{T_2 - T_1} \right)} \quad (4.15)$$

Where

Q_{10}	Temperature coefficient [–]
T	Temperature [$^{\circ}\text{C}$]
R	Rate of biodegradation [–]

For a sandy soil, the value of Q_{10} is typically estimated between 2 and 3.

4.7.2.2 Extension to anaerobic

It is assumed that the biodegradation rate calculated is representative for the soils at Hvorup barracks as well as for the lower groundwater aquifer. The presence of O_2 plays a vital role in the biodegradation of the pollutants, however, the level of oxygen decreases with increasing soil depth. In the same way, the level of nutrients decreases too. So, the degradation process changes from aerobic in the upper soil surface, to anaerobic in the lower horizons of the soil. The rate is assumed to be 100 times lower in the anaerobic region than in the aerobic one.

4.7.3 Samples

In figure 4.5, the sampling wells and pits are indicated. The samples were all taken close to the workshop. Well number 502 was chosen due to the presence of free phase in water (phase of pure gasoline).



Figure 4.5. Location of sampling site

As shown in appendix F.1, there is a lot of different parameters that can influence

biodegradation. A description of the testing procedure and the main parameter for the experiment can be found in appendix F.2.

4.7.4 Biodegradation results

The biodegradation rates for both, zero and first order are shown in table 4.8 for the groundwater samples and table 4.9 for the soil samples, respectively. K_1 lab and K_0 lab is for experiment in lab at room temperature and in aerobic condition. K_1 and K_0 in situ is for biodegradation rate in limestone, lack of nutrient, in anaerobic condition and at low temperature, according to section 4.7.2.1 and 4.7.2.2. It's evident that for anaerobic, low temperature conditions, the biodegradation rate is significantly lower. The figures for all the samples are in appendix F.4 page 139. The half life is calculated from the K_1 in situ value with equation (F.6).

Based on the discussion of results in appendix F.5 page 149 it is evaluated that the experiment is disturbed by leakage or sampling. The biodegradation rate is thus slightly overestimated, as the disturbances are included in the biodegradation rate. It is also evident that the biodegradation is very nutrient-dependant. It is also concluded that the biodegradation primarily follows a 1st order degradation kinetic.

Table 4.8. Biodegradation rate for groundwater sample

Sample number	Time for total degradation [d]	K_1 lab [d^{-1}]	K_1 in situ [d^{-1}]	$t_{1/2}$ [d]	K_0 lab [$\mu\text{g} \cdot \text{L}^{-1}$]	K_0 in situ [$\mu\text{g} \cdot \text{L}^{-1}$]
GW502a	> 30	0.41	0.0010	726	14.48	0.0334
GW502b	29	0.41	0.0010	726	22.07	0.0509
GW512a	28	0.11	0.0003	2743	3.48	0.0080
GW512b	16	0.26	0.0006	1169	14.06	0.0325
GW516a	> 30	0.05	0.0001	5570	2.54	0.0059
GW516b	> 30	0.05	0.0001	5940	2.08	0.0048
GW502Na	5	1.09	0.0025	275	93.84	0.2166
GW502Nb	4	2.46	0.0057	122	107.46	0.2480
GW502Nc	8	0.53	0.0012	570	22.71	0.0524
GW502Nd	5	0.60	0.0014	503	23.61	0.0545

Table 4.9. Biodegradation rate for soil sample

Sample number	Time for total degradation [d]	K_1 lab [d $^{-1}$]	K_1 in situ [d $^{-1}$]	$t_{1/2}$ [d]	K_0 lab [$\mu\text{g} \cdot \text{L}^{-1}$]	K_0 in situ [$\mu\text{g} \cdot \text{L}^{-1}$]
S502Ca	>30	0.003	7.3E-06	94350	0.10	7.3E-06
S502Cb	>30	0.004	9.3E-06	74102	0.17	9.3E-06
S502a	25	0.149	0.0003	2015	3.55	0.0003
S502b	14	8.694	0.0200	35	62.71	0.0200
S510a	3	0.777	0.001	386	24.22	0.0017
S510b	3	0.513	0.001	585	18.70	0.0011
S514a	3	1.147	0.002	262	22.38	0.0026
S514b	3	1.072	0.002	280	17.50	0.0024

It is evident that there is a large variation in the biodegradation rate between these samples due to different nutrition conditions and to differences in the biological activity. Thus it is clear, that biodegradation is a common source of uncertainty. A short comparison of biodegradation rates in shallow aquifers for different regions and conditions can be found in table 4.10. It's evident that the biodegradation measured at Hvorup barracks is lower than the two other locations.

Table 4.10. Comparison between soil biodegradation in Hvorup, Taiwan and North Carolina [Henriksen, 2015a]

	Hvorup	Taiwan	North Carolina
Depth of aquifer [m]	circa 3	1-2	2
BTEX source concentration [$\text{mg} \cdot \text{L}^{-1}$]	11	0.735	10
Temperature [$^{\circ}\text{C}$]	10-13	17-29	15-21
pH [-]	6.5-7	6.8-7.1	4.3
Groundwater velocity gradient [$\text{m} \cdot \text{year}^{-1}$]		840	circa 15
O_2 [$\text{mg} \cdot \text{L}^{-1}$]	7	2.4	7-8
NO_2 [$\text{mg} \cdot \text{L}^{-1}$]		13	7-17
K_1 field [d $^{-1}$]	0.0003-0.0024	0.017-0.020	0.001
Last pollution time	2009	2001	1987-1995

4.8 Groundwater Recharge

The only source for groundwater recharge is precipitation in all its forms, gaseous, liquid and solid. The annual average precipitation is well documented and measured in a fine grid all over Europe. Looking at the average total precipitation for Nordjylland and more especially at data for Nørresundby, values between $600 \text{ mm} \cdot \text{yr}^{-1}$ (1961-1990) and $800 \text{ mm} \cdot \text{yr}^{-1}$ (1990-2000) are reported (DMI, 2013 and Scharling M. [2002]). However, the water contributing to the groundwater recharge is only a fraction of the total precipitation.

The simple water balance can be described as follows:

$$Q_{net} = P_{tot} - EVT - R - \Delta S \quad (4.16)$$

Where

Q_{net}	Net-infiltration [mm · year ⁻¹]
P_{tot}	Total precipitation [mm · year ⁻¹]
EVT	Evapotranspiration [mm · year ⁻¹]
R	All forms of runoff [mm · year ⁻¹]
ΔS	Change in groundwater storage [mm · year ⁻¹]

The surface runoff, including drainage of agricultural land and urban surface water do not contribute to the groundwater recharge, as these waters are usually evacuated immediately to rivers or other open water areas. The surface runoff might be quantified relatively easy by measuring the river discharges in the catchment area, taking into account that there could be an exchange between groundwater and free water body. The evapotranspiration is the sum of two processes, the evaporation, occurring over bare soil and free water areas and the transpiration, being a result of plant metabolism, therefore, occurring over vegetation. It can be very hard to determine the amount that is lost to the groundwater recharge due to evapotranspiration, because it is dependent on many factors. High-frequency measurements of turbulent energy fluxes over different crops in distinct regions clearly shows the influence of the surface cover on the evapotranspiration rate.

Several empirical relationships have been established in order to quantify the evapotranspiration rate, one among those is the PENMAN-MONTEITH EQUATION, used by the FAO, which is presented in appendix D. The actual evapotranspiration has been estimated by GEUS and DMI. The values for 2003 are presented in table 4.11, together with the estimated average annual precipitation.

Table 4.11. Average annual net-precipitation

P_{tot} (1990-2000)	EVT	NP	Unit
895	521	374	mm

The surface runoff for the catchment area can be neglected, as the infiltration capacity of the sandy soil is high and the topography is relatively flat. The surface coverage plays a major role in the amount of water available for infiltration. Fortunately, the upper layer of the catchment area of the aquifer is dominated by sandy soils which have similar properties regarding their retention properties, that's why the relative infiltration rate for farm land depends only on the crop and on the presence or absence of drainages.

In urban areas, a large percentage of the surface is sealed and the precipitation is conducted to open water channels or waste water plants and lead into rivers or into the Fjord.

The net-infiltration is the driving force for the vertical movement of the contaminant released in Hvorup barracks. The surface coverage has to be taken into account in order not to overestimate the vertical velocity of the contaminant. A hydrological correction factor is introduced in order to account for the surface coverage influence on the groundwater recharge.

An average recharge rate can be calculated for the whole area by weighting it with respect to the surface coverage, the respective evapotranspiration rate and a reduction factor r due to paved areas and agricultural drainages. This is shown in table 4.12.

Table 4.12. Weighted recharge rate

Land Use	Area %	r [-]	Recharge rate [mm · yr ⁻¹]
Agricultural	50	1	374
Agri-drained	20	0.7	262
Urban	30	0.3	112
Weighted average			273

A model for the net precipitation has been provided by and is shown in figure 4.6. It's evident that there appears to be no relation between surface coverage and net precipitation. This is probably because coverage has not been accounted for. As such the net precipitation in the urban area is likely to be far less.

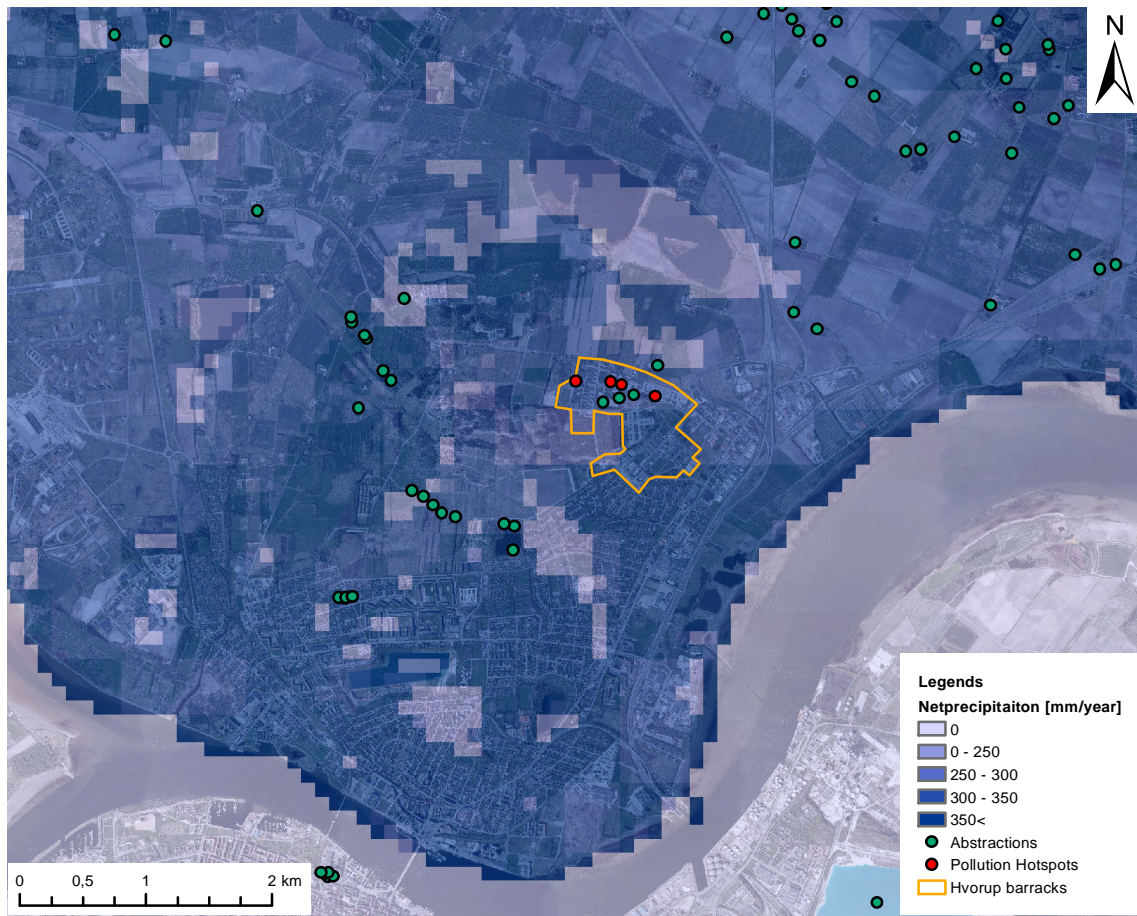


Figure 4.6. Net precipitation in the project area.

Part II

Risk to indoor climate

5. Risk to indoor climate in Hvorup barracks

The volatile compounds in the pollution in Hvorup barracks can diffuse through the soil and penetrate buildings in the area and thereby constitute a risk for indoor air quality. To assess the risk of the concentration of VOCs exceeding the limit for indoor air quality, a gas diffusion analysis is done.

The risk assessment is done for pollution at location A and C, potentially harming the indoor air quality of the canteen and the auto-shop respectively. The air phase concentration for benzene is analyzed in chapter 2.4.2 page 10. The two pollution sites and the potential targets are shown in figure 5.1 and 5.2.

The pollution at location A is close to both a heating central and canteen. It is assumed that the heating central is not a working area, so it is not subject to the limits of benzene concentration, because exposure is limited. The canteen and auto shop are, however, working areas, so an analysis is done to assess the risk of exceeding the limit of benzene concentration in these buildings.

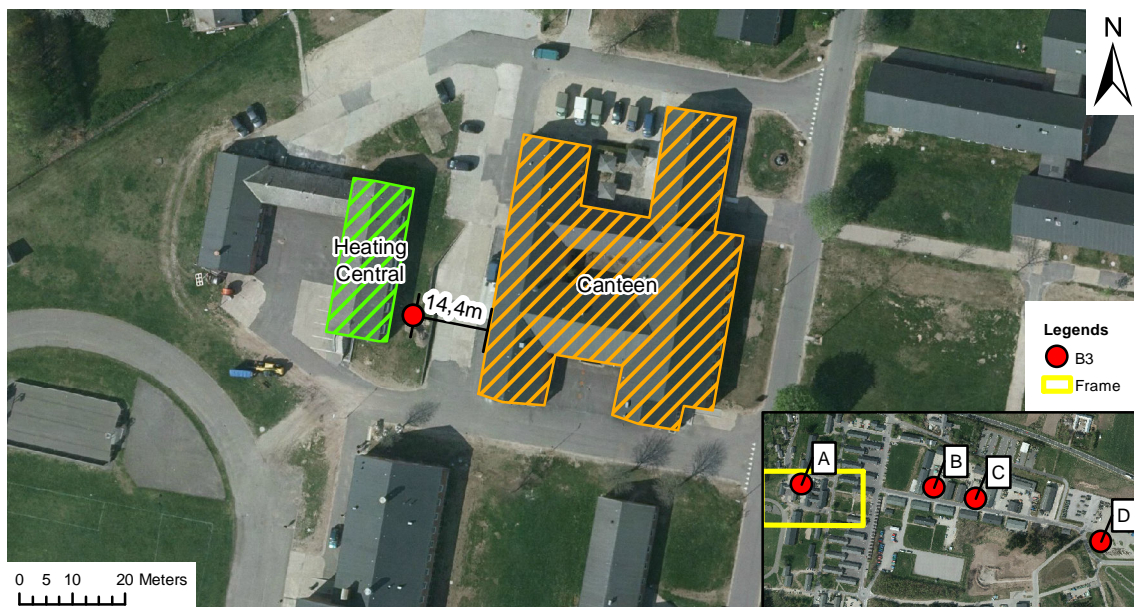


Figure 5.1. The location of pollution site A in relation to nearby buildings.



Figure 5.2. The location of pollution site C in relation to nearby buildings.

The concept model for the gas diffusion analysis is shown in figure 5.3. It shows that the free phase pollution spill diffuses through the unsaturated soil and enters the building. Through this process the chemical is subject to aerobic biodegradation.

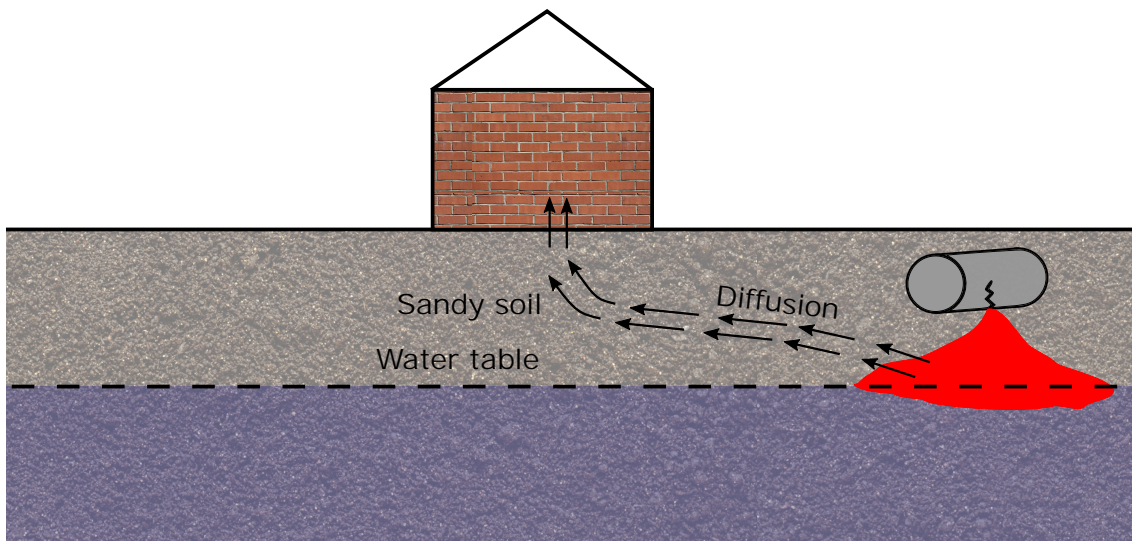


Figure 5.3. Concept model of gas diffusion.

5.1 Analytical Model

As the diffusion process is not dependent on any other vector than concentration gradients the diffusion will result in a spherical spreading centered to the pollution spill. However, as the aim of this calculation is the determination of the concentration in a fixed direction

and distance, only this dimension will be taken into account. A solution of the partial differential equation for a semi-infinite domain and constant pollutant source is given by van Genuchten and Alves:

$$C(x,t) = C_0 \cdot A(x,t) \quad (5.1)$$

with

$$\begin{aligned} A(x,t) = & \cdot \frac{1}{2} \cdot \left[\exp\left(\frac{-x \cdot \sqrt{4D_e K_e}}{2D_e}\right) \cdot \operatorname{erfc}\left(\frac{x - \sqrt{4D_e K_e} \cdot t}{\sqrt{4D_e \cdot t}}\right) \right. \\ & \left. + \exp\left(\frac{x \cdot \sqrt{4D_e K_e}}{2D_e}\right) \cdot \operatorname{erfc}\left(\frac{x + \sqrt{4D_e K_e} \cdot t}{\sqrt{4D_e \cdot t}}\right) \right] \end{aligned} \quad (5.2)$$

Where

C_0	Initial concentration [$\text{mg} \cdot \text{L}^{-1}$]
D_e	Effective diffusion coefficient [$\text{m}^2 \cdot \text{s}^{-1}$]
K_e	Effective 1st order biodegradation rate [d^{-1}]
x	Distance to initial concentration [m]
t	Time [s]

The gas diffusion process will only take place in the air phase of the vadose zone of the upper sand layer, affected by the first order aerobic biodegradation model as presented in 4.7.

As the diffusion of benzene through the porous medium is subject to retardation, the effective diffusion coefficient D , estimated in chapter 4.5 page 22 will be adjusted according to:

$$D_e = \frac{D}{R_a} \quad (5.3)$$

The retardation slows the diffusion process down, as well as it decreases the effective degradation process. The effective biodegradation rate K_e will be introduced:

$$K_e = \frac{K_1}{R_a} \quad (5.4)$$

Penetration into the building

The presence of a building induces a pressure difference in the soil, resulting in a convective flow from the soil into the building. This pressure difference may be caused by different processes:

- Heating, leading to a temperature gradient, resulting in a pressure difference
- Ventilation, leading to a direct pressure difference between the interior of the building and the subsurface.

Once such a pressure gradient is established, minor cracks, wiring looms, etc., in the foundation of the building are the entrance points for the gaseous phase. Assuming that 10% of the accumulated benzene below the foundation enter the building, the maximum concentration of benzene inside the buildings can be calculated by knowing the maximum concentration below the building.

5.2 Input parameters

As it is shown in figures 5.1 and 5.2, the surface above the potential diffusion zone is almost completely sealed. It is assumed a negative soil matrix potential of $pF = 3$ for the sealed soil volume between the contaminant source and the investigated buildings.

The 1st order degradation rate is from the experiments of biodegradation in soil in Hvorup barracks described in chapter 4.7 page 26. The mean of all the samples where no nutrition was added nor any autoclaving is used.

The model input parameters can be calculated and are shown in table 5.1.

Table 5.1. Input parameters

Soil matrix potential, pF	3
Water content [$\text{cm}^3 \cdot \text{cm}^{-3}$]	0.11
Air content [$\text{cm}^3 \cdot \text{cm}^{-3}$]	0.33
Air phase tortuosity [-]	0.41
Diffusion coefficient in air [$\text{m}^2 \cdot \text{d}^{-1}$]	0.049
Effective diffusion coefficient [$\text{m}^2 \cdot \text{d}^{-1}$]	0.0037
Retardation in air [-]	12.8
1st order biodegradation rate [d^{-1}]	0.121
Effective 1st order biodegradation rate [d^{-1}]	$5.28 \cdot 10^{-4}$

The distance between pollution site to the two buildings as well as initial concentration are shown in table 5.2. The initial concentrations of benzene are assessed in chapter 2.4.2 page 10.

Table 5.2. Site distance and initial concentration

	Site A, canteen	Site C, auto-shop
Distance [m]	14.4	17.6
Concentration [$\text{mg} \cdot \text{L}^{-1}$]	0.55	33.5

5.3 Results

The breakthrough curve of benzene inside the two buildings are shown in figure 5.4.

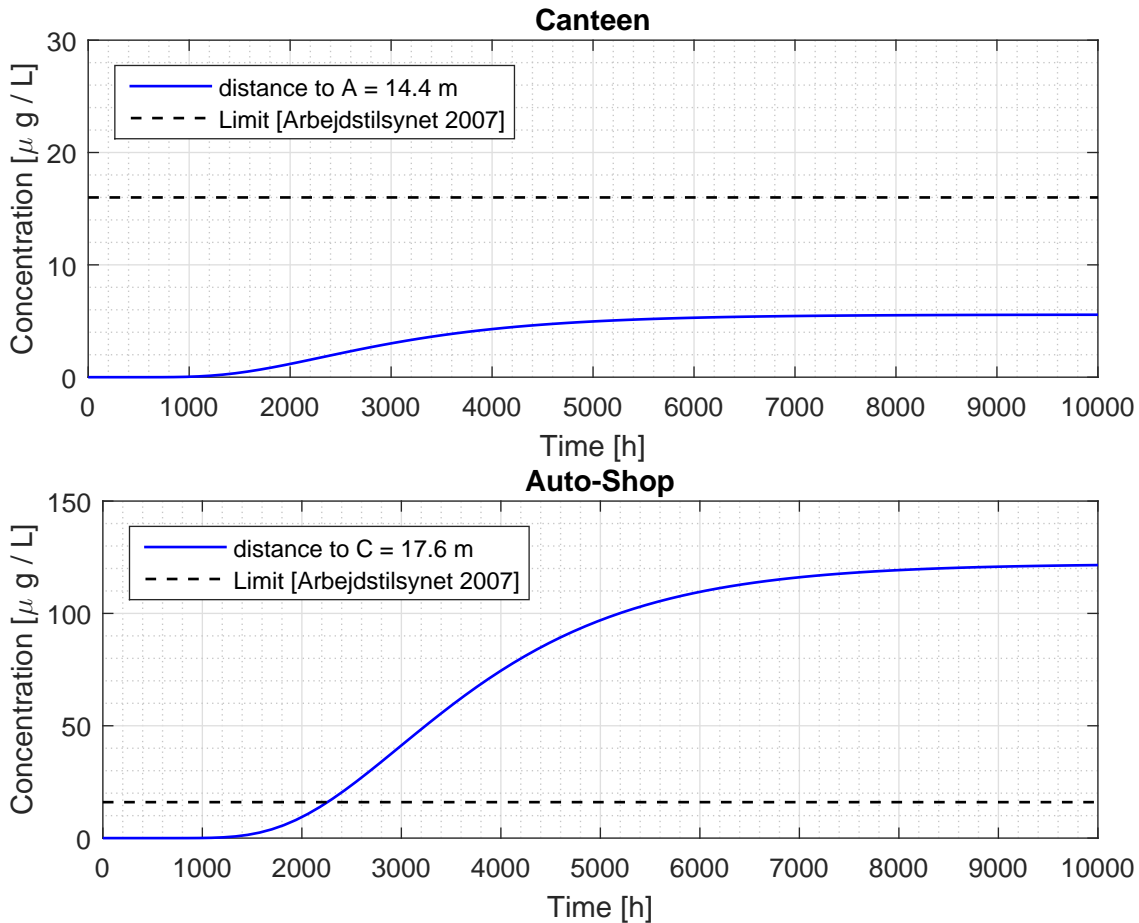


Figure 5.4. Breakthrough curves for benzene in the two buildings

The concentration below the buildings reaches its maximum after about 500 and 550 days for the Canteen and the Auto-Shop respectively. This is indicated by the shape and position of the diffusion curve (figure 5.4) not changing anymore with time.

Table 5.3 shows the largest concentration reached in the two buildings as well as the limit.

Table 5.3. Concentrations under and in the investigated locations and the official limit for indoor air concentration, the reported values are maximum values.

Location	C_0 [$\mu\text{g} \cdot \text{L}^{-1}$]	C_{under} [$\mu\text{g} \cdot \text{L}^{-1}$]	C_{inside} [$\mu\text{g} \cdot \text{L}^{-1}$]	C_{limit} [$\mu\text{g} \cdot \text{L}^{-1}$]
Canteen	550	5.57	0.557	1.60
Auto-shop	33 450	122	12.2	1.60

The reported concentrations are not corrected regarding ventilation of the buildings, nor other activities, that possibly could decrease or increase the indoor concentration of benzene. Arbejdstilsynet [2007] reports a maximum allowable value of $1.60 \mu\text{g} \cdot \text{L}^{-1}$,

which is almost 8 times lower than the calculated inflow concentration for the auto-shop. However, the concentration calculated is the benzene content of the convective-diffusive flux through the foundation, not the actual indoor benzene concentration. The value calculated only indicates, that there is a major risk of trespassing the threshold value of maximum allowable indoor benzene concentration, if the only air exchange of the building with the environment would be through the foundation of the building. The indoor concentration for the canteen is not trespassed by this calculation method.

5.4 Stochastic model

As all the parameters involved in the calculation of the maximum benzene concentration are subject to uncertainty, the variation of the output due to this uncertainty is investigated.

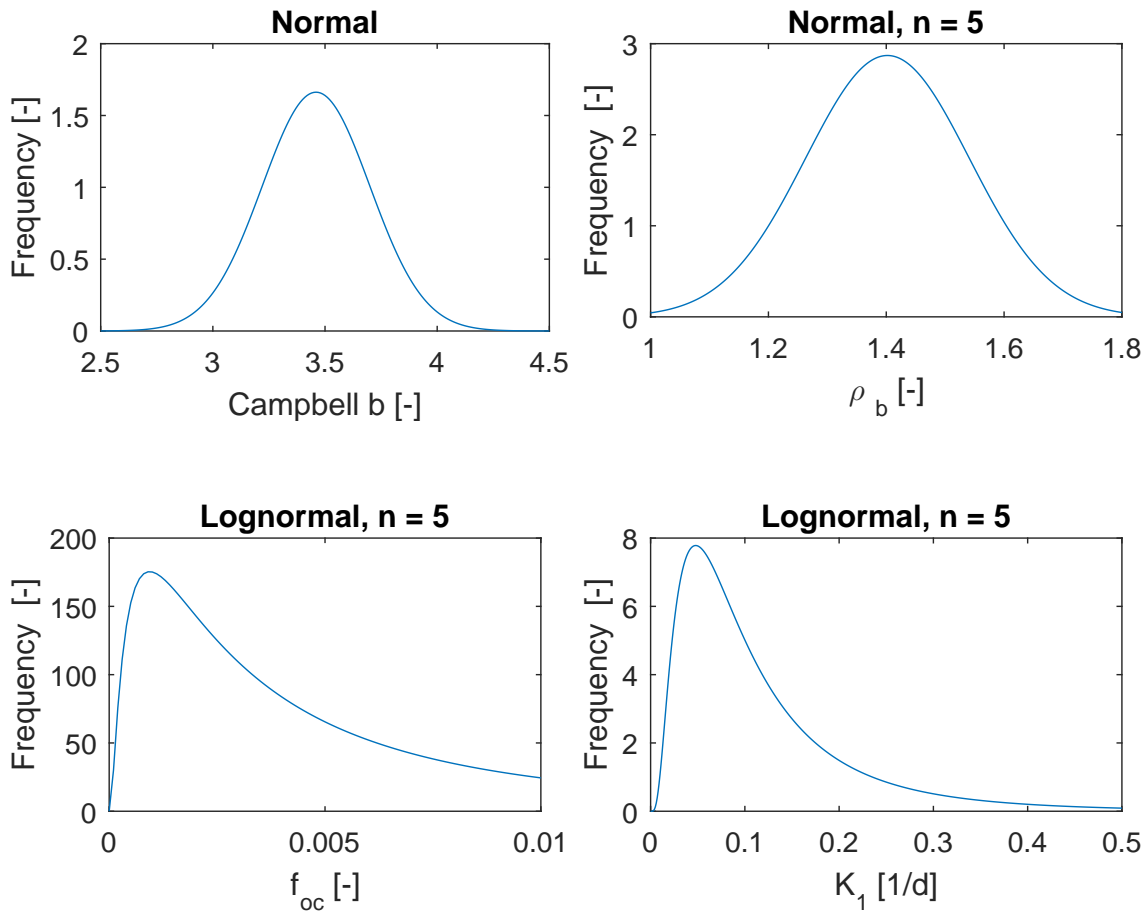
Table 5.4. Distribution types

Campbell parameter b for sand	Normal distribution as determined by the bootstrapped regression analysis
Bulk density ρ_b for sand	Normal distribution, with mean and standard deviation from the Tylstrup sandy soil Hansen [1976]
Organic carbon content f_{oc} for sand	Log-normal distribution with mean and standard deviation from Hansen [1976]
First order biodegradation rate, aerobic conditions	Log-normal distribution from data obtained in chapter 4.7. Mean and standard deviation from all the aerobic condition measurements adjusted according to the temperature
Suction potential ψ	Uniform distribution, lower and upper limits are the assumed potentials occurring in the soil

The most relevant factor to the gas diffusion is most likely the water respectively air content of the porous medium. In order to account for the large range of possibly occurring air contents, the variation of the pF will be set in a second step to vary from $pF = 3$ down to a suction of $pF = 2$. A higher suction than $pF = 3$ is not likely to occur, because the surface is sealed and only very limited evaporation and almost no transpiration is expected. The used distributions are shown in table 5.4

Table 5.5. Parameters of the distributions used in the simulation

	μ	Range [min,max]	σ	CV σ/μ	Distribution
b	3.56	[2.92, 4.43]	1.05	0.29	normal
ρ_b	1.40	[1.10, 2.04]	0.14	0.10	normal
f_{oc}	0.0079	[0.0014,0.15]	0.0014	0.18	log-normal
K_1	0.121	[0.009, 0.23]	0.11	0.92	log-normal
ψ		[-1000, -100]			uniform

**Figure 5.5.** Distributions of the input parameters

The empirical distributions for the maximum concentration are based on a Monte-Carlo simulation with $m = 1000$ randomly generated samples, $n = 1000$ iterations with a fixed matrix suction at $pF = 3$ and fixed time at $t = 2\text{yr}$. The distributions in the buildings are shown in figure 5.6. The visual analysis of the empirical distribution function plots of the estimated mean relative concentrations below the buildings suggests that the results follow a log-normal distribution. The *Lilliefors test* confirms the suggestion.

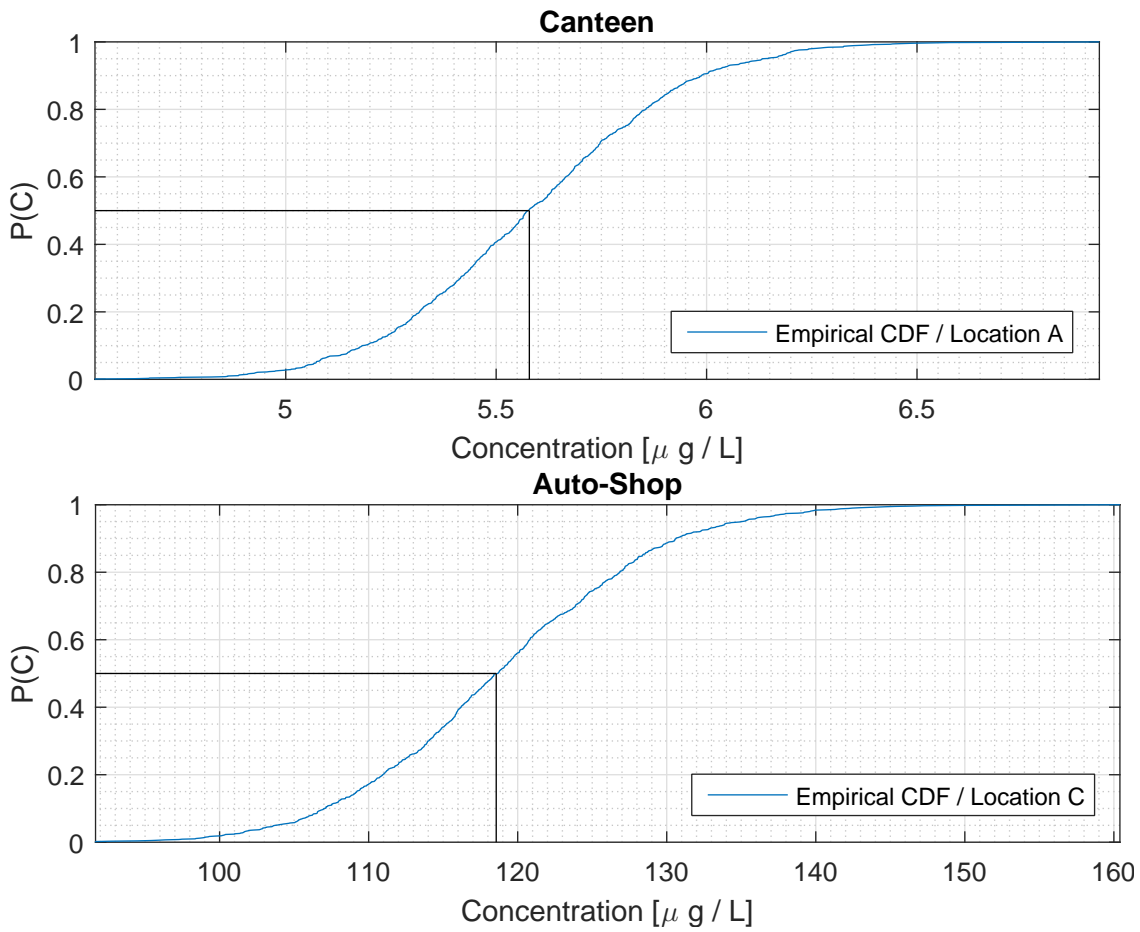


Figure 5.6. Empirical and fitted theoretical distribution functions of the maximum concentration below the buildings. The lines indicate the estimated mean. (Fixed pF).

The stochastic analysis of the evolution below the buildings, at a fixed time big enough to ensure that the maximum achievable concentration has been reached, yields the mean values and a range for the two investigated locations, as shown in table 5.7.

Table 5.6. Means, standard deviations and ranges for the concentrations under the buildings for a fixed negative potential of $pF = 3$.

Location	C mean	C stdev	[min C , max C]
Canteen	5.59	0.104	[4.55, 6.94]
Auto-shop	119.88	89.95	[91.72, 160.47]

The very high standard deviation of the concentration under the Auto-Shop indicates a high spread and/or outliers in the data due to the sensitivity of the model to variations in the input, especially to the biodegradation rate.

The figures 5.8 show the influence of varying water respectively air content to the main

model coefficients. The left figure of figure 5.7 is basically the Campbell retention curve, drawn for the air content, the second one shows the variation of the tortuosity

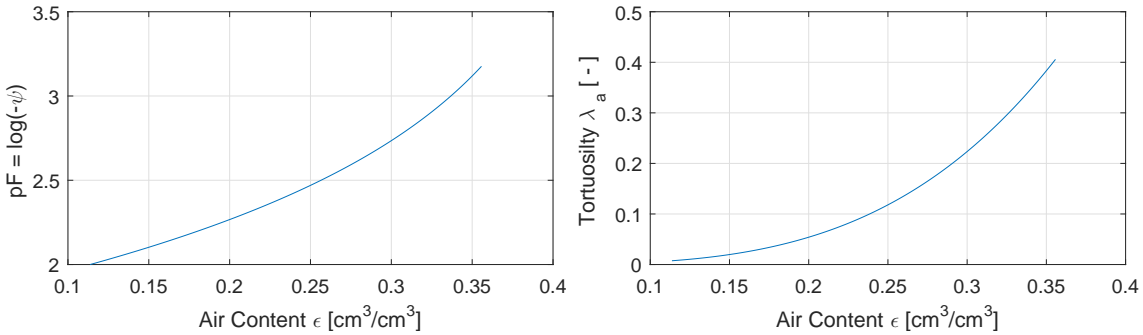


Figure 5.7. Influence of variation of the suction potential to the air content and the tortuosity.

Including the uniform distribution of the suction potential varying between $pF = 3$ and $pF = 2$, the concentration under the buildings will drop, because of the decreasing air, and thus free diffusion path.

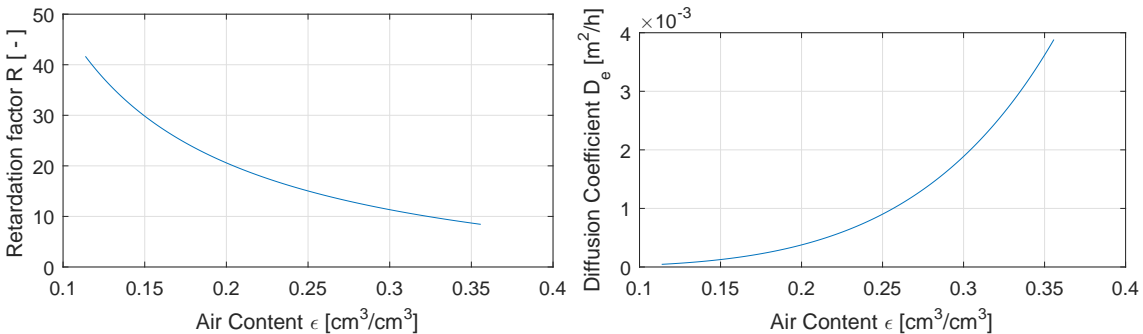


Figure 5.8. Influence of the variation of the suction potential to the retardation and the diffusion coefficient.

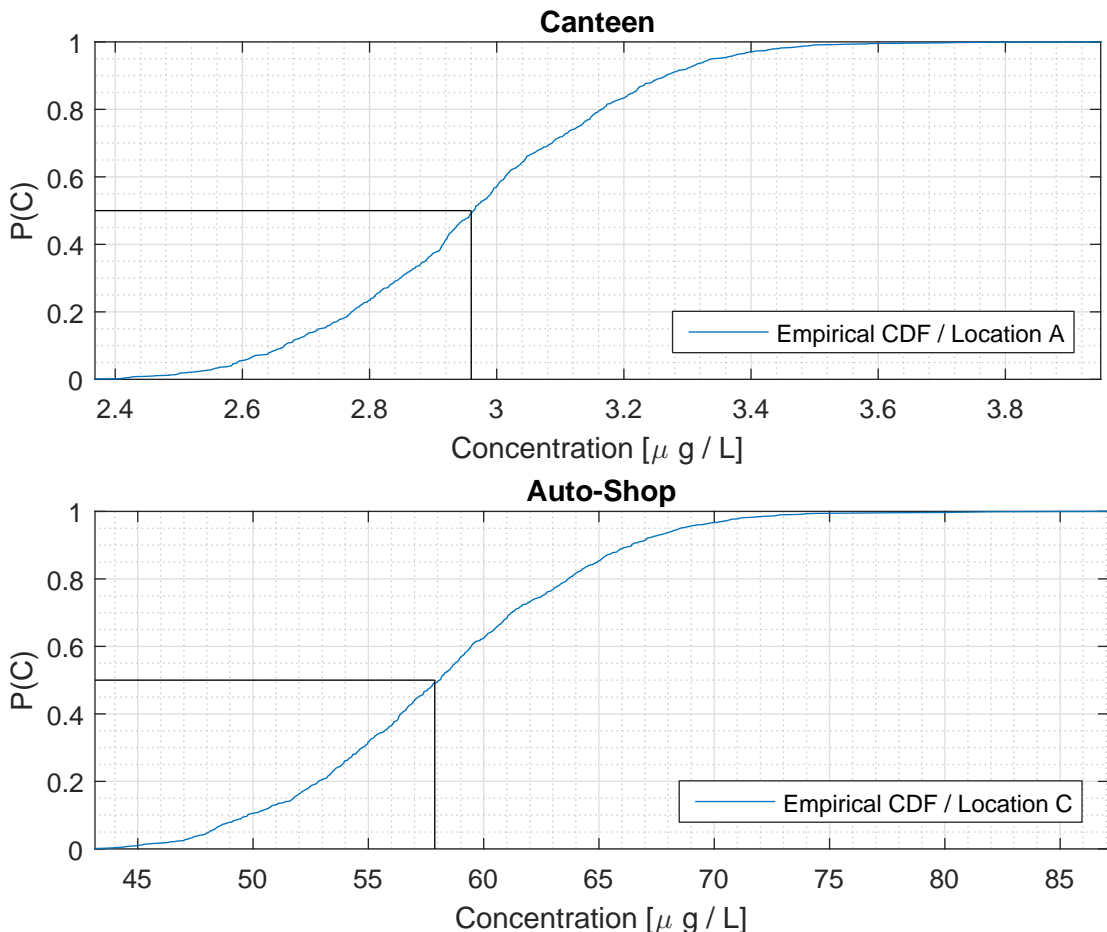


Figure 5.9. Empirical and fitted theoretical distribution functions of the maximum concentration below the buildings. The lines indicate the estimated mean. (uniform distributed pF).

Table 5.7. Means, standard deviations and ranges for the concentrations under the buildings for a uniform distributed pF .

Location	C mean	C stdev	[min C , max C]
Canteen	2.97	0.053	[2.37, 3.95]
Auto-shop	58.22	40.15	[43.15, 87.10]

Figure 5.10 show the results of the Monte-Carlo simulations for the breakthrough curves for benzene below the Canteen and the Auto-Shop respectively. The graph clearly shows the uncertainty in the concentration evolution below the buildings.

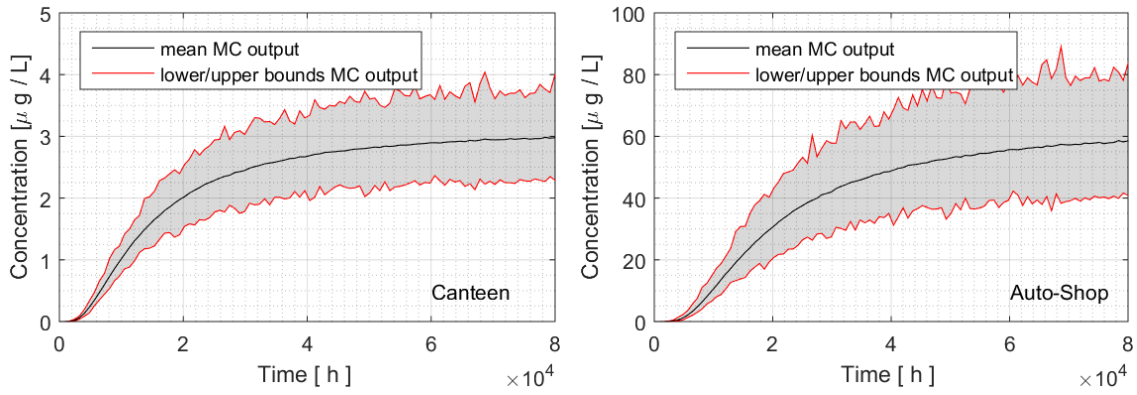


Figure 5.10. Visualization of the Monte-Carlo breakthrough result.

5.5 Parameter sensitivity

The diffusion process depends on many different parameters. The influence of the parameters is shown in figure 5.11. The temperature is changed by 1.5 and 15°C respectively.

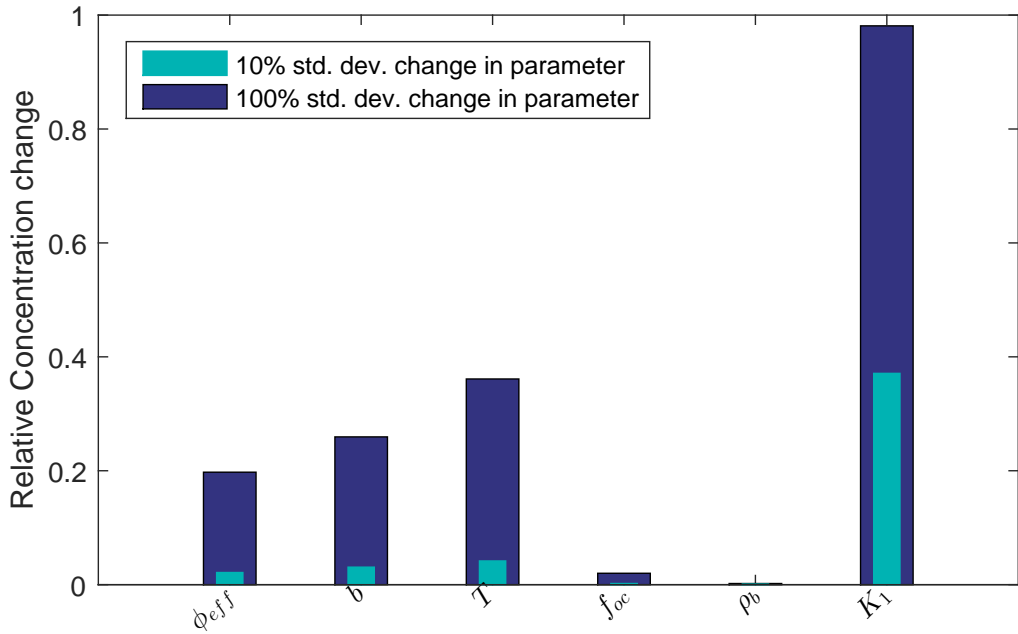


Figure 5.11. Bar diagram showing the model sensitivity to different parameters. The temperature change amounts to 1.5 and 15°C respectively.

In this model, the temperature is no part of the stochastic simulation, but has an quite large effect on the model output by influencing the diffusion coefficient. The largest effect is however due to the change in the biodegradation rate. It needs to be mentioned that there are several parameters not independent from each other. As the saturated water

content is assumed to be equal to the total porosity, it is related to the parameter b via the Campbell model (equation 4.2) and via the equation (4.3) to the bulk density.

5.6 Discussion

Table 5.8. Summary table of the calculated concentrations inside the investigated buildings. C_{inside} are the calculated mean values, $[C_{min} - C_{max}]$ are the respective ranges, C_{limit} is the limit value for indoor air concentrations

Site	C_{inside} [$\mu\text{g} \cdot \text{L}^{-1}$]	$[C_{min} - C_{max}]$ [$\mu\text{g} \cdot \text{L}^{-1}$]	C_{limit} [$\mu\text{g} \cdot \text{L}^{-1}$]
Basic Model			
Canteen	0.557		1.60
Auto-Shop	12.20		1.60
Stochastic Model ($pF = 3$)			
Canteen	0.559	[0.455, 0.694]	1.60
Auto-Shop	11.988	[9.172, 16.047]	1.60
Stochastic Model ($pF \in [2,3]$)			
Canteen	0.297	[0.237, 0.395]	1.60
Auto-Shop	5.822	[4.315, 8.710]	1.60

The differences between the stochastic model and simple model are because a minor change in the parameters, especially the biodegradation rate K_1 , b and the air content (suction potential) have a major effect on the outcome. In order to reduce this uncertainty, especially the input parameters with the biggest influence on the output, K_1 , b and ϕ have to be investigated further.

The water content in the subsurface depends on the recharge, thus on the precipitation and the surface coverage. The soil temperature depends on the surface air temperature. This meteorological variability should be part of the model in a more detailed form, because the parameters depending on them have a large effect on the propagation and concentration of the contaminant.

The estimated dilution factor of 10 between the subsurface and the interior of the buildings is also uncertain, because the actual state of the foundation is not known, as well as the pressure difference between the indoor and subsurface, inducing the presumed convective flux.

Finally, with the presented models, the concentration of benzene inside the buildings will pose a risk to human health only in the Auto-Shop. This is in fact only due to the very high concentration of benzene at the pollution source. According to the model and assuming equal soil conditions between the pollution sources and the buildings, the benzene concentration would not surpass the indoor limit if the concentration at the pollution source would be lower.

Part III

Risk to regional drinking water resource

6. Risk to regional drinking water resource

Analytical model

As pollution has been detected in Hvorup barracks, the risk the pollution poses to the abstractions of the municipality is assessed. The goal of this chapter is to determine the concentration of the pollutant benzene by an analytical model. Chapter 7 approaches the same problem by a numerical approach.

The pollutant is subject to a 3 dimensional transport through layered soil, however this model is simplified into two separate transports processes. The transport model accounts for the two major means of transport in the saturated zone, which are advection and dispersion, as well as the degradation of the pollutant due to biodegradation.

The pollution at location C was gauged to be about $22 \text{ mg} \cdot \text{L}^{-1}$ of benzene in groundwater. As this is considered the highest concentration of benzene in Hvorup barracks, this will be the starting point of the transport model.

The concept model for the risk assessment to the regional drinking water resource is shown in figure 6.1. Two aquifers, separated by a clay layer, reside under Hvorup barracks. A vertical transport estimates the travel time and the biodegradation through the clay lens, a horizontal model assesses the travel time and biodegradation through the fractured limestone to the relocated Lindholm well field as well as to the Nørre Uttrup well field.

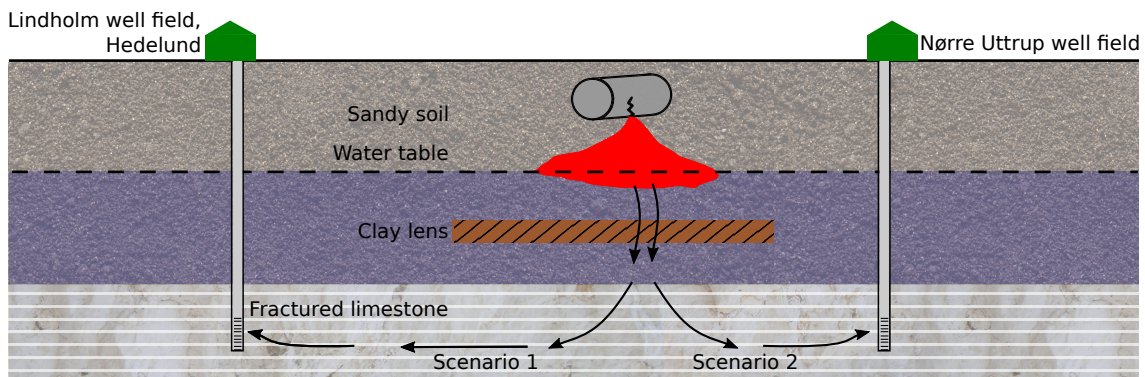


Figure 6.1. Concept model for the risk assessment to the regional drinking water resource.

6.1 Vertical transport

The vertical transport model describes the vertical propagation of the contaminant, assumed to reside near the groundwater table, to the limestone aquifer. It is thus

exclusively a saturated transport model. A low-permeable clay lens is situated in between the pollution source and the limestone aquifer. Because of the low hydraulic conductivity of the clay layer, the transport through this layer is probably the most influencing factor in the vertical transport. The transport through the vadose zone is disregarded.

The concept model for the vertical transport is shown in figure 6.2. It is assumed that the contaminant penetrates an intact clay lens with no major cracks or fractures in it.

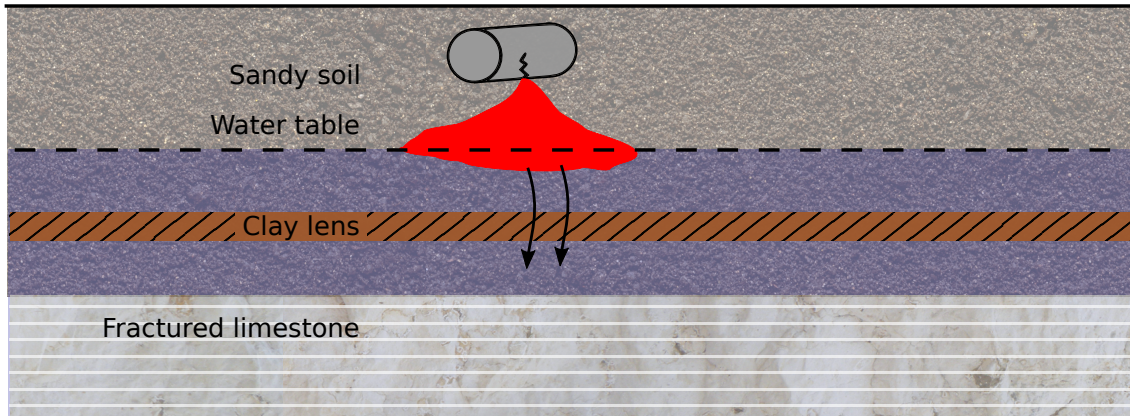


Figure 6.2. Concept model for the vertical transport.

6.1.1 Analytical method

The transport time for the vertical transport is calculated by the following equation, dispersion being disregarded:

$$t = \frac{L_{clay}}{u_{benzene}} \quad (6.1)$$

Where

t	Travel time through clay lens [year]
L_{clay}	Thickness of clay lens [m]
$u_{benzene}$	Velocity of benzene [$\text{m} \cdot \text{year}^{-1}$]

The transport of benzene is assumed to result only from advection. When taking into account retardation as well as effective porosity, the velocity of the chemical is:

$$u_{benzene} = \frac{V_{water}}{\phi_{eff} \cdot R} \quad (6.2)$$

Where

V_{water}	Darcy velocity [$\text{m} \cdot \text{year}^{-1}$]
ϕ_{eff}	Effective porosity [$\text{cm}^3 \cdot \text{cm}^{-3}$]
R	Retardation [-]

The Darcy velocity in the clay lens can be calculated with Darcy's equation:

$$V_{water} = K_{sat} \cdot \frac{\Delta h}{L_{clay}} \quad (6.3)$$

Where

K_{sat}	Vertical saturated hydraulic conductivity of clay [$\text{m} \cdot \text{s}^{-1}$]
Δh	Pressure difference above and below clay lens [$\text{cm H}_2\text{O}$]

The concentration in the limestone aquifer can be calculated by accounting for biodegradation, it is:

$$\begin{aligned} C &= C_0 \cdot \exp(-K_1 \cdot t) && \text{1st order degradation} \\ \text{or} \\ C &= C_0 - K_0 \cdot t && \text{0th order degradation} \end{aligned} \quad (6.4)$$

Where

C	Concentration in limestone [$\text{mg} \cdot \text{L}^{-1}$]
C_0	Initial concentration [$\text{mg} \cdot \text{L}^{-1}$]
K_1	First order degradation rate [d^{-1}]
K_0	Zero order degradation rate [$\text{mg} \cdot \text{L}^{-1}$]

6.1.2 Input parameters

The nearest drilling that is evaluated to effectively delineate the clay layer in thickness is drilling 26.5360, where the soil type was identified at every 1 m. The thickness of the clay layer here is about 3 m. The location of the drilling is shown in figure 6.3 and it is about 600 m away from the pollution site.

The pressure difference over the clay layer is assumed to be the pressure difference between the upper and lower aquifer. The closest drilling where measurements of hydraulic head for both aquifers above and below the clay lens are available, is drilling 26.3999. The difference in hydraulic head is about 10 cm. However at this location the thickness of the clay lens is only 50 cm, and is thus evaluated as not representative for Hvorup barracks.

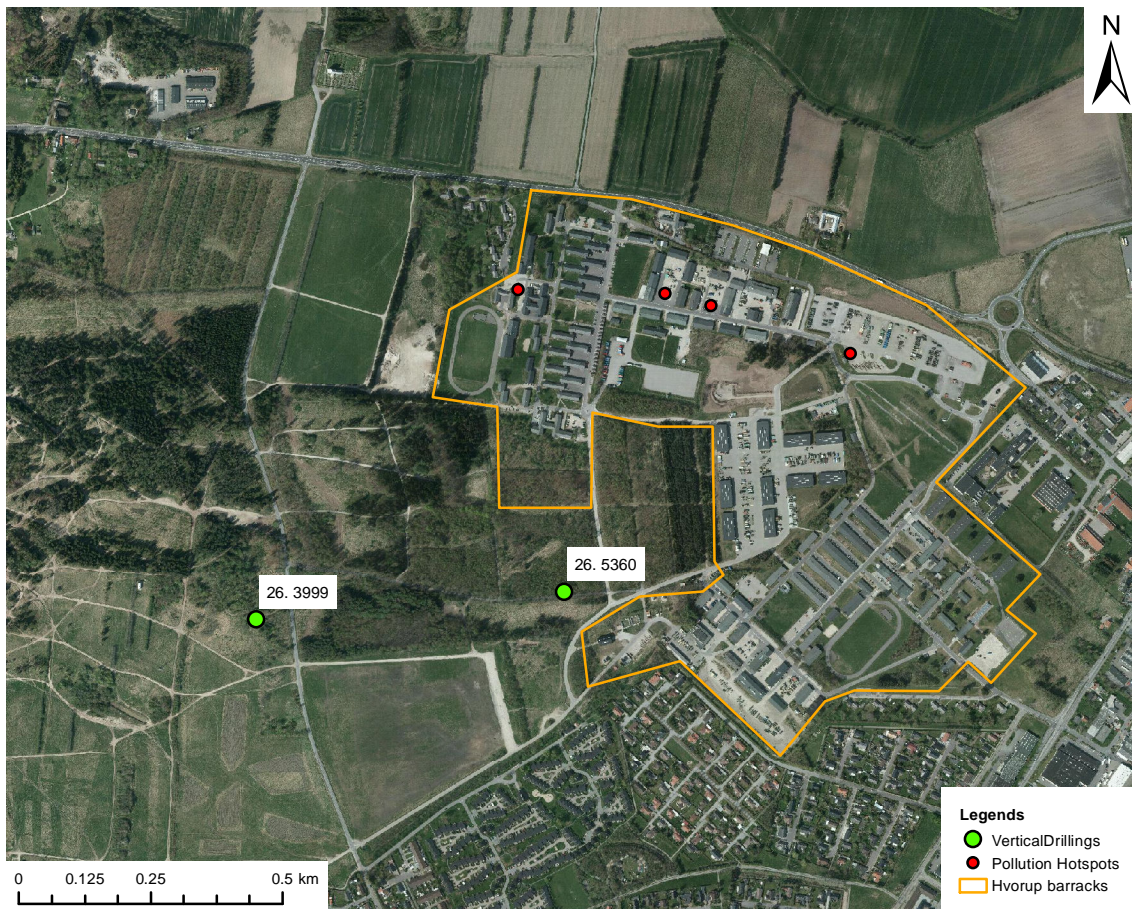


Figure 6.3. Drillings used for clay thickness and difference in hydraulic head.

Head measurements done during field trips the 10th of September and the 29th of October 2013 show a water table at pollution site C in the upper aquifer of about 7 - 7.5 m [Brigitte et al., 2013]. A potential map of the lower aquifer has been created by NIRAS, shown in figure 6.4. The difference in hydraulic head between the two aquifers can be estimated to be roughly between 2.5 - 3 m. This is thus assumed to be the pressure difference over the clay layer.

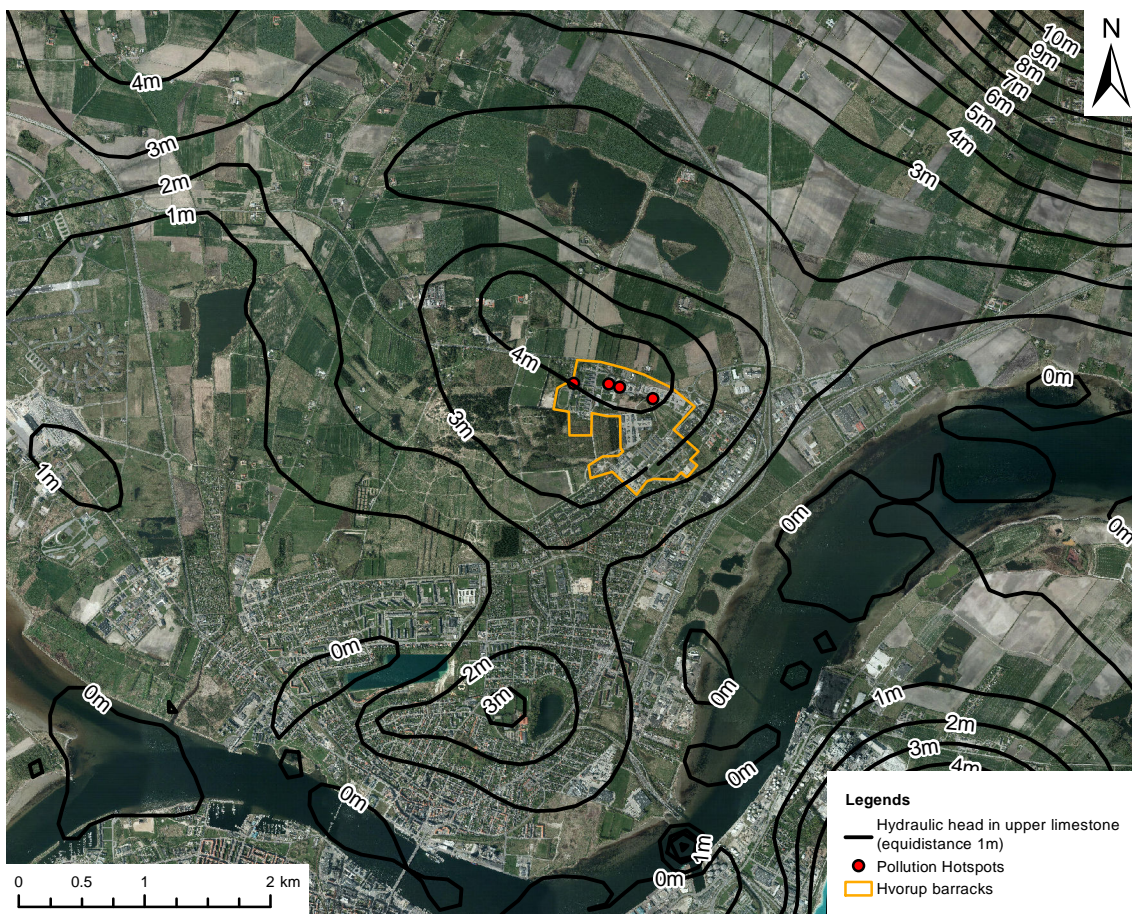


Figure 6.4. Potential map of lower aquifer [Niras, n.d.]

No measurements of the vertical saturated hydraulic conductivity of clay have been found. The mean of the limits described in appendix A.1 page 105 is used, which is $2.17 \cdot 10^{-9} \text{ m} \cdot \text{s}^{-1}$ for horizontal saturated hydraulic conductivity. Assuming a vertical anisotropy for clay of 3, the vertical conductivity will be $7.23 \cdot 10^{-10} \text{ m} \cdot \text{s}^{-1}$. The effective porosity of a clayey soil from Roskilde is presented in chapter 4.6.2 page 24, and is about 7 %.

The sorption coefficient for clay is calculated in chapter 4.6.2 page 24 and is about $0.132 \text{ L} \cdot \text{kg}^{-1}$. Neglecting hysteresis and assuming full saturation, the water content is equal to the total porosity. Both bulk density and total porosity are presented in chapter 4.6.2 page 24, and the retardation factor can be calculated by equation 4.11 page 24.

The initial concentration was assessed to be about $22 \text{ mg} \cdot \text{L}^{-1}$. The biodegradation rates in Hvorup barracks have been estimated in chapter 4.7 page 26. The biodegradation rate in the clay layer is assumed to be the average in situ biodegradation rate from the groundwater samples without autoclaving nor nutrition addition.

The entire table of parameters used is shown in table 6.1

Table 6.1. Parameters used for vertical transport through the clay lens

Thickness of clay lens	3 m
Pressure difference	2.75 m
Anisotropy factor	3
Vertical hydraulic conductivity	$7.23 \cdot 10^{-10} \text{ m} \cdot \text{s}^{-1}$
Effective porosity	7 %
Sorption coefficient of clay	$0.132 \text{ L} \cdot \text{kg}^{-1}$
Bulk density of clay	$1.53 \text{ g} \cdot \text{cm}^{-3}$
Water content / total porosity of clay	0.45
Retardation of benzene	1.45
Initial concentration	$22 \text{ mg} \cdot \text{L}^{-1}$
1st order degradation rate	$5.00 \cdot 10^{-4} \text{ d}^{-1}$
0th order degradation rate	$2.26 \cdot 10^{-2} \text{ } \mu\text{g} \cdot \text{L}^{-1}$

6.1.3 Results

The travel time can be estimated, and the results are shown in table 6.2.

Table 6.2. Travel time for benzene through the clay lens

Darcy velocity	$0.02 \text{ m} \cdot \text{yr}^{-1}$
Chemical velocity	$0.21 \text{ m} \cdot \text{yr}^{-1}$
Travel time	14.6 yr

By accounting for either 1st order or 0th order biodegradation, the concentration in the fractured limestone below pollution site C is shown in 6.3.

Table 6.3. Concentration in limestone, accounting for biodegradation

	1st order	0th order
Concentration in limestone	$1.54 \text{ mg} \cdot \text{L}^{-1}$	$21.7 \text{ mg} \cdot \text{L}^{-1}$

It's evident that, by assuming no increase in the biodegradation rate with increasing contaminant concentration, the biodegradation in the clay sediment is almost negligible. However it was concluded, in the analysis of biodegradation, that the groundwater samples primarily followed a 1st order biodegradation. It was thus evaluated, that the maximum degradation rate was not reached in the microcosms.

It is thus evident from table 6.3 that the concentration of benzene is reduced from $22 \text{ mg} \cdot \text{L}^{-1}$ to $1.54 \text{ mg} \cdot \text{L}^{-1}$ through the clay lens.

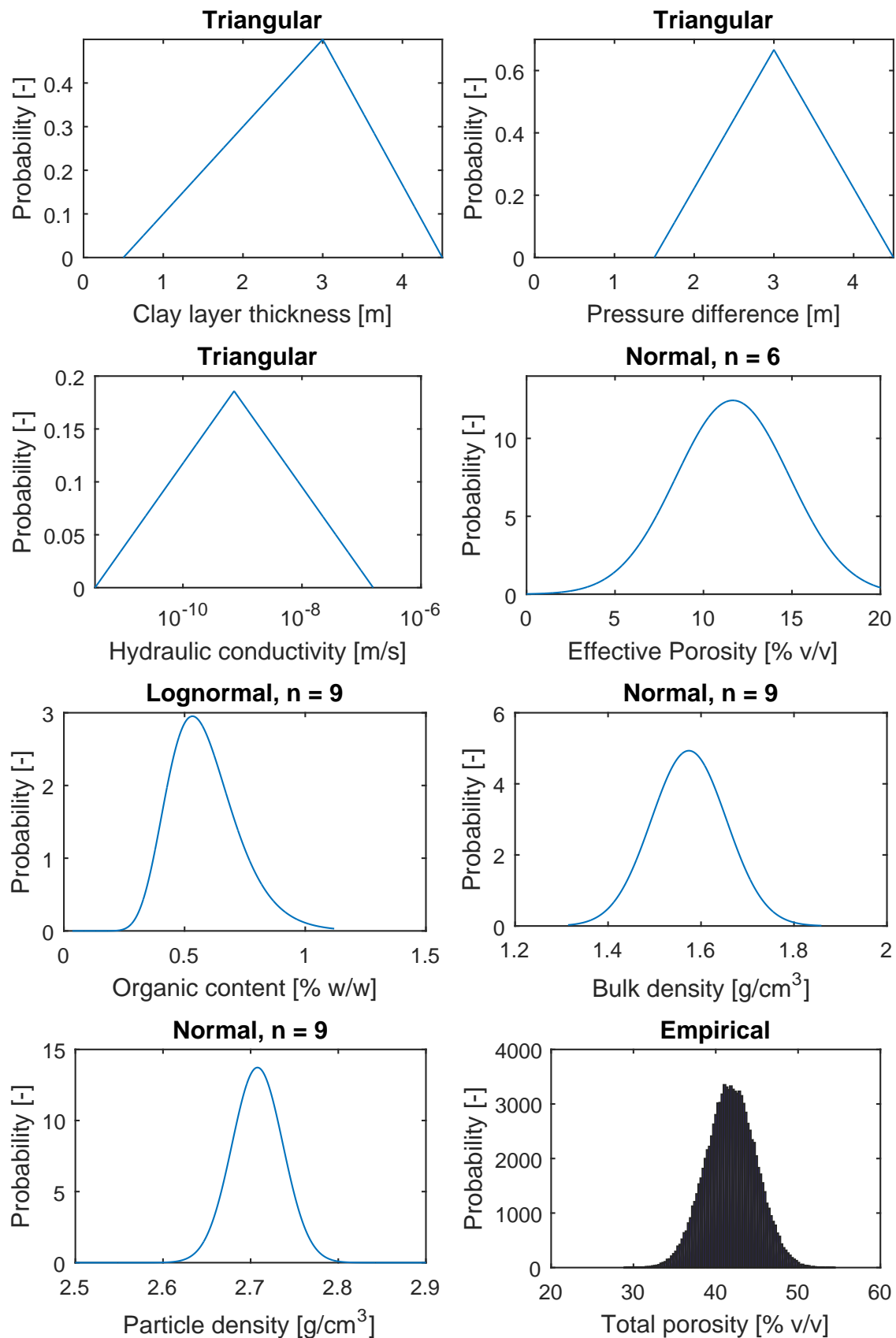
6.1.4 Stochastic model on vertical transport

A stochastic analysis is done on this model, where the uncertainties regarding the parameters are taken into account. The inputs used in getting the distributions are shown in table 6.4.

Table 6.4. Distribution types

Clay layer thickness	Triangular distribution with 0.5 m and 4.5 m as limits
Pressure difference over clay	Triangular distribution. Season variation is likely to be 1 m. Measurements for head in pollution site C were in the range 7-7.5 m. Thus the limits for the distribution are ± 1.5 m.
Vertical hydraulic conductivity of clay	Log triangular distribution with limits from Spitz and Morene [1996] for horizontal hydraulic conductivity and assuming vertical anisotropy of 3
Effective porosity of clay	Normal distribution with values of standard deviation and mean from all clay soils from Hansen [1976]
Organic content of clay	Normal distribution with values of standard deviation and mean from all clay soils from Hansen [1976]
Bulk density of clay	Normal distribution with values of standard deviation and mean from all clay soils from Hansen [1976]
Particle density of clay	Normal distribution with values of standard deviation and mean from all clay soils from Hansen [1976]
Total porosity / water content of clay	Empirical distribution calculated from bulk density of clay and particle density of clay from Hansen [1976]
Retardation of benzene in clay	Empirical distribution calculated from bulk density, organic content and total water content of clay from Hansen [1976]
1st and 0th order biodegradation rate	Lognormal distribution with values of standard deviation and mean from all groundwater samples adjusted for anaerobic, nutrient limited conditions in chapter 4.7 page 26 where no autoclaving occurred nor nutrients added

The distributions are shown in 6.5. The n value above the graphs denote the amount of measurements used to calculate mean and standard deviation. The empirical distribution for retardation is calculated based on the distributions for the three parameters, that are used to calculate it.



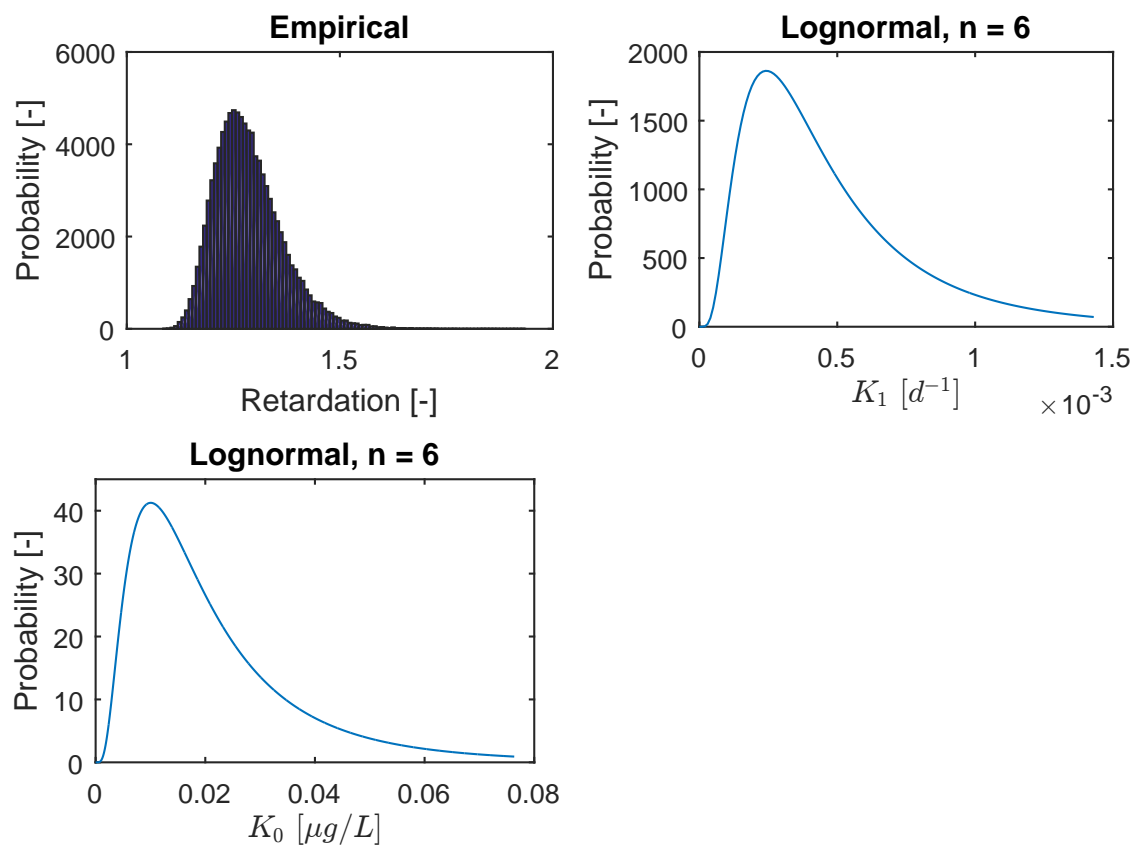


Figure 6.5. Distribution of the parameters

The travel time is then calculated with 1000 Monte Carlo simulations. The cumulative distribution for the travel time is seen in figure 6.6.

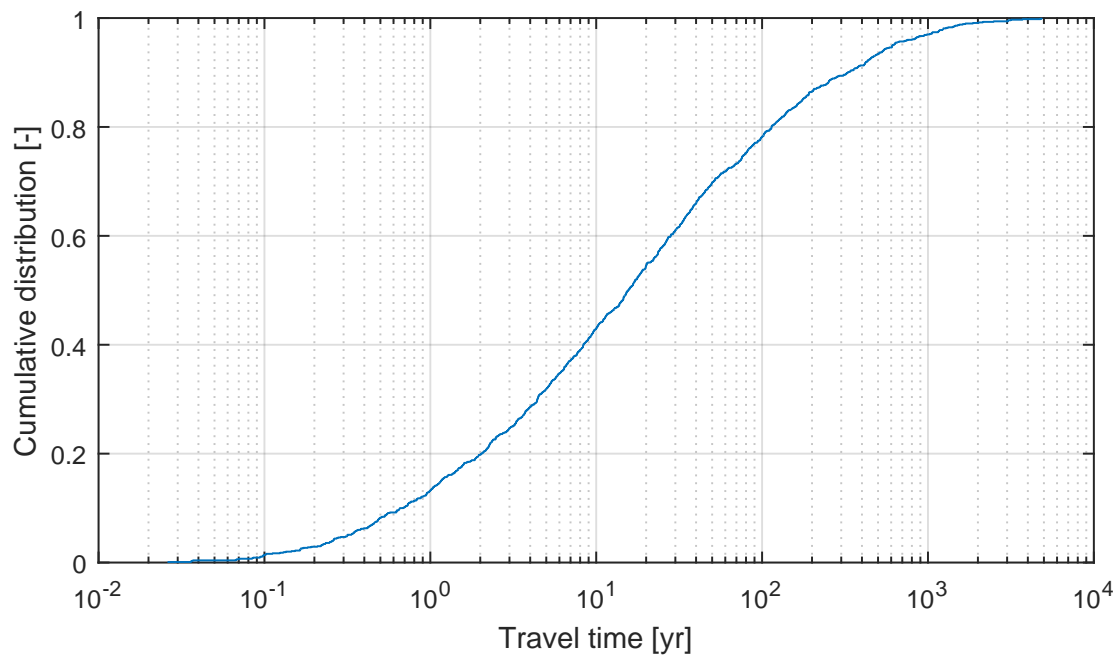


Figure 6.6. Cumulative distribution of travel time.

The concentration is calculated and its distribution for concentration in limestone is shown in 6.7.

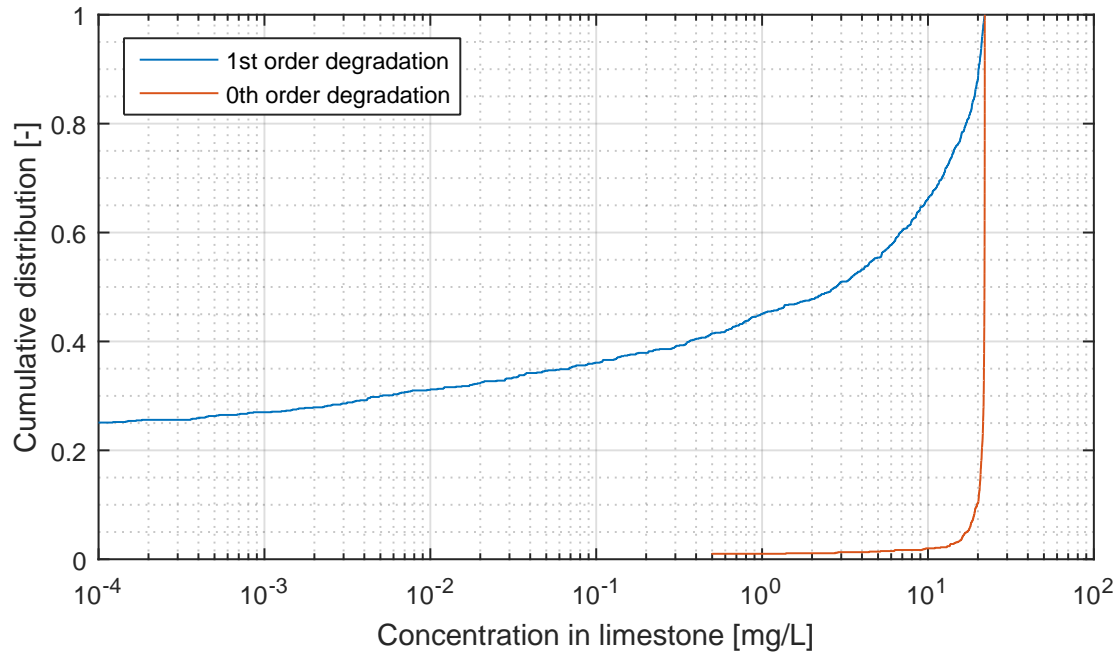


Figure 6.7. Concentration of benzene in limestone.

6.2 Horizontal transport

The horizontal transport from pollution site to the water abstractions is analyzed. The horizontal transport is assumed to occur only inside the limestone layer. The transport is calculated, using an analytical solution for advection, dispersion, retardation and biodegradation.

As it is uncertain at this point in which direction the pollution will flow in the limestone, two different scenarios are investigated. In scenario 1, it is assumed that the direction of flow is towards the relocated Lindholm well field. In scenario 2 it is assumed that the direction of flow is towards the Nørre Uttrup well field. The two scenarios are shown in figure 6.8.

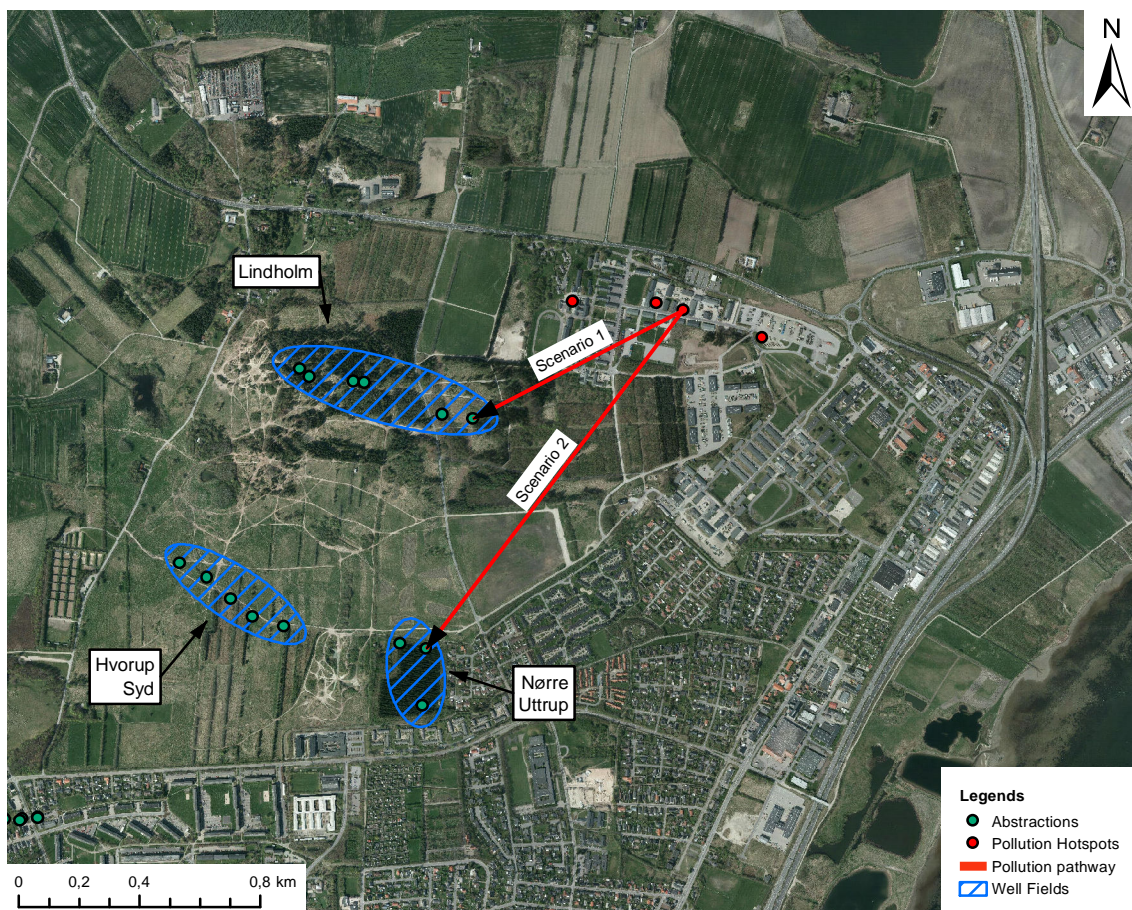


Figure 6.8. The scenarios of horizontal transport.

6.2.1 Analytical method

The analytical solution to advection and dispersion is the following:

$$C(L,t) = C_0 \cdot \left[\frac{1}{2} \cdot \text{ERFC} \left(\frac{R \cdot L - u \cdot t}{\sqrt{4 \cdot D \cdot R \cdot t}} \right) + \frac{1}{2} \cdot \text{ERFC} \left(\frac{R \cdot L + u \cdot t}{\sqrt{4 \cdot D \cdot R \cdot t}} \right) \cdot \exp \left(\frac{L \cdot u}{D} \right) \right]$$

(6.5)

Where

L	Distance [m]
D	Dispersion [m]
$ERFC(x)$	Complementary error of x [-]

D in the analytical solution is a combination of both dispersion and diffusion. However in the saturated zone the diffusion is neglected, as diffusion has an insignificant contribution to the transport.

The transport of benzene is assumed to result only from advection. When taking into account effective porosity, the velocity of the chemical is:

$$u_{benzene} = \frac{V_{water}}{\phi_{eff} \cdot R} \quad (6.6)$$

Where

v_{water}	Darcy velocity [$\text{m} \cdot \text{yr}^{-1}$]
ϕ_{eff}	Effective porosity [$\text{cm}^3 \cdot \text{cm}^{-3}$]
R	Retardation [-]

The Darcy velocity can be calculated with Darcy's equation:

$$V_{water} = K_{sat} \cdot \frac{\Delta h}{L} \quad (6.7)$$

Where

K_{sat}	Horizontal saturated hydraulic conductivity of fractured limestone [$\text{m} \cdot \text{s}^{-1}$]
Δh	Pressure difference between pollution site and abstraction well [$\text{m H}_2\text{O}$]
L	Distance between pollution site and abstraction well [m]

Dispersion can be calculated by dispersivity and mean velocity of chemical as follows:

$$D = \alpha \cdot U \quad (6.8)$$

Where

α	Chemical dispersivity [m]
----------	---------------------------

6.2.2 Input parameters

As the pressure in the relocated Lindholm well field will decrease due to water abstraction, it is evaluated that the potential map shown in figure 6.4 is inaccurate. The potential from the groundwater model is thus used instead. As the hydraulic head in the limestone in Hvorup barracks is also significantly different for the calibrated groundwater model, the calibrated groundwater model is used for the head in the limestone in the barracks as well.

For scenario 2, both the hydraulic head in the limestone in Hvorup barracks as well as in Nørre Uttrup well field are retrieved from the potential map shown in figure 6.4.

The hydraulic conductivity of fractured limestone in the model is assumed to be the mean of the two measurements described in appendix A.1 page 105.

The effective porosity of fractured limestone is the secondary or fissure porosity. The fissure porosity and retardation are retrieved from chapter 4.6.3 page 25. As the limestone responsible for the transport of the chemicals is expected to be very fractured, the effective porosity is assumed to be in the high end, i.e. $1 \text{ cm}^3/\text{cm}^3$.

The retardation of benzene in fractured limestone is assumed to be exclusively due to diffusion between the mobile and immobile volume, meaning any retardation by sorption is disregarded. The retardation is calculated in chapter 4.6.3 page 25. As the effective porosity is assumed to be in the high end, the corresponding low value of retardation is chosen as well.

The chemical dispersivity dispersion is largely dependent on scale. Spitz and Morene [1996] suggests a relationship between chemical dispersivity and scale as follows:

$$\alpha/l = [0.01; 1] \quad (6.9)$$

Where

$$l \mid \text{Distance [m]}$$

However that relation is indifferent to soil type. Three measurements for fractured limestone aquifers are shown in table 6.5, they are added to the suggested relation from Spitz and Morene [1996] as shown in figure 6.9.

Table 6.5. Literature values for longitudinal dispersivity in fractured limestone [Gelhar et al., 1992]

Scale [m]	Thickness of aquifer [m]	α_L [m]
122	15	15
490	30.5	6.7
32 000	61	20

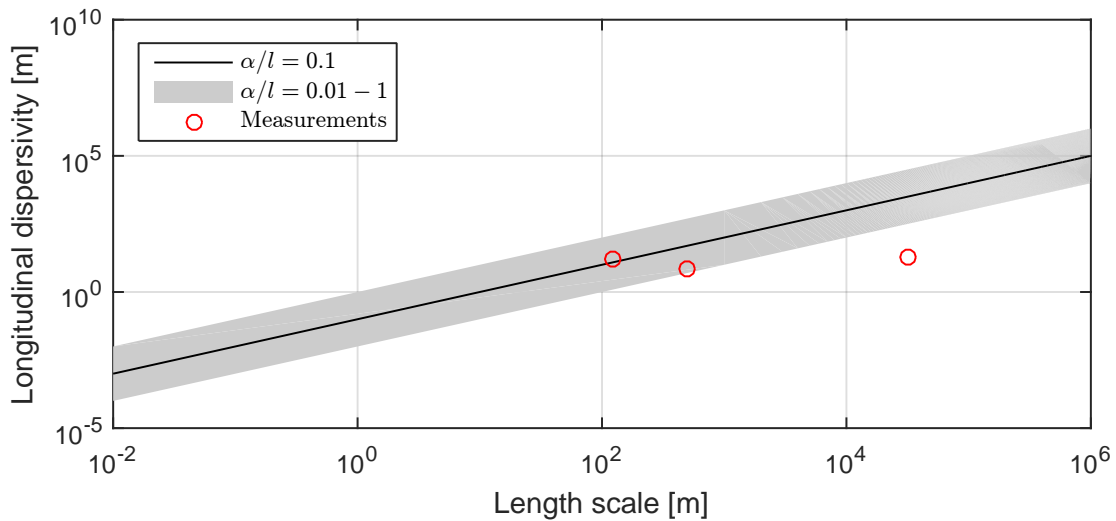


Figure 6.9. Field scale dispersion in fractured limestone.

It's evident that two of the measurements are within the suggested relationship, and one is significantly outside. Based on this it is evaluated that the dispersion for fractured limestone is in the low range of the suggested relation, i.e. $\alpha/l = 0.01$.

As no measurements for biodegradation potential are available, it is assumed that it is equivalent to the groundwater samples in chapter chapter 4.7 page 26 in situ. 0th order biodegradation is excluded as it was evaluated that this kinetic model was not applicable to the site.

The parameters for the horizontal transport model are shown in table 6.6.

Table 6.6. Parameters used for horizontal transport

	Scenario 1	Scenario 2
Hydraulic head, limestone in Hvorup barracks [m]	3.15	4.5
Hydraulic head, water abstraction [m]	2.01	2
Distance [m]	784	1409
Hydraulic conductivity [$\text{m} \cdot \text{s}^{-1}$]	$5.8 \cdot 10^{-4}$	$5.8 \cdot 10^{-4}$
Effective porosity [$\text{cm}^3 \cdot \text{cm}^{-3}$]	0.156	0.156
Retardation [-]	43	43
Dispersivity [m]	7.84	14.09
1st order degradation rate [d^{-1}]	$5.00 \cdot 10^{-4}$	$5.00 \cdot 10^{-4}$

6.2.3 Results

The calculated Darcy velocity and mean velocity are shown in table 6.7.

Table 6.7. Mean velocity of chemical

	Scenario 1	Scenario 2
Hydraulic gradient [$\text{m} \cdot \text{m}^{-1}$]	$1.45 \cdot 10^{-3}$	$1.77 \cdot 10^{-3}$
Darcy velocity [$\text{m} \cdot \text{s}^{-1}$]	$8.41 \cdot 10^{-7}$	$1.03 \cdot 10^{-6}$
Mean velocity, excl. retardation [$\text{m} \cdot \text{s}^{-1}$]	$8.41 \cdot 10^{-5}$	$1.03 \cdot 10^{-4}$

The breakthrough curve for benzene in the abstractions can be calculated for both scenario 1 and 2. They're shown in figure 6.10. It is evident that the concentration of benzene exceeds the limit for drinking water from Miljøministeriet [2014] in both Nørre Uttrup well field and the relocated Lindholm well field.

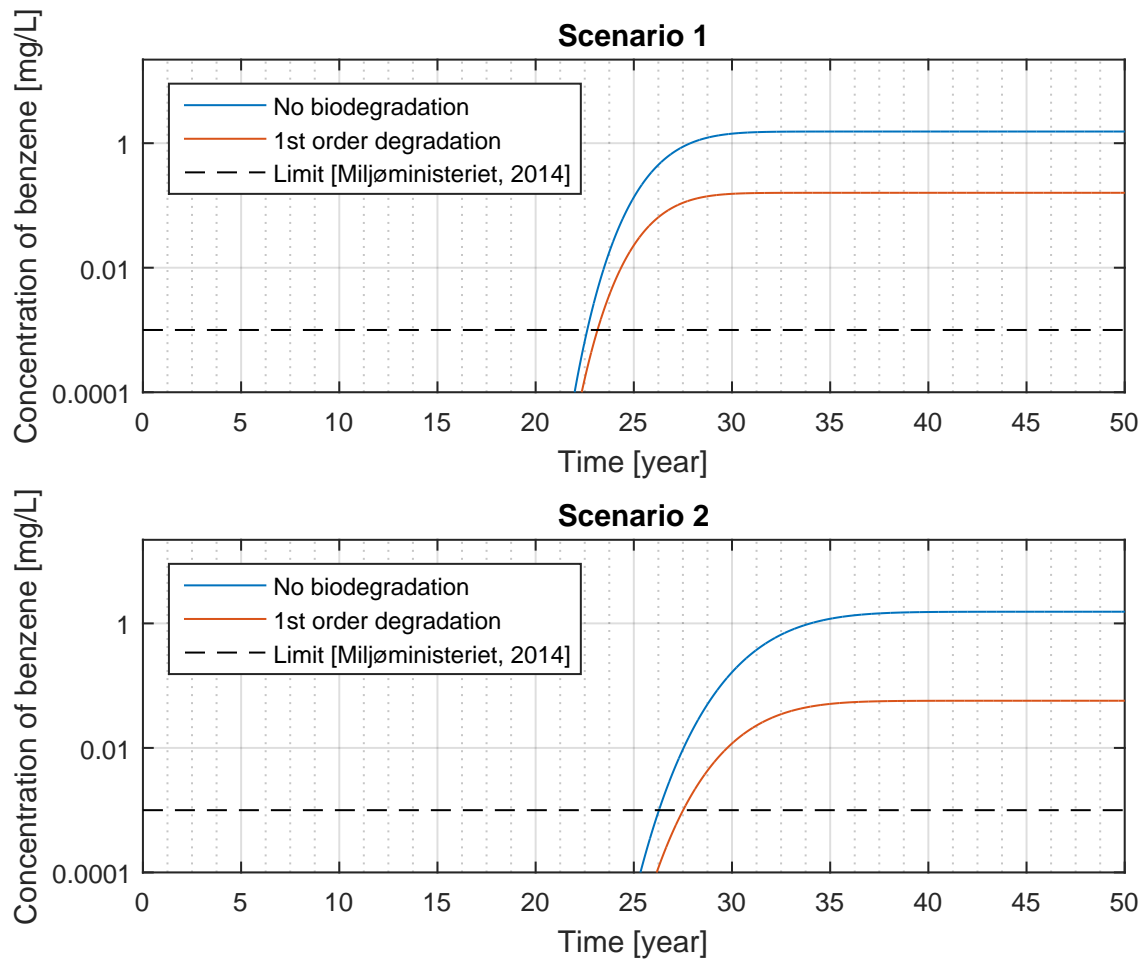


Figure 6.10. Breakthrough curves for scenario 1 and 2

6.2.4 Stochastic model on horizontal transport

A stochastic model is done on the horizontal transport, where the uncertainties in estimating the horizontal transport as well as the uncertainties estimating the vertical transport are taken into account. The distribution for the parameters in the horizontal transport remain the same. The inputs used in getting the distributions for vertical transport are shown in table 6.8.

Table 6.8. Distribution types

Head in limestone in Hvorup barracks	Uniform distribution with lower limit as the calculated head from the groundwater model and with upper limit as the head from potential map supplied by Niras
Head in limestone in relocated Lindholm well	No distribution
Head in limestone in Nørre Uttrup well	Uniform distribution with lower limit as the calculated head from the groundwater model and with upper limit as the head from potential map supplied by Niras
Hydraulic conductivity of fractured limestone	Log trapezoidal distribution where the outer limits are the limits for fractured limestone from Spitz and Morene [1996] and the inner limits are the two measurements.
Effective porosity	Log uniform distribution between limits from GEUS [2011]
Total porosity	Normal distribution with values of standard deviation and mean from limestone measurements as described in appendix A.2 page 110
Relationship of dispersion, a/l	Log trapezoidal distribution where more weight is added to the lower end of the relation supplied by Spitz and Morene [1996]
1st order biodegradation rate	Lognormal distribution with values of standard deviation and mean from all groundwater samples adjusted for anaerobic, nutrient limited conditions in chapter 4.7 page 26 where no autoclaving occurred nor nutrients added

The distributions are shown in figure 6.11. The empirical distribution for retardation is calculated based on the distributions for the two parameters that are used to calculate it.

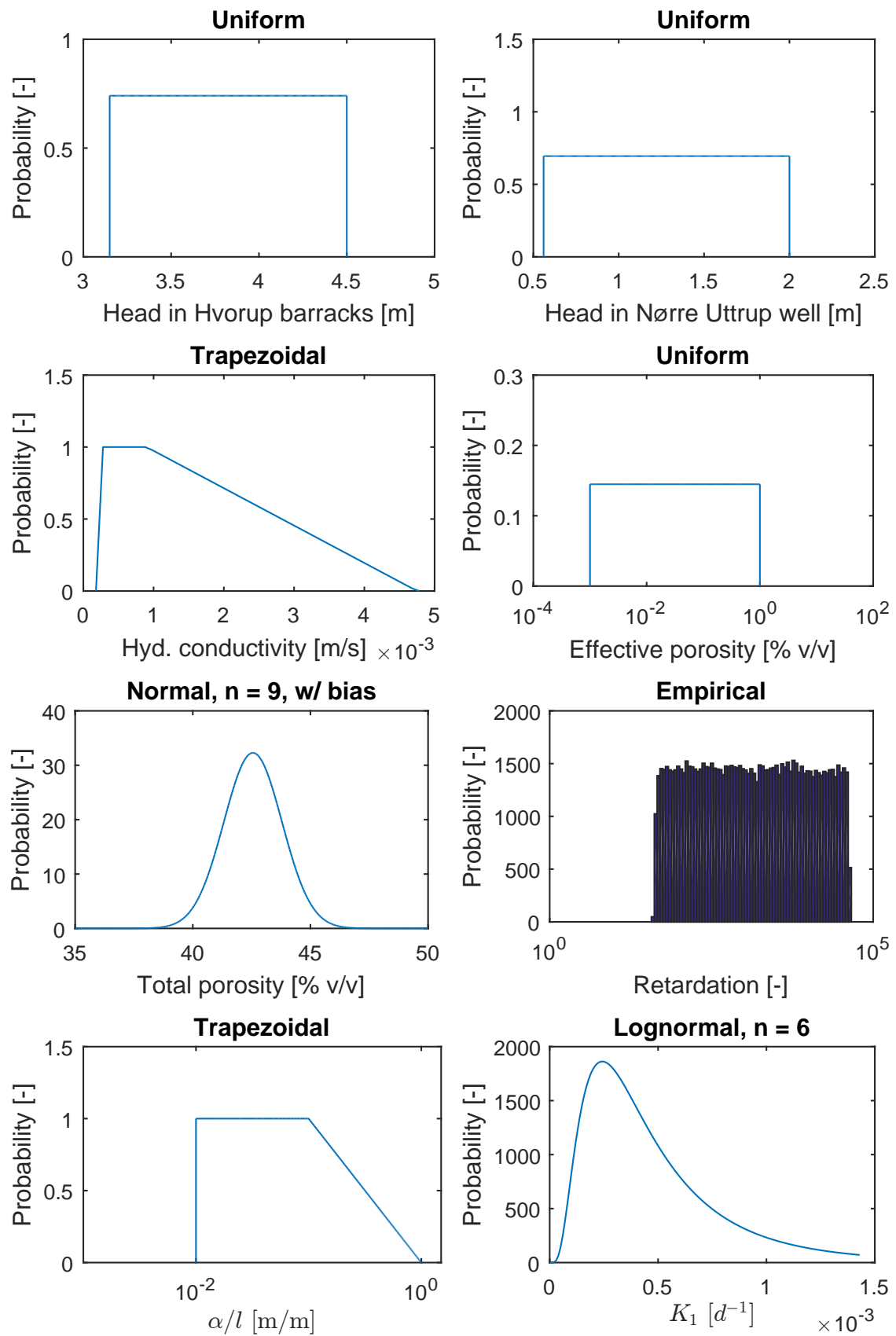


Figure 6.11. Distribution of the parameters

Although effective and total porosity are expected to be related, no data is available to examine this relation. The relation is thus ignored in the stochastic model.

The cumulative distribution of the concentration in the abstraction wells in both scenarios is shown in figure 6.12.

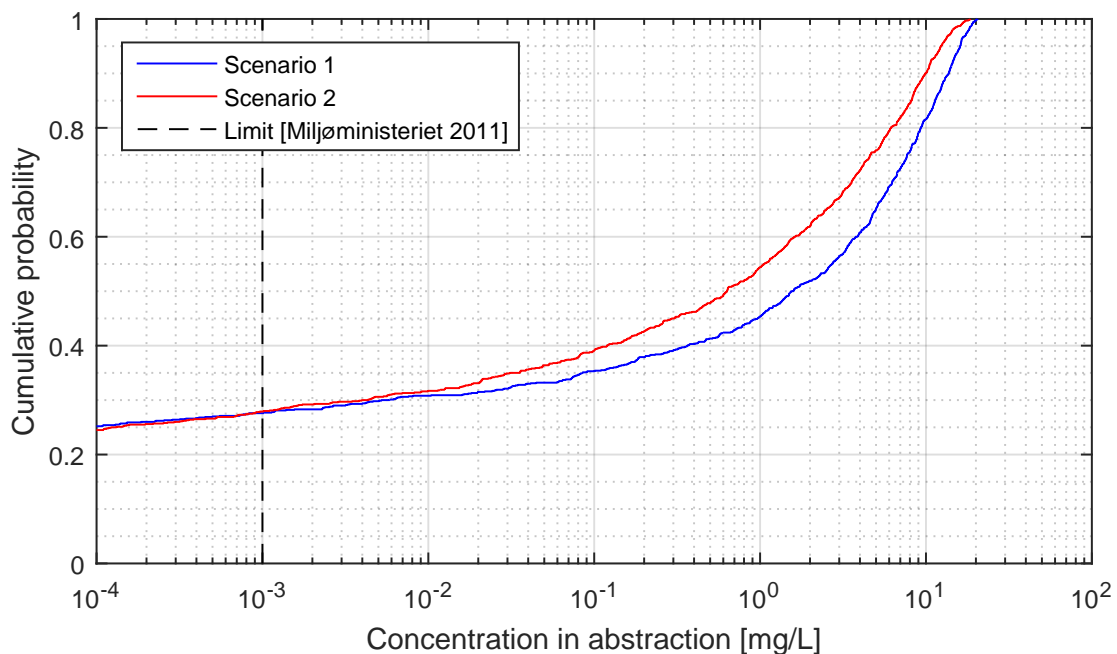


Figure 6.12. Concentration of benzene in abstraction well.

It is evident that the uncertainties of the input parameters for the horizontal and vertical model greatly affect the results. It is evident that only about 27 % of the 1000 monte carlo simulations resulted in a concentration of benzene below the limit for drinking water. It is thus likely that the concentration of benzene exceeds the limit for drinking water in the abstraction well.

6.3 Parameter sensitivity

The sensitivity of the parameters for both the horizontal and vertical transport model are shown in figure 6.13. It shows that the four most sensitive parameters are hydraulic conductivity and biodegradation for both clay and fractured limestone. The sensitivity analysis is only done for scenario 2.

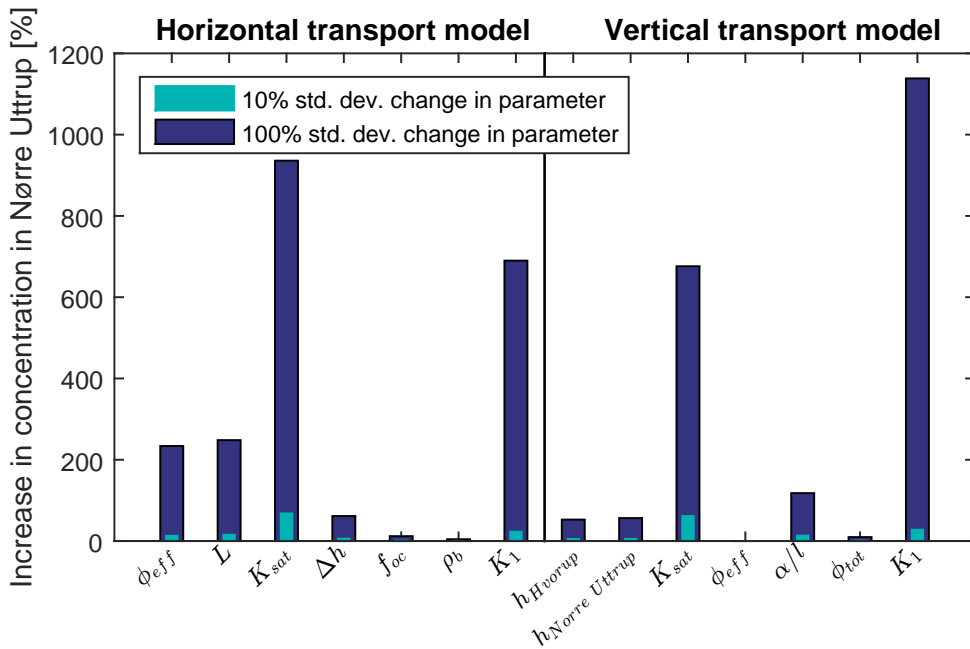


Figure 6.13. Parameter sensitivity.

6.4 Discussion

The stochastic analysis shows that the uncertainties surrounding the input parameters to the model greatly influence the results. The uncertainties of the hydraulic conductivity for the clay and fractured limestone as well as biodegradation potential have been shown in chapter 6.3 page 67 to have a significant impact on the results. In order to reduce the uncertainties of the results, the biodegradation as well as hydraulic conductivity for the fractured limestone and clay have to be investigated further.

The vertical transport is in the analytical model reduced to a penetration of a clay lens, however the pollutant in reality has to travel through the sandy soil as well. The vertical transport time and thus the biodegradation of the pollutant is underestimated. However this is to the conservative side.

Transverse dispersion has also been excluded. Transverse dispersion will reduce the amount of pollution transported to the abstraction well, and has been found in the numerical transport model to have a significant effect on the concentration in Nørre Uttrup well field. As this is excluded it is likely that the spread of pollutant is overestimated.

The biodegradation for the fractured limestone has been assumed to be equal to the biodegradation for the sandy soil adjusted for anaerobic conditions and lack of nutrition. Previous studies have found that the biodegradation potential in the fractured limestone is almost as high as for the low depth sandy soil [Henriksen, 2015b]. It is thus evaluated that the real difference in biodegradation is relatively low.

Fractured limestone is also a dual domain system, meaning some of the water volume resides in immobile pores with likely poor biodegradation. The biodegradation potential is thus in this case overestimated, as the decrease in biodegradation in the immobile volume is ignored. However by comparison with similar studies of biodegradation in soil the biodegradation found in the experiment at Hvorup barracks is already at the low end. It can thus be evaluated that although the dual domain nature is ignored, the biodegradation in the mobile volume is underestimated as well.

The analytical solution does not take flow direction of the groundwater into account. It is evident from the numerical model in chapter 7 page 71 that the pollution is not transported towards the relocated Lindholm well field, but only Nørre Uttrup well field. It is also evident that the pollution has to travel further than a direct path from pollution site to abstraction well, as it was assumed in this chapter.

7. Risk to regional drinking water resource

Numerical model

A numerical model is done to further assess the risk of the pollution plume reaching the municipality abstractions. The purpose of the model is to investigate the transport of pollutants while accounting for the heterogeneity of the subsurface.

The numerical model is done in the commercial software GMS. It is split into two models:

A **groundwater model** using the MODFLOW module in GMS. This describes the flow of groundwater.

A **transport model** using the MT3DMS module in GMS. This describes the transport of chemicals.

7.1 Groundwater model

The groundwater model is a steady-state, three-dimensional finite-difference model that implements a multi-layered geological model as well as a recharge of the aquifer that varies geographically.

The model is first setup to be able to determine the hydraulic head in the project area. The model is then calibrated so the hydraulic head matches the measurements in the area.

7.1.1 Input parameters

The model consists of the following elements:

- Boundary conditions
- Geological model
- Recharge
- Streams
- Abstractions
- Layer properties
 - Horizontal hydraulic conductivity
 - Vertical hydraulic conductivity

These elements are described in the following chapters.

7.1.1.1 Boundary conditions

The groundwater model uses two different types of boundary conditions: Prescribed head boundaries and no-flow boundaries. Prescribed head boundaries ensure a specified head in a cell and no-flow boundaries ensure that no flow occurs through the cell.

Prescribed head boundaries are specified in Limfjorden as well as the two streams that delineate the model. The boundary is shown in figure 7.1. The boundary at the streams is located just outside the location of the streams to allow for cells inside the model that are defined as drainage. Prescribed head boundaries are also located at the lake in the southwestern area. This is to account for a water abstraction that maintains a low water table in this area.

The prescribed head is defined in points on the boundary, and GMS then interpolates between the points to get the prescribed head in the boundary cells. The head in the points is retrieved from the potential map that's introduced in chapter 4.8 page 30. The prescribed head boundaries are automatically assigned to the top most layer that is wet in the model. For all layers below the top layer the boundary condition is no flow.

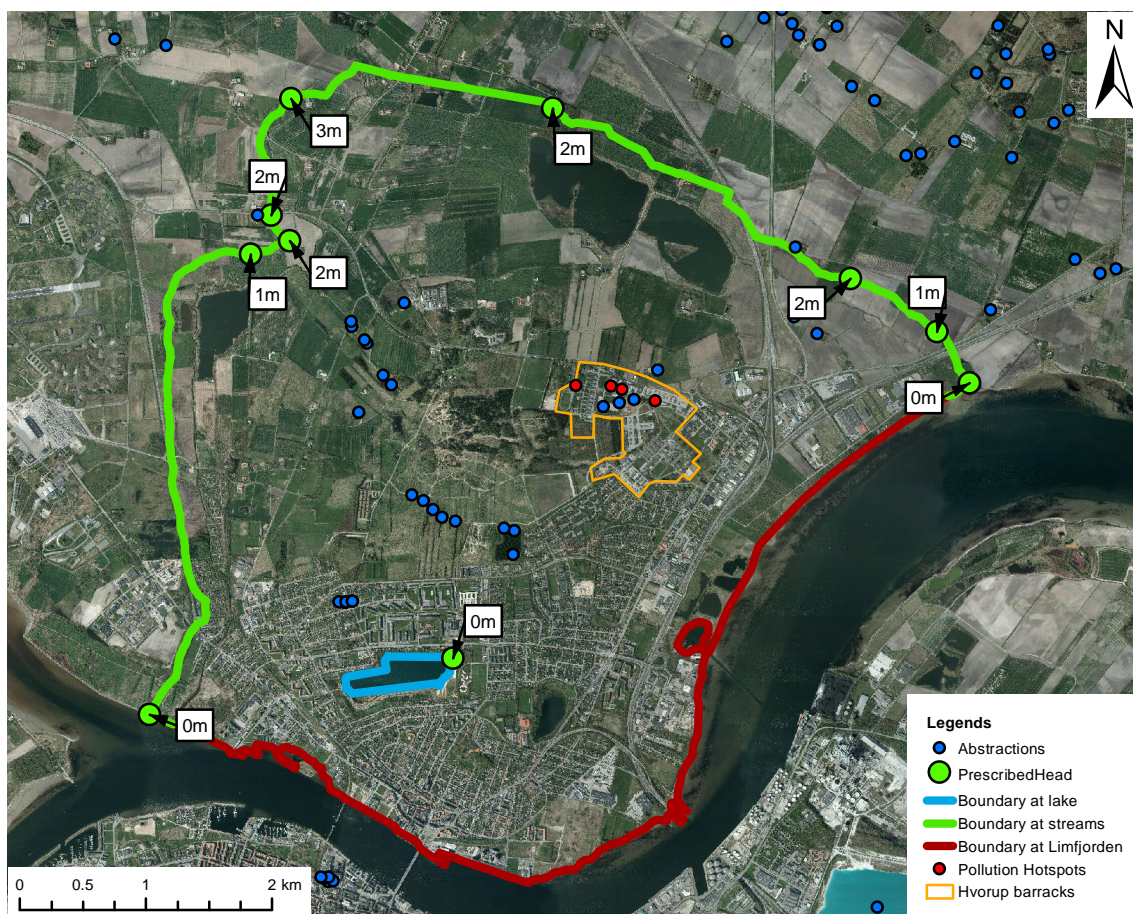


Figure 7.1. Boundary conditions.

7.1.1.2 Geological model

A geological model for the entire area of the groundwater model is available. The geological model has been supplied by NIRAS. It is a grid of cells with a cell size of 100×100 m. It consists of 13 layers with a bottom elevation of every layer as well as a terrain elevation.

The soil layers are shown in table 7.1. The two top layers are top soil. Following this are three sand and four clay layers and then four limestone layers. The second last limestone layer is presumably the low permeable horizon in the limestone that separates the lower groundwater into two aquifers. The layers will onwards be referenced by soil type, i.e. sand is sand layer 1, 2, and 3. Layer 10 and 11 will onwards be referenced as upper limestone, and layer 13 will be referenced as lower limestone.

A cross-section of the geological model is shown in figure 7.3. The location of the cross-section is shown in figure 7.2.

Table 7.1. Soil layers in the geological model ordered after depth

- | | |
|---------------|----------------------|
| 1. Top soil 1 | 8. Sand 3 |
| 2. Top soil 2 | 9. Clay 4 |
| 3. Clay 1 | 10. Danian limestone |
| 4. Sand 1 | 11. Limestone |
| 5. Clay 2 | 12. Limestone |
| 6. Sand 2 | 13. Limestone |
| 7. Clay 3 | |



Figure 7.2. Location of cross-section.

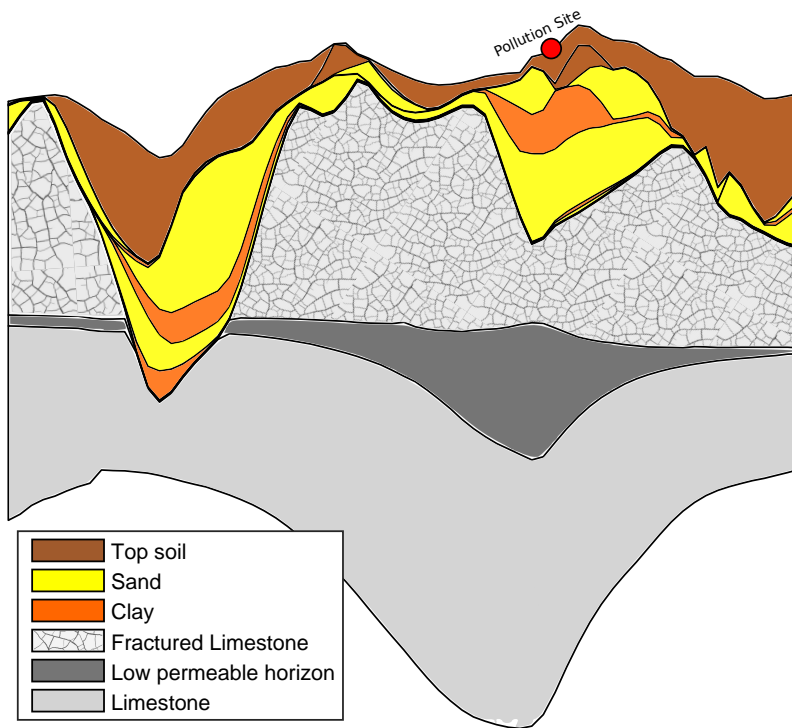


Figure 7.3. Cross-section of geological model.

The upper limestone layer is presumably more fractured than the lower. Because of this it is likely that the two limestone layers do not share similar hydraulic properties.

7.1.1.3 Recharge

The data for net-precipitation presented in chapter chapter 4.8 page 30 is implemented in the model. As evapotranspiration is already included in the data, a model for evapotranspiration is not implemented into the groundwater model.

7.1.1.4 Streams

All streams in the model area are implemented as drains. For drainage cells a conductance is specified as a description of the rate of flow between groundwater and drainage. This factor is a combination of both the area of permeable surface for the drainage as well as the hydraulic conductivity and thickness of said surface. The conductance is calculated with the following equation:

$$C = \frac{K \cdot A}{L} \quad (7.1)$$

Where:

C	Conductance [$\text{m}^2 \cdot \text{s}^{-1}$]
K	Hydraulic conductivity of surface [$\text{m} \cdot \text{s}^{-1}$]
A	Area of surface [m^2]
L	Thickness of surface [m]

In GMS it is possible to specify the conductance per unit length of the stream. The streams in the model are shown in figure 7.4.

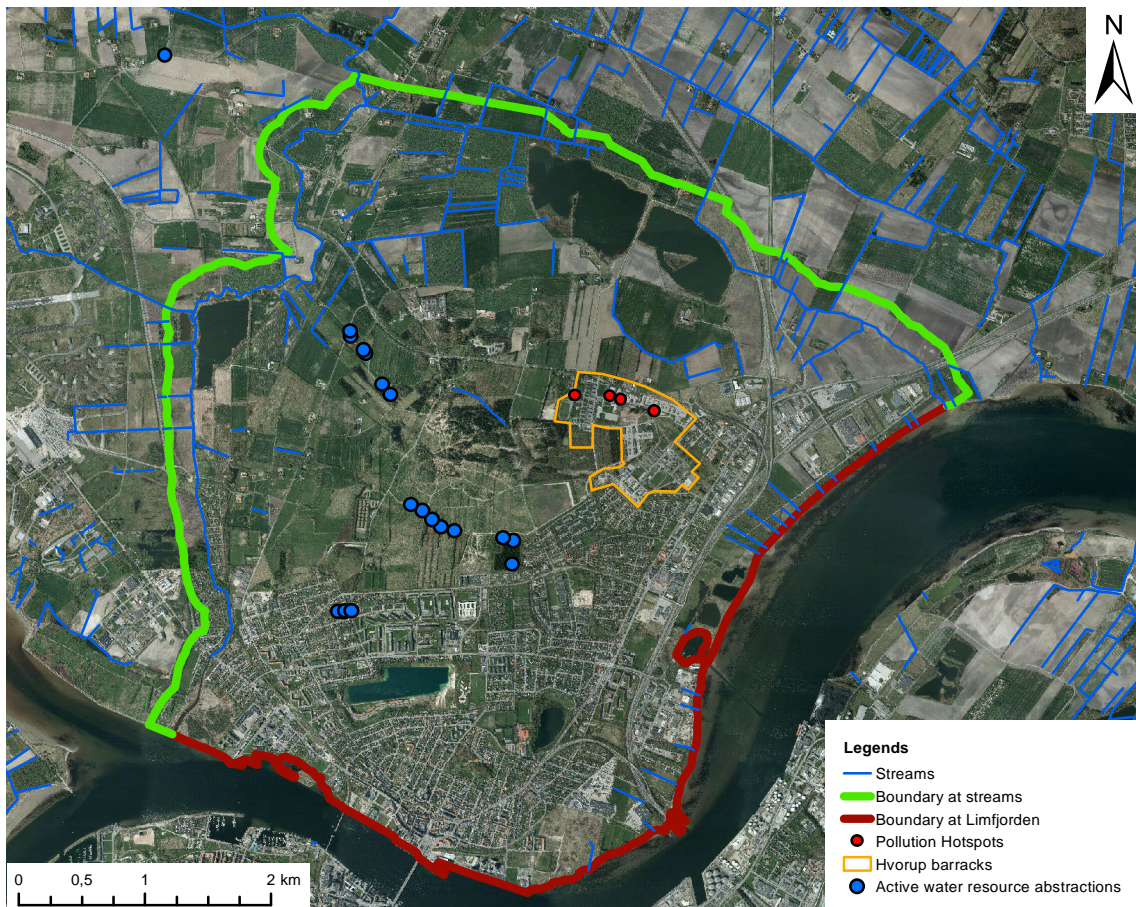


Figure 7.4. Streams in the groundwater model.

A rough estimation of the conductance for the streams is done. The hydraulic conductivity from riverbed lining materials have been determined in the range $1.3 \cdot 10^{-10}$ to $2.0 \cdot 10^{-2} \text{ m} \cdot \text{s}^{-1}$, although values in the range $1.7 \cdot 10^{-10}$ to $1.0 \cdot 10^{-3} \text{ m} \cdot \text{s}^{-1}$ were predominate [Calver, 2001].

The area of surface is almost directly proportional to the water table, as shown in figure 7.5 for a stretch of Guldbækken in Svenstrup [Nielsen et al., 2015]. This indicates that estimation of width of water table from orto photos is sufficient in determining the area of surface.

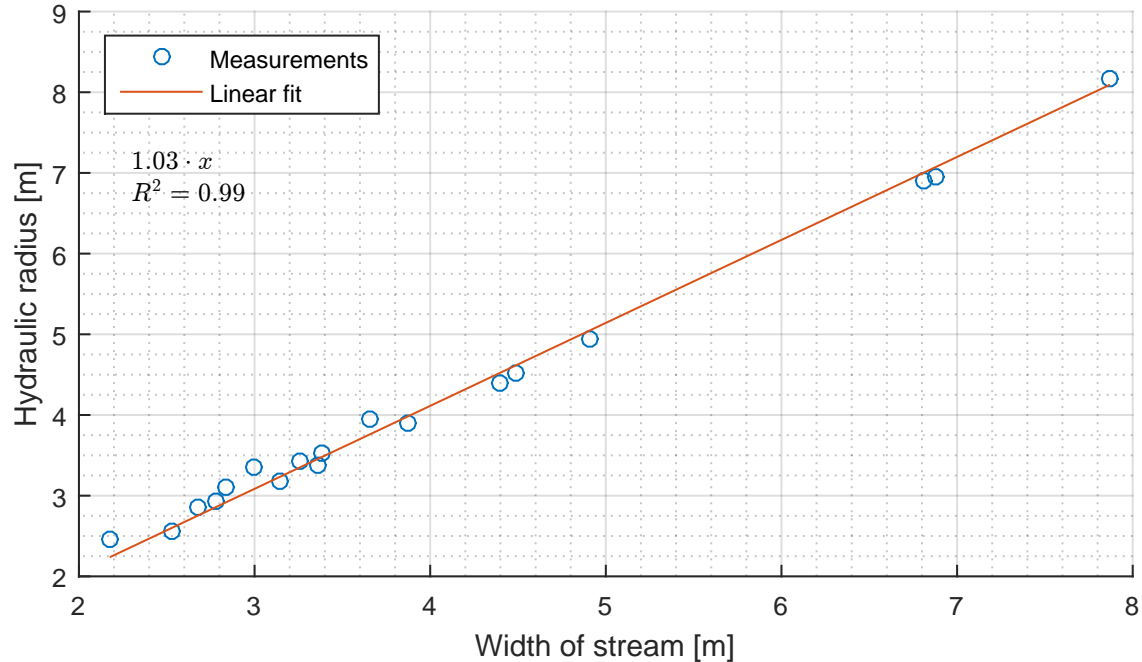


Figure 7.5. The surface area of a stream in relation to the width of the water table.

As the streams in the groundwater model all are of varying sizes, three different conductances are determined. One for Lindholm Å, one for Lerbækken and one for all other streams in the model. The thickness of the river bed sediment is unknown. It is thus assumed to be in the range of 0.2 - 1 m. The results for the conductance are shown in table 7.2. The width of the streams are determined by measurements from orto photos. As the smaller streams all vary in size, a width for these is assumed equal to 0.4 m.

Table 7.2. The range of conductance of Lindholm Å, Lerbækken and smaller streams

Stream	Width [m]	A [m ² · m ⁻¹]	L [m]	K _{sat} [m · s ⁻¹]	C [m ² · s ⁻¹ · m ⁻¹]
Lindholm Å	4 - 9	4 - 9	0.2 - 1	1.7 · 10 ⁻¹⁰ - 1.0 · 10 ⁻³	7 · 10 ⁻¹⁰ - 5 · 10 ⁻²
Lerbækken	2	2	0.2 - 1	1.7 · 10 ⁻¹⁰ - 1.0 · 10 ⁻³	3 · 10 ⁻¹⁰ - 1 · 10 ⁻²
Other streams	0.4	0.4	0.2 - 1	1.7 · 10 ⁻¹⁰ - 1.0 · 10 ⁻³	7 · 10 ⁻¹¹ - 2 · 10 ⁻³

As shown there's a great uncertainty on the values of conductance. As the range is very large for the conductance, the log mean is used for the groundwater model. The log mean is calculated as follows:

$$\bar{C} = \exp\left(\frac{1}{2} \cdot (\log(C_{lower}) + \log(C_{upper}))\right) \quad (7.2)$$

Where:

\bar{C}	Log mean of conductance [$m^2 \cdot s^{-1} \cdot m^{-1}$]
C_{lower}	Lower limit of conductance [$m^2 \cdot s^{-1} \cdot m^{-1}$]
C_{Upper}	Upper limit of conductance [$m^2 \cdot s^{-1} \cdot m^{-1}$]

The values of conductance used in the groundwater model are shown in table 7.3, calculated with equation (7.2).

Table 7.3. The conductance of Lindholm Å, Lerbækken and smaller streams

Stream	C [$m^2 \cdot s^{-1} \cdot m^{-1}$]
Lindholm Å	$6 \cdot 10^{-6}$
Lerbækken	$2 \cdot 10^{-6}$
Other streams	$4 \cdot 10^{-6}$

7.1.1.5 Abstractions

As the intent of this groundwater model initially is to match the observations of hydraulic head in the area, the abstractions that were in use during the measurements of the water table will have to be included in the model.

The abstractions that are included are Lindholm, Hvorup Syd and Nørre Uttrup well field as well as the three abstractions inside the barracks that supplied the barracks with water that have now been closed.

No data is available for the abstraction amount for the individual abstractions, but data for the abstraction amount per year for the water plants is available. It is thus assumed that the abstractions are distributed evenly among the abstraction wells connected to the water plant. As the distance between the abstraction wells for a water plant is relatively small, this assumption is expected to have a very small impact on the groundwater model.

As the head observations in the area are a collection of measurements from the previous years, the abstractions should reflect this. The mean of the abstraction amount from 2002-2014 is used. The data for the abstractions are shown in appendix G page 153. It shows that the variation in abstraction amount per year is relatively small.

The abstractions are implemented as wells within a layer range in the model. The layer range corresponds to the top and bottom of the filters. Only one of the wells abstracts above the fractured limestone.

7.1.1.6 Saturated hydraulic conductivity

The saturated hydraulic conductivity has to be defined for each layer.

The hydraulic properties of the limestone aquifer

The limestone aquifer is divided into areas of high and low conductivity because of fractures. The conditions during sedimentation and the fluctuations of the water table in the geological past play a major role in the distribution and density of pores and fissures.

During flow in fractured limestone, the larger fractures are exposed to a higher concentration of CO_2 , released from differences in HCO_3^- concentrations, biological activity and the faster turnover of the pore-water. This leads to a higher dissolution of CaCO_3 from the soil matrix and thus, increases the fracture size leading to a larger hydraulic conductivity. The upper part of the aquifer is more affected by the presence of these preferential flow paths, because the fissure density decreases with depth [Price et al., 1993].

A major role in the horizontal hydraulic conductivity of the limestone is the layering. Interfaces between layers of different hardness as well as interfaces between limestone and flint also contribute to high hydraulic conductivities. For the vertical hydraulic conductivities, however, tectonic factors contribute to a high conductivity, especially for the harder types of limestone. [GEUS, 2011]

For now the limestone aquifer is only separated into two layers. The upper layer is assumed to be fractured, and the lower is assumed to be only partially fractured. It is assumed that the hydraulic conductivity for the lower layer is then 10% of the upper layer. The two layers are separated by the low permeable horizon, as shown in figure 7.3. This low permeable horizon is assumed to have properties similar to clay, although the actual properties are likely to be limestone mixed with clay.

Values

The saturated hydraulic conductivities will be derived from literature and previous measurements. The values for saturated horizontal hydraulic conductivity used in the model are shown in table 7.4. As the measurements of hydraulic conductivity for clay do not seem to match the literature values, the measurements are excluded, and the literature values are used instead.

Table 7.4. The horizontal saturated hydraulic conductivity for the different soil types

Soil type	K_{sat}	Source
	[m · s ⁻¹]	
Sand	$1.68 \cdot 10^{-5}$	Average of measurements on top soil in Hvorup barracks and Tylstrup
Top soil	$1.68 \cdot 10^{-5}$	Same as for sand
Clay	$2.36 \cdot 10^{-7}$	Average of limits for clay from Spitz and Morene [1996]
Low permeable horizon	$2.36 \cdot 10^{-7}$	Same as for clay
Fractured Limestone	$5.8 \cdot 10^{-4}$	Average of measurements from single-well tracer test and pumping test
Deep/non-fractured limestone	$5.8 \cdot 10^{-5}$	10% of fractured limestone

Factors for vertical anisotropy are used to define the values of saturated vertical hydraulic conductivity. The values are shown in table 7.5. As no measurements of the vertical hydraulic conductivity have been found, the vertical anisotropy of all layers is assumed to be equal to 3.

Table 7.5. The vertical anisotropy for the different soil types

Soil type	K_h/K_v
	[−]
Sand	3
Top soil	3
Clay	3
Fractured limestone	3

7.1.1.7 Results

The hydraulic head in the upper limestone layer is shown in figure 7.6. It shows that there's a peak in hydraulic head northwest of Hvorup barracks, with a maximum hydraulic head of 2.4 m above sea level.

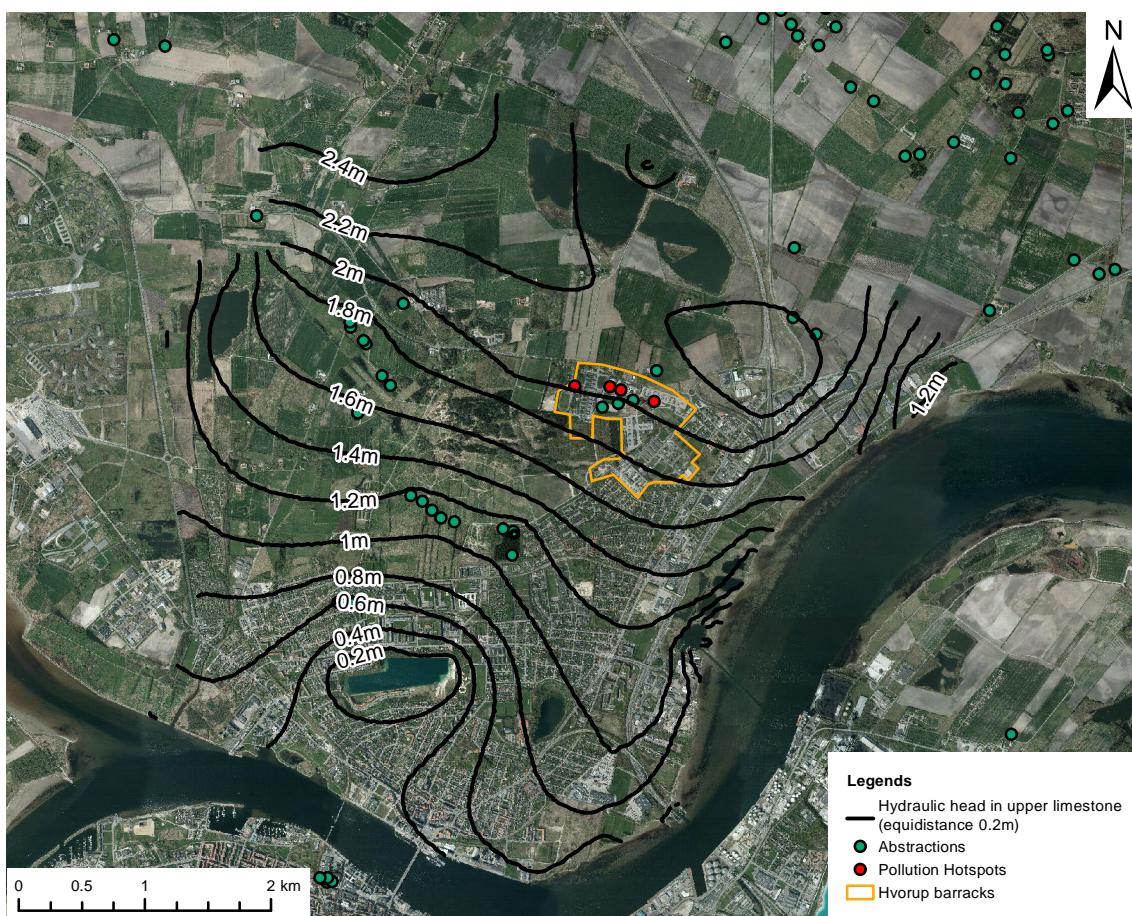


Figure 7.6. Hydraulic head in the upper limestone layer.

7.1.2 Calibration

The groundwater model is calibrated to better reflect the observations of hydraulic head in the area. Before deciding on the parameters that are subject to calibration, a sensitivity analysis is done on the parameters in the groundwater model.

7.1.2.1 Sensitivity

A sensitivity analysis is done on the hydraulic conductivity of the layers as well as the conductance and factors of anisotropy. A 5% and 25% increase is done on all the parameters, and the change in RMS of observed head and calculated head is calculated. The sensitivity of all the parameters are shown in figure 7.7. As the hydraulic conductivity of the top soil is tied to sand, it is also changed as the hydraulic conductivity of sand is changed.

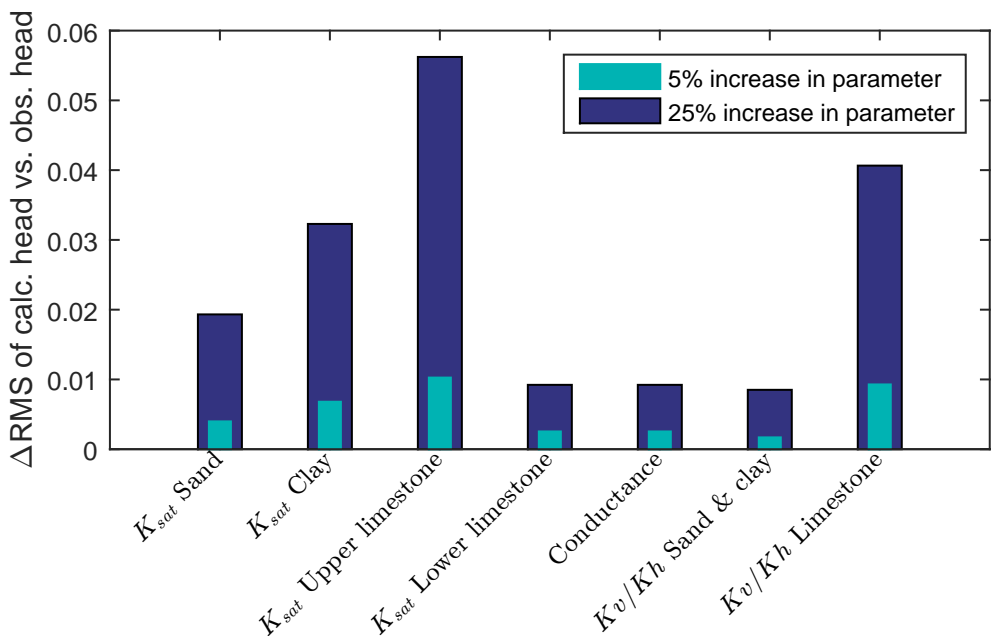


Figure 7.7. Sensitivity analysis on the parameters included in the groundwater model.

It would perhaps be more interesting to see the sensitivity of the parameters in relation to the uncertainty. However the groundwater model is incapable of executing when using the maximum values of conductance or minimum values of hydraulic conductivity for clay.

It is evident that the horizontal hydraulic conductivity of the upper limestone is the most sensitive parameter. As such this parameter will be calibrated. As the values of conductance were based on very rough estimates, this is also calibrated.

The calibration is done with the Parameter Estimation (PEST) tool within GMS. In GMS this is an automatic process, where only limits for the parameters need to be specified.

The conductance of Lindholm Å, Lerbækken and the smaller streams are tied, meaning the relation between the conductances before and after calibration are identical.

7.1.2.2 Zones of hydraulic conductivity

Based on the knowledge that the hydraulic conductivity of fractured limestone is affected by fluctuations in water table as well as preferential flow path, additional zoning of the hydraulic conductivity in the upper, fractured limestone layer (layer 11) is done. The zones are shown in figure 7.8. Although tectonic disturbances as well as changes in hardness and content of flint also influence the hydraulic conductivity, no data for this has been found for the project area.

Zone 1 is the zone where the water table resides inside the fractured limestone. Zone

2 is the zone where high flow rates are occurring. Both the water table and flow rate used in determining the zones are based on the results from the groundwater model after calibration without zoning.

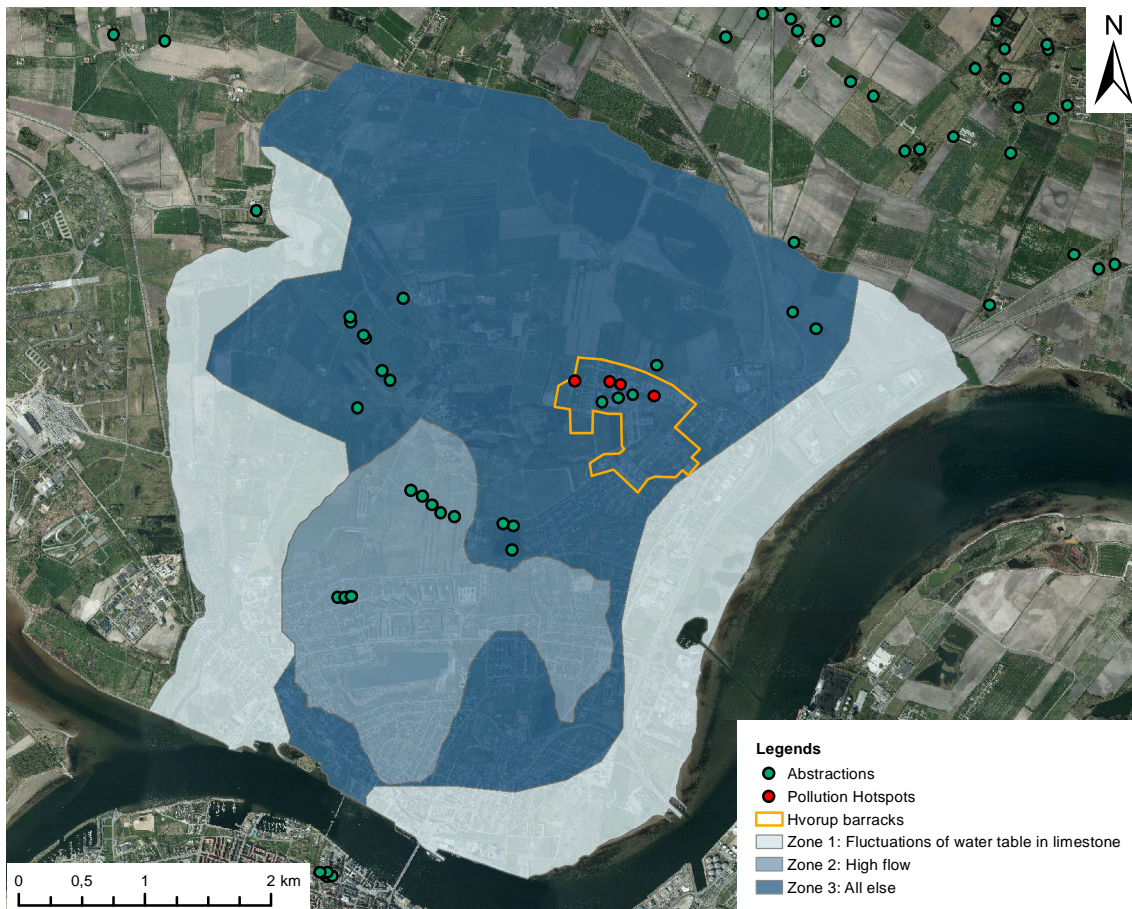


Figure 7.8. The zones of hydraulic conductivity in the limestone

The calibration for the limestone is then a calibration of conductance and the three zones of fractured limestone. The zones are not tied during the calibration.

7.1.2.3 Observations of hydraulic head

Many observations of hydraulic head are available for the area within the groundwater model. However as these measurements will be the foundation for the calibration, it's evaluated that only quality measurements will be used. The observations used for calibration are shown in figure 7.9. The 12 observations are picked as they have more than three measurements from the same intake and have a well-defined depth of intake.

The value of hydraulic head is the median of all measurements in the observation for all but three observations. For these the water level has been evaluated from visual inspection of the water table curve. The three measurements have been changed because of their

close proximity to the lake and the old slaughterhouse where significant water abstractions have been occurring in the past. As such the water table is evaluated from the most recent measurements.



Figure 7.9. The observations of head used for calibration. [GEUS, 2015]

The observations are implemented in GMS as an observation point. The observation is applied to the proper layer, determined by the depth of the intake for the observation.

It's evident from figure 7.9 that there's a lack of observations east and north of Hvorup barracks. Because of this it's difficult to determine the interface between Lerbækken and the groundwater aquifer as well as the location of the regional peak in groundwater table.

However the observations north and east of Hvorup barracks that are excluded either have few measurements or fail to specify the depth of the intake.

7.1.2.4 Results

The hydraulic head in the upper, fractured limestone layer is shown in figure 7.10. It's evident that the peak in hydraulic head is now located northeast of Hvorup barracks with a maximum head of 3.4 m.

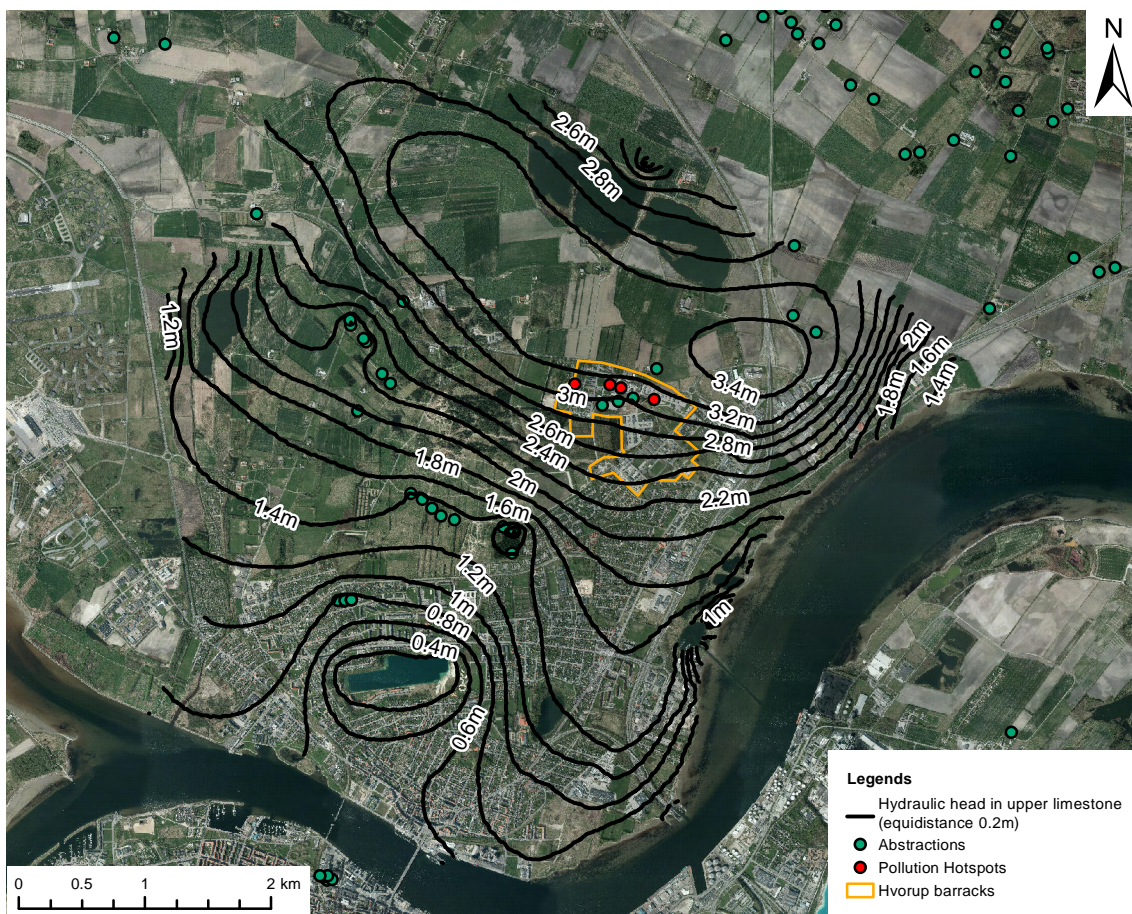


Figure 7.10. Hydraulic head in the upper limestone layer after calibration.

The observed hydraulic head compared to the calculated head is shown in figure 7.11. The variation in measured water table in the observations is also displayed. For the variation in measured water table the 5% highest and lowest measurements are excluded as they are evaluated by visual inspection to be errors.

Root mean square has dropped from 1.04 m to 0.63 m due to calibration. It's evaluated that the difference between calculated and observed head is acceptable. The greatest deviation between observation and calculation is the observation of 5.3 m. Unfortunately this measurement is close to Hvorup barracks as shown in figure 7.9 and is also the observation with the greatest hydraulic head. As such it is likely that the groundwater model underestimates the peak of groundwater table and the water table gradient between pollution sites and abstraction wells.

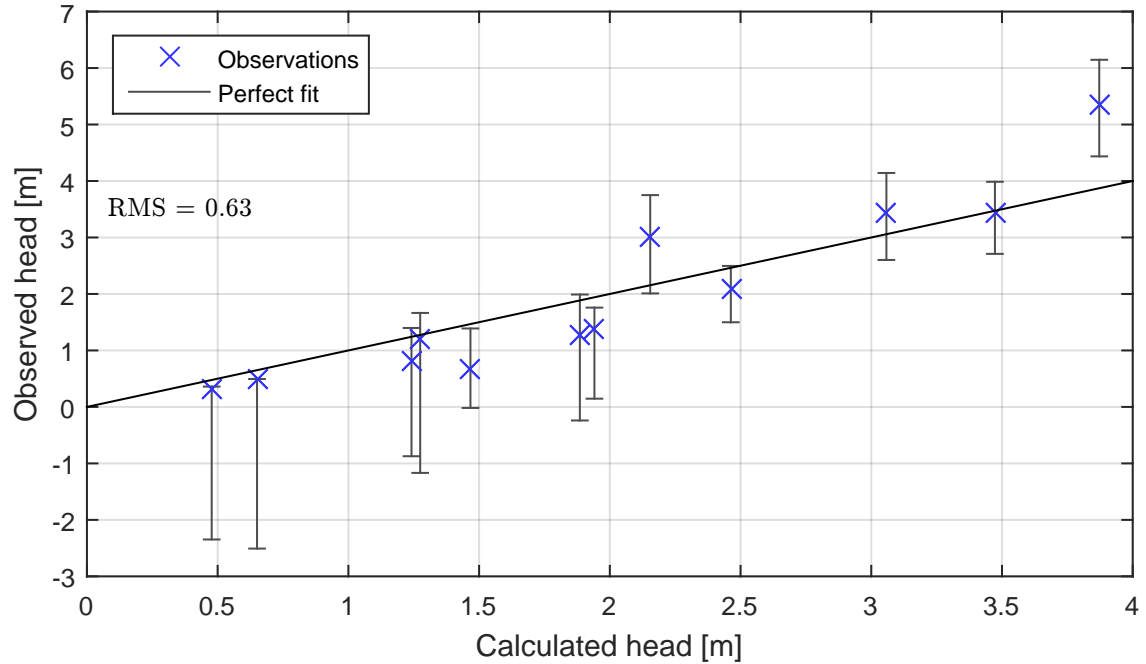


Figure 7.11. The hydraulic head in the observations compared to the calculated hydraulic head in the groundwater model

The values of the calibrated parameters are shown in table 7.6. The values of hydraulic conductivity for zone 1 and 2 are higher than zone 3, which fits with the intention of the zoning.

Table 7.6. The parameters after calibration

Conductance, Lindholm Å	$7.00 \cdot 10^{-10} \text{ m} \cdot \text{s}^{-1}$
Conductance, Lerbækken	$2.06 \cdot 10^{-10} \text{ m} \cdot \text{s}^{-1}$
Conductance, other streams	$4.43 \cdot 10^{-11} \text{ m} \cdot \text{s}^{-1}$
K_{sat} , zone 1	$3.36 \cdot 10^{-4} \text{ m}^2 \cdot \text{s}^{-1} \cdot \text{m}^{-1}$
K_{sat} , zone 2	$9.92 \cdot 10^{-4} \text{ m}^2 \cdot \text{s}^{-1} \cdot \text{m}^{-1}$
K_{sat} , zone 3	$1.81 \cdot 10^{-4} \text{ m}^2 \cdot \text{s}^{-1} \cdot \text{m}^{-1}$

7.1.3 Conclusion

The groundwater model has been calibrated. As all measurements of hydraulic head in the area have been used for the calibration, no measurements are available for validating the model.

The groundwater model is evaluated to be a good model for the project area, as the

difference in hydraulic head for most of the observations are inside the range.

Through further single-parameter manual calibration with the calibrated parameters as an outset, it has also become evident that no significant improvement in difference between calculated and observed head is possible by only changing a single parameter.

7.2 Transport model

The transport of contaminants is simulated using MT3DMS in conjunction with MODFLOW. MT3DMS is a transport model that can handle dispersion, sorption and biodegradation. The calibrated groundwater model is used to calculate the hydraulic head in the model area.

7.2.1 Input parameters

In order to limit the calculation time the model area for the MT3DMS is reduced. The new model area is shown in figure 7.12. It has two different model extents: One extent for the layers above the fractured limestone, around the pollution hotspot. And another extent in the fractured limestone from pollution hotspot to the water abstractions. It is evident that the horizontal spreading in the upper layers is very limited, which is why such a small model extent can be permitted.

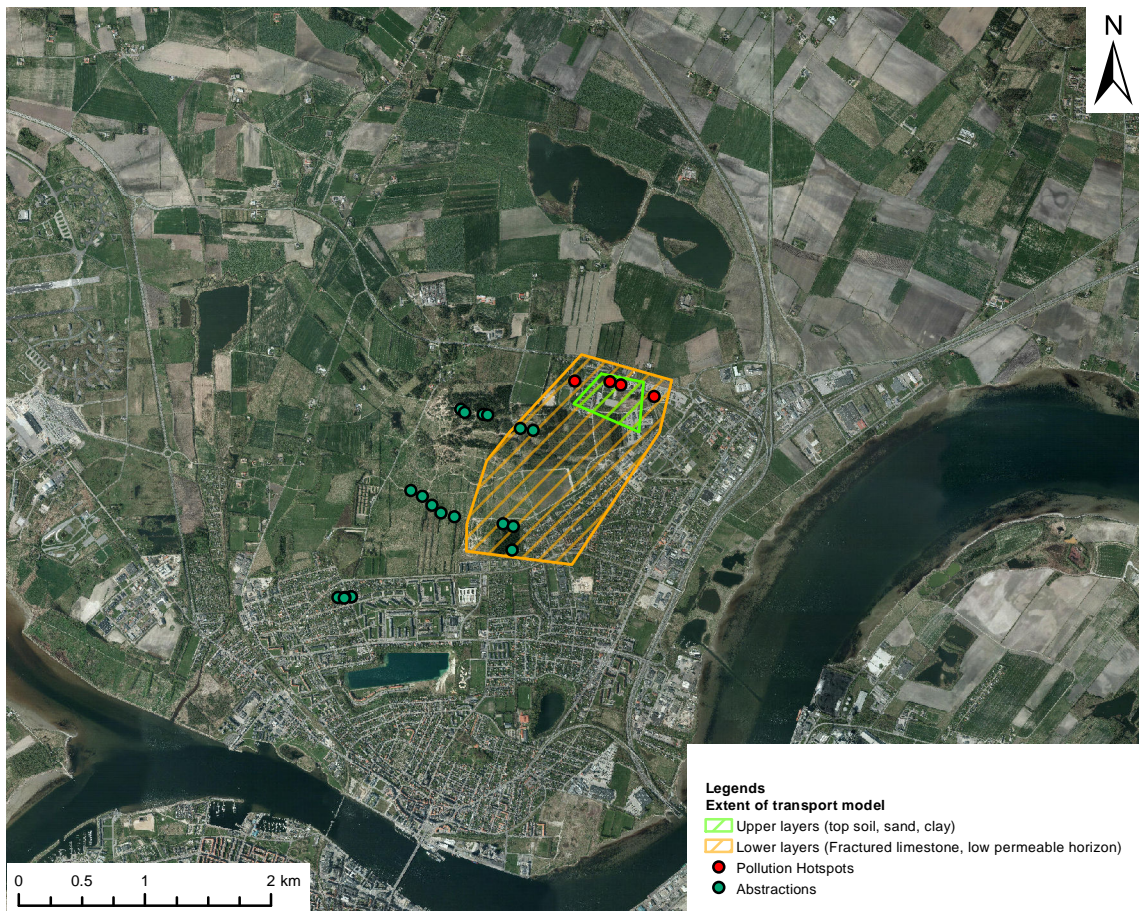


Figure 7.12. The extent of the transport model

The hydrocarbon measurement in pollution location C is used. Based on the analysis of the benzene content in chapter 2.4.1 page 9 it is assumed that the initial concentration is 22 mg/L. The pollution is inserted as a constant concentration at pollution site C in layer 2, as this is the location of the water table of the upper aquifer.

The parameters for the layers in the transport model are shown in table 7.7. The retardation in top soil, sand and clay are from sorption, calculated in chapter 4.6.2. The retardation in fractured limestone is from the diffusion between the immobile and mobile volume, calculated in chapter 4.6.3. The biodegradation is the average of all groundwater samples with no nutrition added nor any autoclaving while adjusted for anaerobic, nutrition limited conditions. It is assumed that the biodegradation is the same for top soil, sand, clay and fractured limestone and is unrelated to depth. The dual domain nature of fractured limestone is not taken into account. It is thus assumed that the biodegradation rate in the limestone matrix is the same as for the fissures.

The values for horizontal and vertical transverse dispersion are default values in GMS.

Table 7.7. The parameters for the transport model. (a) is calibrated in chapter 7.2.2

	Top soil & sand	Clay	Frac. limestone
Effective porosity [% cm ³ · cm ⁻³]	21	7	0.01
Retardation [-]	1.52	1.45	43
1st order biodegradation [d ⁻¹]	5.00 · 10 ⁻⁴	5.00 · 10 ⁻⁴	5.00 · 10 ⁻⁴
Horizontal dispersivity	0	0	(a)
Horizontal transverse dispersivity	0	0	10% of (a)
Vertical transverse dispersivity	0	0	1% of (a)

7.2.2 Calibration of longitudinal dispersion

As MT3DMS is a numerical solution it is subject to numerical dispersion. Numerical dispersion is not a phenomenon that occurs in reality. The analytical solution in chapter 6 page 49 does not have numerical dispersion, and is thus used as a measurement for what the dispersion in MT3DMS is supposed to be, due to field dispersivity. The transport model is calibrated so that it fits with a dispersivity relation of $\alpha/l = 0.01$, i.e. the same as the analytical model.

The longitudinal dispersivity in MT3DMS is adjusted so that the total dispersion fits the dispersion from the analytical solution. As it becomes evident that the pollution at Hvorup barracks is primarily transported to Nørre Uttrup well field, this will become the location where the dispersion is fitted.

The pollutant for the calibration starts in the limestone layer. Because of this the dispersivity in the other layers is not calibrated and will be assumed to be non-existent.

As the analytical model involves a direct transport path from Hvorup barracks to Nørre Uttrup well field, the distance that the pollutant has to travel is longer. In order to have the breakthrough occur at the same time, the distance for the analytical model is changed to 1650 m (up from 1409 m).

The breakthrough curve by assuming no dispersivity in the upper limestone layer is shown in 7.13. It shows that numerical dispersion is occurring, but is less than field dispersion in the analytical solution. Figure 7.14 shows the two breakthrough curves with a longitudinal dispersivity of 9 m. It is evident that the analytical model and MT3DMS have similar amounts of dispersion, and it is thus evaluated that this is a good fit.

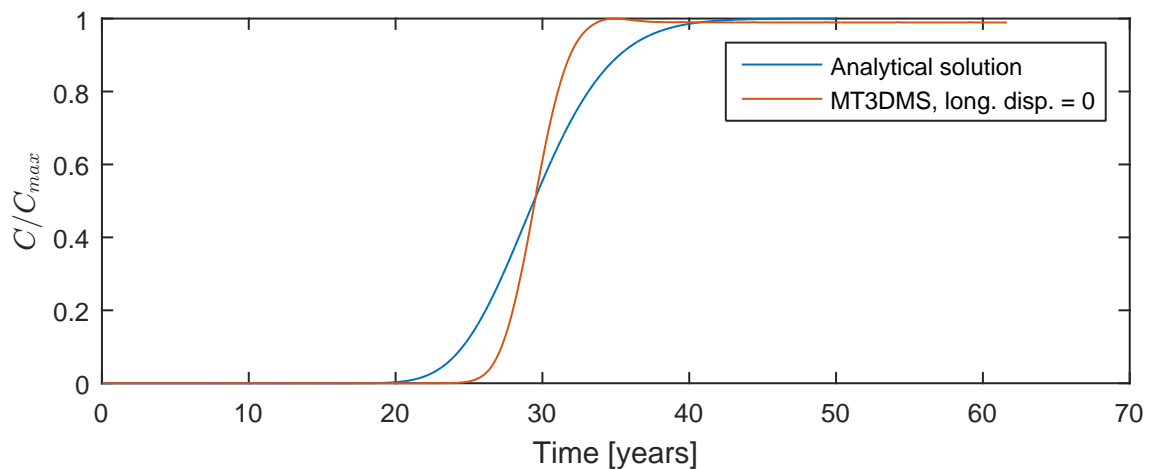


Figure 7.13. The breakthrough curve in Nørre Uttrup well from the MT3DMS model with a longitudinal dispersivity of 0 m compared to the analytical solution

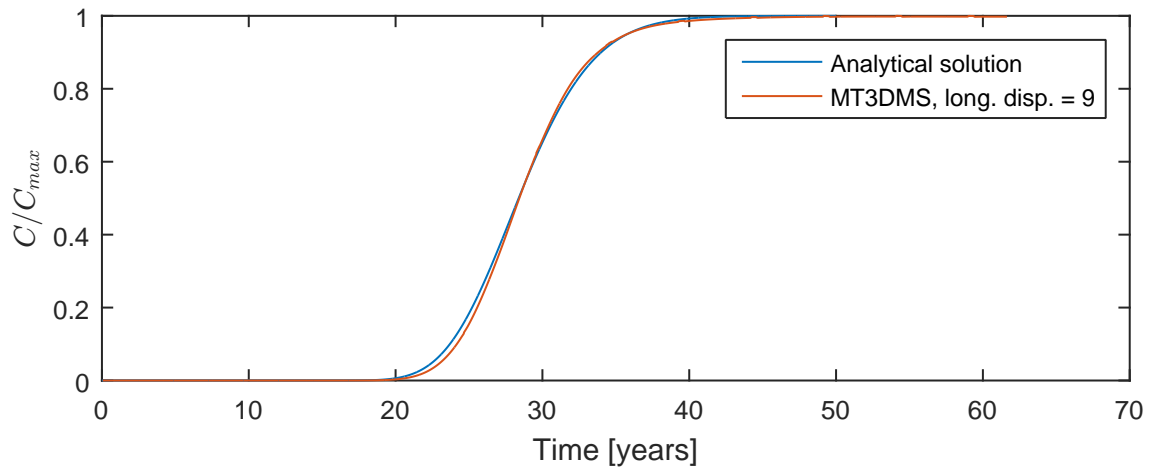


Figure 7.14. The breakthrough curve in Nørre Uttrup well from the MT3DMS model with a longitudinal dispersion of 9 m compared to the analytical solution

7.2.3 Results

The results from the transport model in layer 11, the upper fractured limestone from which the municipality abstracts drinking water, are shown in figure 7.15. It shows that the pollution is transported towards Nørre Uttrup well field and that the concentration in Nørre Uttrup well field does not exceed the limit for benzene in drinking water of $1 \mu\text{g} \cdot \text{L}^{-1}$ [Miljøministeriet, 2014].

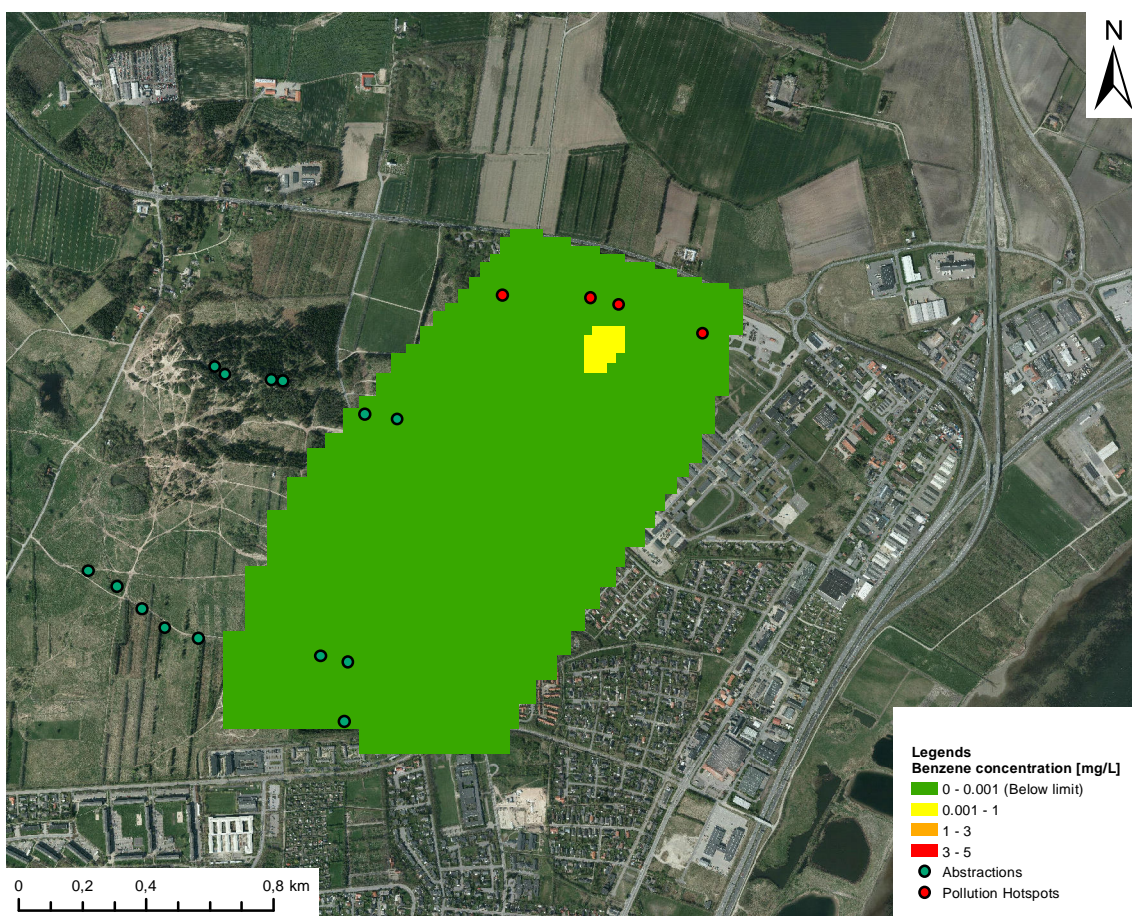


Figure 7.15. Benzene concentration in the fractured limestone with biodegradation

7.2.4 Parameter sensitivity

A sensitivity analysis on the parameters used in the calculation of hydraulic head is shown in figure 7.16. It shows that the hydraulic conductivity of the lower limestone as well as the conductance have a negligible influence on the concentration in Nørre Uttrup well. The values of anisotropy and hydraulic conductivity, however, impact the concentration in Nørre Uttrup well. It also shows that the values of anisotropy are more influential than horizontal hydraulic conductivity. As the values of anisotropy are just assumptions in this study, it is problematic in regards to a risk assessment.

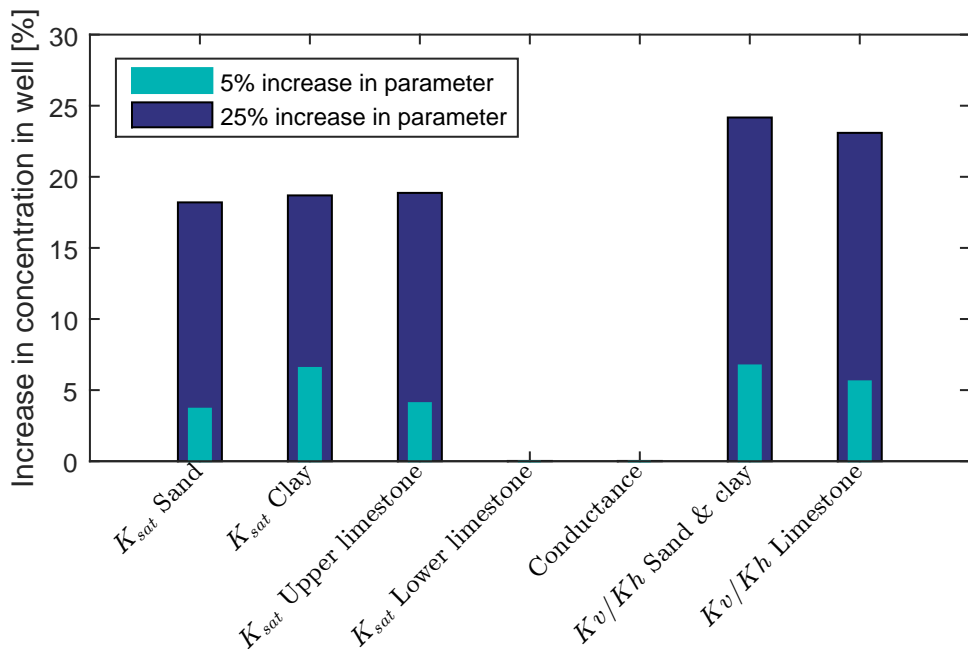


Figure 7.16. Benzene concentration in the fractured limestone with biodegradation

7.2.5 Discussion

The groundwater model is not stable enough to allow for a stochastic model. The effect of the uncertainties of the parameters on the numerical transport model are unknown. It can be expected that the uncertainties of the input parameters affect the numerical transport model somewhat the same as for the analytical model, however the hydraulic conductivity affects both the groundwater flow model and transport model, and its effect is thus greater for the numerical model.

The uncertainties of biodegradation for the analytical model, described in chapter 6.4, are present for the numerical model as well. The effect of the dual domain of fractured limestone on biodegradation can be implemented in the numerical transport model, but this has not been done due to time limitations.

The method of assembling the geological model is unknown. Assuming that it is based on interpolation of layer depths for soil profiles, the quality of the geological model is dependent on the amount of soil profiles. Especially the clay thickness is uncertain. In the analytical solution it was estimated that the thickness of the clay lens is 3 m at pollution site C, however the thickness of the clay lens in the geological model is between 7.5 and 11 m. The penetration of the clay lens is responsible for over half of the biodegradation in the analytical model, and the thickness of this lens is thus very important.

The calibrated hydraulic conductivity between pollution site and well field is lower than the one used in the analytical model by a factor of 3. As the method of calibration is likely not to be appropriate for finding the true hydraulic conductivity, this factor is still

very uncertain. The hydraulic conductivity is however close to the two measurements of hydraulic conductivity of fractured limestone that have been done south of Limfjorden.

It is also possible that if Nørre Uttrup well field is shut down the pollution will be transported to the relocated Lindholm well field instead. Indeed, because the flow path of the pollutant in the numerical model is likely to be very conditional, the transport from pollution site to the relocated well field can not be simply disregarded by flow paths from this model.

As the groundwater model is intended to be an alternative to the analytical model done in chapter 6 page 49, the results of the two models are compared. The comparison is shown in figure 7.17 where there's no biodegradation in any of the two models. It is evident that there's a significant reduction in pollution for the MT3DMS-model. This is due to recharge as well as transverse dispersion. This factor reduces the concentration in the abstraction well by a factor of about 22. It is thus evident that this dilution has a significant impact on the transport of chemicals.

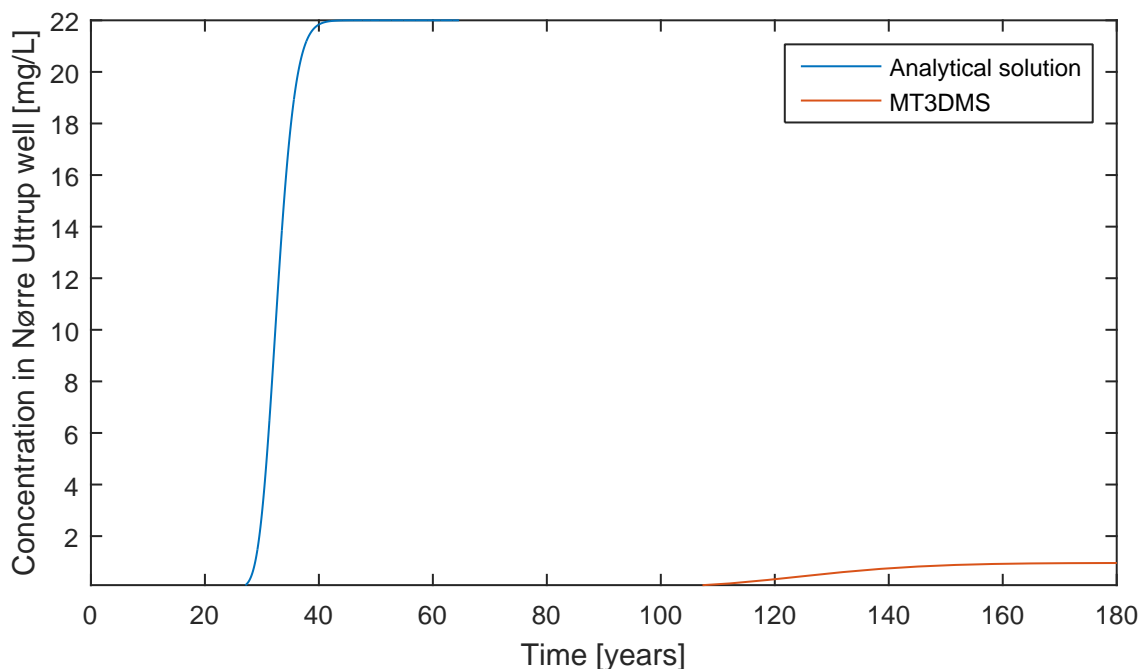


Figure 7.17. Comparison between analytical solution and MT3DMS

The results of the stochastic model for scenario 2 in the analytical model can then be adjusted to account for the dilution factor. The concentration in the abstraction well is divided by 22, and the result is shown in figure 7.18. It is evident that the dilution factor is not enough to say with certainty that the concentration does not exceed the limit for drinking water by the analytical solution.

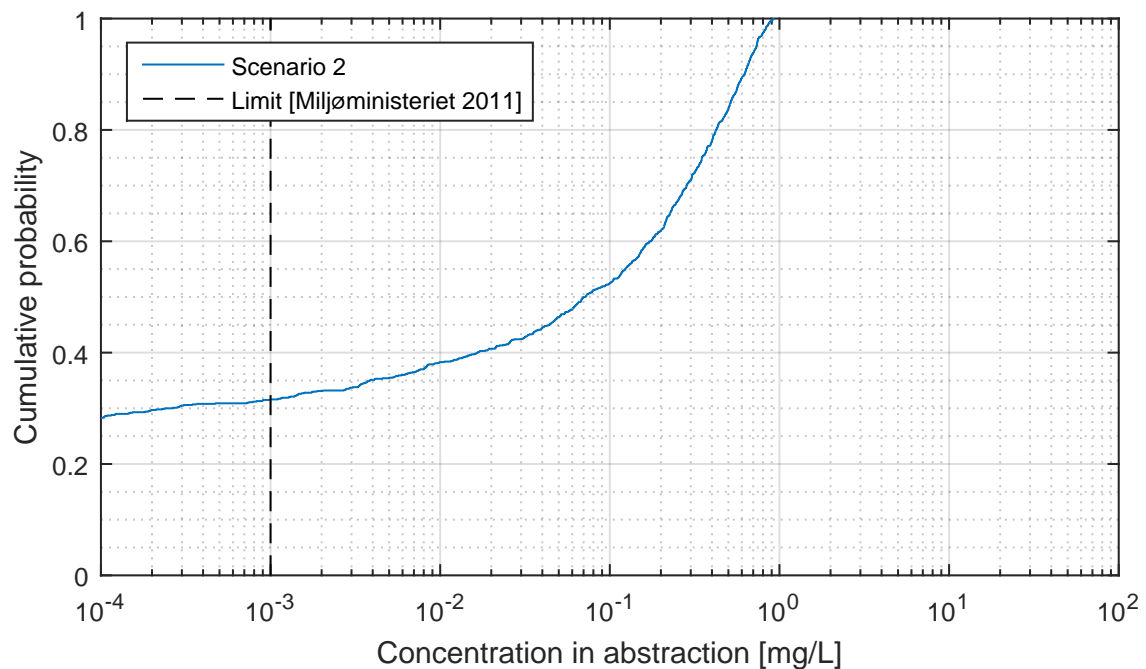


Figure 7.18. Comparison between analytical solution and MT3DMS

As the groundwater model includes more than the analytical model it is evaluated that it provides a more accurate description of the spread of concentration. It is thus evaluated that although the analytical model clearly shows that the concentration of pollution exceeds the limit for drinking water, this is because it underestimates the vertical transport time and excludes dilution. However because the properties of the clay lens as well as horizontal hydraulic conductivity are very uncertain, it can not safely be concluded that the pollution does not reach Nørre Uttrup well field. It can also not be concluded that the pollution does not reach the relocated Lindholm well field.

Part IV

Conclusion

8. Conclusion

Based on the investigation of transport of pollutant from soil to nearby buildings in Hvorup barracks it is concluded that there is a low risk of indoor air pollution at the canteen. However for the auto shop it is likely that the pollution concentration exceeds the limit for working area environment. It is possible that due to a high ventilation rate in the auto shop there is probably little accumulation of the contaminant in the air.

Based on the investigation of transport of pollutant from pollution site to Nørre Uttrup well field and the relocated Lindholm well field it is concluded that the contaminant is diluted, biodegraded, and retarded to the extent that the concentration of contaminant does not exceed the limit for drinking water.

It can be concluded that the Lindholm well field can be safely relocated to Hedeby plantation, as the pollutant at Hvorup barracks will not travel towards this location.

However due to the uncertainties of the input parameters for both the investigation of indoor air pollution and pollution of regional drinking water resource the conclusion is not unconditional.

Because of this it is suggested that the benzene concentration inside the buildings as well as the abstractions of the municipality is monitored frequently.

Bibliography

- Aalborg Forsyning, 2013.** Aalborg Forsyning. *Grønt regnskab 2013*, 2013. URL <http://www aalborgforsyning.dk/media/125712/groenne-regnskaber-2013-aalborg-forsyning-vand-as.pdf>.
- Aalborg Kaserner, 2011.** Aalborg Kaserner. *Velkommen til Aalborg Kaserner*, 2011. URL http://www.forsvaret.dk/trr/documents/trr/generel_velkomstfolder.pdf.
- Aalborg Kommune, 2013.** Aalborg Kommune. *Vandforsyningsplan 2013-2024 for Aalborg Kommune*, 2013. URL http://www.forsyningaalborg.dk/media/234133/vandforsyningsplan_2013-2024_-_vedtaget_plan.pdf.
- American Petroleum Institute, 2001.** American Petroleum Institute. *Alcohols and Ethers: A Technical Assessment of Their Application as Fuels and Fuel Components*. American Petroleum Institute, 2001.
- Arbejdstilsynet, 2007.** Arbejdstilsynet. *At-vejledning - Stoffer og materialer - C.0.1*, 2007. URL <http://arbejdstilsynet.dk/~/media/at/at/04-regler/05-at-vejledninger/c-vejledninger/c-0-1-graensevaerdilisten/c-0-1-graensevaerdilisten-2007%20pdf.ashx>.
- Brigitte et al., 2013.** Anne-Mette Brigitte, Nielsen Peter, Overvad Jensen, Søren Holm Andersen, Emil Aagaard Thomsen, Kristoffer Nielsen and Nicolai Midtiby. *Assessment of Pollutant Transport in OSD no. 33*. Aalborg University, 2013.
- Calver, 2001.** Ann Calver. *Riverbed permeabilities: Information from Pooled Data*. 2001.
- Claes, 2011.** Niels Claes. *Water and chemical transport in limestone*, 2011. URL http://projekter.aau.dk/projekter/files/52713292/final_thesis2.pdf.
- FBE, 2009.** Forsvarets Bygnings- & Etablissementstjeneste FBE. *581 Hvorup kaserne. orienterende forureningsundersøgelse*, 2009. URL http://www2.forsvaret.dk/temaer/groenneetablissementer/konkurrence/Documents/FBE-Gr%C3%B8netab_h%C3%A6fte2_aalborg_FINAL_WEB.pdf.
- FBE, 2010a.** Forsvarets Bygnings- & Etablissementstjeneste FBE. *581 Hvorup kaserne. orienterende forureningsundersøgelse*, 2010. URL <http://www aalborg.dk/media/3235025/hvorup-kaserne-tilladelse-monteringsboringer.pdf>.

-
- FBE, 2012.** Forsvarets Bygnings- & Etablissementstjeneste FBE. *581 Hvorup kaserne. supplerende forureningsundersøgelse ved varmcecentral*, 2012. URL
<http://www aalborg.dk/media/3235025/hvorup-kaserne-tilladelse-monteringsboringer.pdf>.
- FBE, 2010b.** Forsvarets Bygnings- & Etablissementstjeneste FBE. *581 Hvorup Kaserne - Supplerende forureningsundersøgelse*. 2010.
- Gelhar et al., 1992.** Lynn W. Gelhar, Claire Welty and Kenneth R. Rehfeldt. *A Critical Review of Data on Field-Scale Dispersion in Aquifers*, 1992. URL
http://www.cof.orst.edu/cof/fe/watershd/fe537/labs_2007/gelhar_et_al_reviewfieldScaleDispersion_WRR1992.pdf.
- GEUS, 2015.** GEUS. *JUPITER-databasen*, 2015. URL
<http://www.geus.dk/DK/data-maps/jupiter/Sider/default.aspx>.
- GEUS, 2011.** GEUS. *Kortlægning af kalkmagasiner*, 2011. URL
http://gk.geus.info/xpdf/geovejledning_8_kalk_final_net.pdf.
- Hansen, 1976.** Lorens Hansen. *Soil Types at the Danish State Experimental Stations*. 1976.
- Henriksen, 2015a.** Kaj Henriksen. *Lecture in soil and groundwater*. 2015.
- Henriksen, 2015b.** Kaj Henriksen. *Supervisor meeting*. 2015.
- Hsieh, 1994.** Dennis P. H. Hsieh. *Intermedia Transfer Factors for Contaminants Found at Hazardous Waste Sites: Benzene*, 1994. URL
<https://www.dtsc.ca.gov/AssessingRisk/Upload/benzene.pdf>.
- Johansen et al.** O. M. Johansen, M. L. Pedersen and J. B. Jensen. *Effect of groundwater abstraction on fen ecosystems*. Elsevier.
- Loll and Moldrup, 2000.** P. Loll and P. Moldrup. *Soil Characterization and Polluted Soil Assessment*. Aalborg University, 2000.
- Majid, 2006.** Editor Hassanizadeh S. Majid. *Theory and Applications of Transport in Porous Media, Vol. 20*. 2006.
- Miljøministeriet, 2014.** Miljøministeriet. *Bekendtgørelse om vandkvalitet og tilsyn med vandforsyningssanlæg*, 2014. URL
<https://www.retsinformation.dk/forms/r0710.aspx?id=160400>.
- Nielsen et al., 2013.** Anne-Mette Brigitte Nielsen, Peter Overvad Jensen, Søren Holm Andersen, Emil Aagaard Thomsen, Kristoffer Nielsen and Nicolai Midtiby. *Assessment of Pollutant Transport in OSD no. 33*. 2013.
- Nielsen et al., 2015.** Emil Nielsen, Niels Fræhr, Claus Liltorp and Victor G. Ludvigsen. *Sewer system in Svenstrup*. Aalborg University, 2015.

- Niras, n.d.** Niras. *Potential map*. n.d.
- Price et al., 1993.** M. Price, R. A. Downing and W. M. Edmunds. *The Chalk as an Aquifer*. 1993.
- Sander, 1999.** R. Sander. *Compilation of Henry's Law Constants for Inorganic and Organic Species of Potential Importance in Environmental Chemistry*. Unpublished, 1999.
- Scharling M., 2002.** C. Kern-Larsen Scharling M. *Klimagrid Danmark, Nedbør og fordampning 1990–2000, Beregningsresultater til belysning af vandbalancen i Danmark*. Tech. Rep. 02-03. Danish Meteorological Institute, 2002.
- Spitz and Morene, 1996.** Karlheinz Spitz and Joanna Morene. *A practical guide to groundwater and solute transport modelling*. (ISBN: 987-0-471-13687-5), 1996.
- Stockmarr, 2005.** J. Stockmarr. *Groundwater quality monitoring in Denmark*. Bull. Geol Surv. Denmark and Greenland, 7, 33-36, 2005.
- Thomsen et al., 2004.** R. Thomsen, V. H. Søndergaard, Sørensen and Kurt Ingvard. *Hydrogeological mapping as a basis for establishing site-specific groundwater protection zones in Denmark*. Hydrogeology Journal, 2004.
- van Genuchten and Alves.** M. Th. van Genuchten and W. J. Alves. *Analytical Solutions of the One-Dimensional Convective-Dispersive Solute Transport Equation*.
- Vejdirektoratet, 2011.** Vejdirektoratet. *3. Limfjordsforbindelse - VVM-redegørelse »> Miljøvurdering - Del 2*, 2011. URL [http://www.vejdirektoratet.dk/DA/vejprojekter/limfjorden/Documents/Rapport380_milj%C3%B8_2\[1\].pdf](http://www.vejdirektoratet.dk/DA/vejprojekter/limfjorden/Documents/Rapport380_milj%C3%B8_2[1].pdf).
- Vert et al., January 2012.** M. Vert, Y. Doi, K.H. Hellwich, M. Hess, P. Hodge, P. Kubisa, M. Rinaudo and F. Schué. *Terminology for biorelated polymers and applications (IUPAC Recommendations 2012)*. 84, 377–410, 2012. doi: 10.1351/PAC-REC-10-12-04. URL <http://www.degruyter.com/view/j/pac.2012.84.issue-2/pac-rec-10-12-04/pac-rec-10-12-04.xml>.

Part V

Appendix

Appendix A

Soil and hydrological properties

The data used for estimating the soil and hydrological properties are presented in this appendix. The soil and hydrological properties of sand and clay as well as fractured limestone are all originate from literature. Own measurements of soil properties and small scale hydrological properties of fractured limestone are also included.

A.1 Hydraulic conductivity

Multiple sources for hydraulic conductivity of the soils are used. The full data set is shown in table A.1 . The location of the five sampling sites is shown in figure A.1.

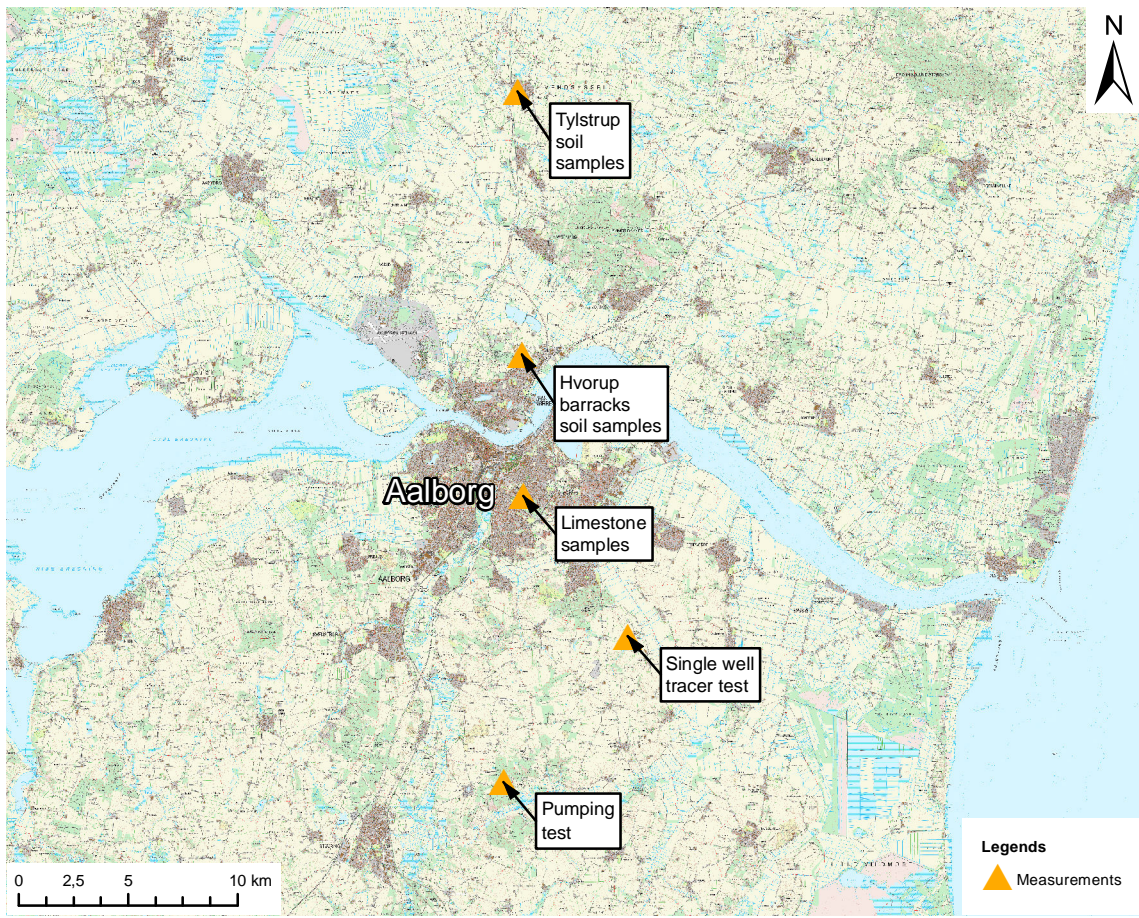


Figure A.1. Location of the five sampling sites.

Table A.1. Values of horizontal saturated hydraulic conductivity from literature and experiments close to or inside Hvorup barracks. STD: Standard deviation. A ? denotes that this is unknown.

Literature			
Soil type	Range of K_{sat} [$\text{m} \cdot \text{s}^{-1}$]		Reference
Sand	4.75 -	$9950 \cdot 10^{-6}$	Spitz and Morene [1996]
Clay	0.1 -	$4720 \cdot 10^{-10}$	Spitz and Morene [1996]
Limestone	4.72 -	$943 \cdot 10^{-12}$	Spitz and Morene [1996]
Fractured limestone	1.8 -	$47.5 \cdot 10^{-4}$	Spitz and Morene [1996]
Measurements on top soil (sand) in Hvorup Barracks			
Test type	K_{sat} [$\text{m} \cdot \text{s}^{-1}$]	(STD)	Reference
Constant head	$8.59 \cdot 10^{-6}$	$(1.07 \cdot 10^{-6})$	3-22 (2015)
Constant head	$8.17 \cdot 10^{-6}$	$(1.80 \cdot 10^{-6})$	3-22 (2015)
Constant head	$1.42 \cdot 10^{-5}$	$(2.33 \cdot 10^{-6})$	3-22 (2015)
?	$3.30 \cdot 10^{-5}$	$(1.90 \cdot 10^{-5})$	3-16 (2014)
Constant head	$1.83 \cdot 10^{-5}$		D012 (2013)
Slug test	$1.07 \cdot 10^{-5}$		D012 (2013)
Measurements on top soil (sand) in Tylstrup			
Test type	K_{sat} [$\text{m} \cdot \text{s}^{-1}$]	(STD)	Reference
?	$2.43 \cdot 10^{-5}$	$(1.44 \cdot 10^{-5})$	Hansen [1976]
Measurements on top soil (clay) in various locations in Denmark			
Location	K_{sat} [$\text{m} \cdot \text{s}^{-1}$]	(STD)	Reference
Askov	$4.7 \cdot 10^{-5}$		Hansen [1976]
Roskilde	$7 \cdot 10^{-6}$	$(1 \cdot 10^{-6})$	Hansen [1976]
Rønhave	$6 \cdot 10^{-6}$		Hansen [1976]
Blangstedgaard	$3.3 \cdot 10^{-5}$	$(1.3 \cdot 10^{-5})$	Hansen [1976]
Silstrup	$2.9 \cdot 10^{-5}$	$(1.4 \cdot 10^{-5})$	Hansen [1976]
Ødum	$8.5 \cdot 10^{-6}$	$(7.1 \cdot 10^{-7})$	Hansen [1976]
Tystofte	$9.5 \cdot 10^{-6}$	$(7.1 \cdot 10^{-7})$	Hansen [1976]
Large scale measurements of deep fractured limestone			
Test type	K_{sat} [$\text{m} \cdot \text{s}^{-1}$]	(Range)	Reference
Single well tracer test	$9 \cdot 10^{-4}$		Claes [2011]
Pumping test	$2.6 \cdot 10^{-4}$	$(1.7 \cdot 10^{-4} \text{--} 3.9 \cdot 10^{-4})$	Jøphansen et al. [2011]

A.2 Soil properties of soils from Tylstrup, Roskilde and Golfparken

Soil and hydrological properties of a sandy soil from Tylstrup, a clay soil from Roskilde as well as fractured limestone from Golfparken are presented. The measurements of the limestone from Golfparken are done by the project group. However because of unreliable results of the limestone, literature values are presented for this as well.

The hydraulic conductivity as well as organic carbon content appear in the tables as calculated values. The method of calculation is denoted with these symbols:

† The mean is calculated by weighting the values by the thickness of the soil layer they were measured for.

‡ The organic carbon content f_{oc} is calculated based on the empirical relationship presented by *Romano and Santini* (1997)

$$f_{oc} = 0.58 \cdot f_{OM}$$

The average vertical hydraulic conductivity is the weighted harmonic mean:

$$\bar{K} = \frac{\sum_{i=1}^n z_i}{\sum_{i=0}^n \frac{z_i}{K(z_i)}}$$

where

n	number of layers
z_i	thickness of layer i (weighting factor)
$K(z_i)$	Hydraulic conductivity at depth z_i

The pore sizes are divided into groups according to:

ϕ_{macro}	macro-pores	$> 30 \text{ }\mu\text{m}$
ϕ_{meso}	meso-pores	$30 - 0.2 \text{ }\mu\text{m}$
ϕ_{mini}	mini-pores	$< 0.2 \text{ }\mu\text{m}$

Particle density and bulk density are denoted ρ_s and ρ_b respectively.

Sandy soil from Tylstrup

Table A.2. Particle size distribution (Tylstrup) and organic content after [Hansen, 1976]
Particle size and organic content

Depth [cm]	Clay	Silt	Fine sand	Coarse sand	f_{OM}	$f_{OC} \ddagger$	Units
0-28	3.7	6.2	75.8	12	2.3	1.33	[% g · g ⁻¹]
28-52	4.4	8.4	75.7	9.7	1.8	1.04	[% g · g ⁻¹]
52-76	7.6	5.9	81.2	4.5	0.8	0.464	[% g · g ⁻¹]
76-100	2.9	2.3	93.6	0.2	0.4	0.232	[% g · g ⁻¹]
mean †	4.61	5.72	81.34	6.82	1.36	0.79	[% g · g ⁻¹]

Table A.3. Water retention measured at indicated negative pressure cm H₂O head and vertical saturated hydraulic conductivity (Tylstrup) after [Hansen, 1976]

Water retention									
Depth [cm]	0	16	50	100	150	500	1500	15000	K_s [cm · h ⁻¹]
0-28	0.441	0.402	0.381	0.294	0.219	0.177	0.137	0.023	6.84
28-52	0.540	0.431	0.345	0.234	0.155	0.122	0.092	0.051	15.12
52-76	0.435	0.340	0.307	0.234	0.158	0.128	0.106	0.069	2.88
76-100	0.483	0.434	0.414	0.277	0.096	0.057	0.039	0.027	10.08
mean †	0.473	0.402	0.362	0.261	0.159	0.123	0.0952	0.0417	6.099 #

Table A.4. Densities and pore size distributions (Tylstrup) after [Hansen, 1976]

Density and porosity

Depth cm	ρ_s [g · cm ⁻³]	ρ_b [g · cm ⁻³]	ϕ_{macro} [% v/v]	ϕ_{meso} [% v/v]	ϕ_{mini} [% v/v]	ϕ_{tot} [% v/v]
0-28	2.61	1.39	14.6	22.2	7.3	44.1
28-52	2.67	1.24	30.5	18.4	5.1	54.0
52-76	2.69	1.58	20.1	16.5	6.9	43.5
76-100	2.67	1.4	20.6	25	2.7	48.3
mean †	2.66	1.40	21.18	20.59	5.72	47.34

Clay soil from Roskilde

Table A.5. Particle size distribution (Roskilde) and organic content after [Hansen, 1976]
Particle size and organic content

Depth[cm]	Clay	Silt	Fine sand	Coarse sand	f_{OM}	$f_{OC} \ddagger$	Units
0-27	10.1	22.8	57.7	6.8	2.6	1.51	[w/w]%
27-50	18.6	17.0	61.10	2.7	0.6	0.35	[w/w]%
50-80	18.2	18.5	62.0	0.8	0.5	0.29	[w/w]%
80-100	27.6	24.40	46.4	1.1	0.5	0.29	[w/w]%
mean †	17.98	20.50	57.51	2.92	1.09	0.61	%[w/w]

Table A.6. Water retention measured at indicated negative pressure cmH_2O head and vertical saturated hydraulic conductivity (Roskilde) after [Hansen, 1976]

Water retention									
Depth[cm]	0	16	50	100	150	500	1500	15000	K_s [cm · h ⁻¹]
0-27	0.429	0.393	0.358	0.314	0.297	0.250	0.216	0.096	4.32
27-50	0.453	0.417	0.378	0.332	0.313	0.272	0.235	0.139	0.72
50-80	0.450	0.426	0.387	0.349	0.330	0.289	0.255	0.194	2.88
80-100	0.450	0.426	0.404	0.389	0.383	0.364	0.339	0.271	2.16
mean †	0.445	0.415	0.380	0.343	0.328	0.289	0.257	0.170	1.728 #

Table A.7. Densities and pore size distributions (Roskilde) after [Hansen, 1976]

Density and porosity

Depth cm	ρ_s [g · cm ⁻³]	ρ_b [g · cm ⁻³]	ϕ_{macro} [% v/v]	ϕ_{meso} [% v/v]	ϕ_{mini} [% v/v]	ϕ_{tot} [% v/v]
0-27	2.59	1.41	11.5	22.4	9.0	42.9
27-50	2.67	1.54	12.1	19.3	13.9	45.3
50-80	2.67	1.57	10.1	15.5	19.4	45.0
80-100	2.70	1.58	6.1	11.8	27.1	45.0
mean †	2.65	1.52	10.14	17.50	16.87	44.50

Limestone from Golfparken

Samples of limestone were collected from Golfparken, as shown in figure A.1. For all of the samples experiments were conducted to measure macroporosity, bulk density and particle density. For three of the samples a constant head experiment was conducted to get the small scale hydraulic conductivity. The methods are explained in appendix B page 113.

The results are shown in table A.8 for porosity and densities and table A.9 for saturated hydraulic conductivity.

Table A.8. Measured Limestone soil properties

Sample #	sat mass [g]	oven dry mass [g]	ϕ_{tot} †[cm ³ · cm ⁻³]	ρ_s ‡[g · cm ⁻³]	ρ_b § [g · cm ⁻³]
S4	171.08	126.14	0.45	2.33	1.29
S5	172.51	129.24	0.43	2.32	1.32
S6	165.60	124.21	0.41	2.15	1.27
S7	170.57	127.01	0.43	2.29	1.29
S8	167.25	123.99	0.43	2.22	1.26
S9	163.71	121.67	0.42	2.13	1.24
S10	164.96	123.34	0.41	2.15	1.26
S11	163.89	121.40	0.42	2.15	1.24
S12	171.41	128.46	0.43	2.29	1.30
mean	166.86	124.31	0.42	2.20	1.27

The total porosity, particle density and bulk density appear in the tables as calculated values. The method of calculation is denoted with these symbols:

† Assumption: Total water content equals total void space (temperature corrected)

‡ from $\phi_{tot} = 1 - \frac{\rho_s}{\rho_b}$

§ from (dry mass)/(total volume) of sample

Table A.9. Measurements of saturated hydraulic conductivity

Sample #	Δh [cm]	T [K]	Q [cm ³ · s ⁻¹]	K_s [cm · s ⁻¹]	K_s [cm · h ⁻¹]
KI	200	294.15	1.803	0.002295	8.263
KII	100	294.45	1.716	0.004369	15.731
KIII	100	294.75	0.855	0.002177	7.837

The effective porosity ϕ_{eff} and the organic content were not measured. The values are retrieved from [Claes, 2011] instead. The values are shown in table A.10.

Table A.10. ϕ_{eff} from Claes (2011), f_{OC} from Janniche (2010)

Sample #	ϕ_{eff} [cm ³ · cm ⁻³]	f_{OC} [-]
a	0.17	0.001-0.005
b	0.26	
c	0.09	
d	0.14	
e	0.12	
mean	0.156	

The secondary porosity or fissure porosity for fractured limestone is shown in A.11.

Table A.11. Fissure porosity of fractured limestone

Fissure porosity [% cm ³ · cm ⁻³]	Reference
0.01	[Price et al., 1993]
0.001 - 1	[GEUS, 2011]

Appendix B

Methods

B.1 Collecting Soil Samples

During several field trips, intact soil samples were collected. The method to perform the sampling is described hereunder.

The equipment used for collecting the intact soil samples were:

- Hammering head
- Metal ring
- Hammer

Hammering head sample ring method of soil collection is done manually. Before the samples were collected, it was necessary to establish the depth of the holes, which was measured using a folding wooden scale. Next the guide cylinder was placed at the desired depth of sampling.

The hammering head with the metal ring inside were placed on top of the soil. The hammering head was held firmly to avoid vibrations. It was then hit with the hammer until the line of the metal ring is almost covered by soil. The sample was then removed from the soil with the use of a tiny garden shovel. The excess of limestone was carefully removed from the soil the use of the garden shovel, assuring that the soil is in undisturbed state. The lids were then put on the top and bottom of the sample to prevent the soil from moving out of the ring.

Top layer samples The samples were collected at Hvorup barracks, during the *Mini-Project*, part of the module *Experimental Hydrology* in autumn 2015.

Limestone Samples The total depth of the pit was 125 cm. In total 10 vertical and three horizontal samples were taken.

The collected soil samples are used to get information about particle size distribution, organic matter content, porosity and hydraulic conductivity.

B.2 Sieving analysis

The purpose of the sieving analysis is to determine the particle size distribution of soil samples and to achieve basic textural knowledge about the soil. From the particle size distribution curve the hydraulic conductivity can be estimated.

B.2.1 Setup

The procedure is based on and further described in the standard DS/CEN ISO/TS 17892-4. A grain size analysis is done by determining the weight related distribution of the soil grains according to size in the sand and gravel fraction (0.06 mm – 60 mm).



Figure B.1. Sieving Tower

The grain size is defined as the mesh width of the finest square sieve, through which the particle can pass.

Apparatus:

- Sieves, mesh widths must provide an indicative description of the material, smallest mesh width should be 0.063 mm
- Shaker machine
- Scale, weight accuracy, 0.1 g

- Sieve brush
- Bowls in corrosion resistant material
- Pressure sprayer/liquid sprayer
- Tub with sieve holder
- Drying oven for 50 and 105°C, respectively

Equipment calibration

The sieves do not need to be calibrated before execution of experiment. However, these should be checked for flaws in the mesh such as holes or remaining particles. The sieves must be calibrated annually in order to prove the actual mesh width, and it must be documented that the mesh width lies within what is approved for the sieve in question. The calibration is done by means of calibration balls designed especially for the particular mesh width. Preparing test sample If more than 90% of the particles are larger than 0.063 mm, a screening must be done. If more than 10% of the particles are smaller than 0.063 mm, a hydrometer analysis must be done. If an overall grain curve is wanted, both experiments must be carried out. The necessary weight of soil used for the test depends on the estimated d_{90} (the mesh width through which 90% of the material can pass). A sample size is weighed (W) and dried at 105°C to a constant weight.

- The sample is placed in the vacuum desiccator after which it is weighed (W_s) (Dry weight A) when it has reached room temperature, and the water content is determined.
- The dry sample is placed in a bowl, tray or tub where it is covered with water. The sample must stand for at least 1 hour with regular stirring of the sample.
- For sample with particles larger than 5 mm, it can be necessary to part the sample and treat the coarse particles separately.
- A parts of the sample (max. 150 g) is placed on a 2 mm sieve under which a 0.063 mm sieve is placed. It is important that there is only the sample amount on each sieve which it can carry which is why it may be necessary to wash out more than once.
- With the pressure sprayer, wash until the water running down on the 0.063 mm sieve is clear. If necessary, stir lightly in the sample with a brush or spatula, figure B.5.
- The part of the sample on the 0.063 mm sieve is washed out, figure B.6. If there is more sample than appropriate, remove some of the sample and save it in a bowl, and the wash out can be done in several steps. No pressure should be applied to the 0.063 mm sieve. If stirring of the sample is needed, do so lightly with a soft brush.
- The sample on the sieve is washed out until the water running from it is completely clear. The washed out sample is collected in a tub.
- Remnant on the sieves is collected and dried at 105°C until a constant weight is achieved.
- If the washed out sample is being used for hydrometer, the water amount can be reduced at max. 50°C.

-
- If the washed out sample is not going to be used, it is dried at 105°C until a constant weight is achieved (W3).
 - When the sample has a constant weight, it is put in the vacuum desiccator until the temperature reaches room temperature.
 - The dried sample is weighed (W1).
 - If a hydrometer analysis is being done on the washed out samples, de-ionized water must be used for the wash out or the wash out can be done with tap water.

The soil samples used in the sieving analysis were oven dried samples. The soil samples have been dried for 24 hours at 105°C and afterwards cooled for one hours in the vacuum desiccator. The samples were covered and stored in a closed plastic box at room temperature until the sieving analysis. The experiment and sample preparation were conducted as the particle guide uk (2015) on moodle.aau dictates. Procedure for experiment Coarse screening Coarse screening must be done if the sample is estimated to have particles over 16 mm. Coarse screening is done on sieves 63, 32 and 16 mm.

- The dried sample is crumbled by hand so that any clumps are crushed.
- The sample is screened for 20 min. in the shaker machine.
- The content remaining on the sieves is weighed.
- The screenings from the 16 mm sieve is weighed (W2) (Dry weight B) and saved for fine screening.

Fine screening The fine screening is usually done with the 8, 4, 2, 1, 0.5, 0.25, 0.125 and 0.063 mm sieves. In case of very uniform samples, other sieves can be used. The screenings from the 16 mm sieve is used for fine screening. Should coarse screening not be necessary, the entire sample from the wash out will be used, and, and W1 and W2 are therefore the same.

- Above-mentioned sieves are collected in consecutive order, and the sample is poured onto the 8 mm sieve or the sieve with the largest mesh width.
- The sieve tower is placed in the shaker machine and screened for 20 min.
- The screening remnants on each sieve are transferred to bowls and weighed.
- Tap a couple of times on the side of each sieve until it is removed so that any remnants fall through.
- Each sieve is placed with the bottom up on a large piece of paper, and the backside is lightly brushed off so that particles sitting in the mesh have loosened. On the sieves 0.5 mm and under, brushing must only be done lightly with a soft brush.

Sieve remnants on each sieve must not exceed specified values. Is this the case, the total sample is divided into smaller parts, and each part is screened individually, and the sieve remnants are the collective amount on each sieve. If the screenings on sieve 0.063 mm exceed by a few per cent, it is indicative that the wash out has been incomplete or that the specific sieve is defective. Experimental equipment: Sieves, shaker machine, scale and sieve brush. The samples were gently crushed by hand until the samples were homogeneous. The sample size was determined from the D90 estimation to around 100g (particle guide

uk). The appropriate sieving tower (see appendix) was cleaned and the sample was added to the top sieve. The mesh size ranged from 12mm to 0,063mm. The sieving tower was placed in the shaker machine for 20 min. Thereafter the sieve content was weighted and registered. Calculations Screenings on the 64, 32 and 16 mm sieves are calculated in % of A. The screenings from the fine screening are calculated in % of B. The values found are divided by 100 and multiplied by the percentage of screenings on the 16 mm sieve by which the screenings are stated in % of A. Reporting The screenings on each sieve in % of the dry weight of the total sample A, is plotted into a coordinate system as a function of the sieve dimension. The screening percentages are plotted in the y-axis in an arithmetic scale, and the sieve dimensions in the axis of abscissas in a logarithm scale.

B.3 Suction Box

It can be separated in three major classes, the macro-porosity, the meso-porosity and the micro-porosity, each of those having completely different functions and properties regarding fluid transport. The macro-porosity is the fraction of the total porosity with pores larger than $30 \mu\text{m}$. In terms of potentials, it is the fraction of pores that is emptied at a negative pressure of $\text{pF} = 2$, or $-100 \text{ cm H}_2\text{O}$. It can also be referred to as the air content at field capacity, thus very important when dealing with gas transport through porous medium. The meso-pores are the water filled pores at field capacity up to a pF of 4.2, the permanent wilting point. In the saturated zone, the macro-porosity is, together with the meso-porosity, responsible for the fluid movement. The micro-pores contain the residual water, the fraction of the water that is coated to the minerals.



Figure B.2. Sample

All intact samples were weighted and placed in a box on top of fully water saturated kaolinite clay for 120 hours. During this time the samples were becoming fully saturated. Before being placed in the box the lids were removed from the samples and white pieces of cloths were placed on the bottom of the sample cylinders and fastened with rubber rings to prevent the samples from being disturbed.



Figure B.3. Vacuum Pump

After this the samples were weighed again and placed in the suction box with a suction level of -100 cm . A foil tray with water was also in the box to ensure that the box remained moist.

A sand/kaolin box from AAU Laboratory is used soil parameter measurements. The apparatus consists of the following parts, referring to B.4.

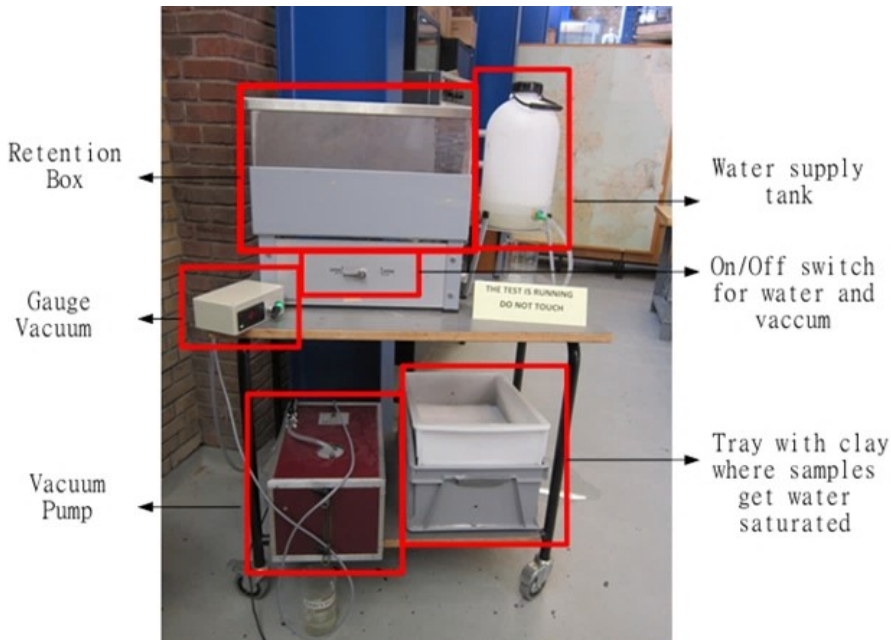


Figure B.4. Retention Box

Retention box contains a layer of kaolinite, which is saturated with water from the water tank to the right of the box. By applying the water-saturated clay, a vacuum corresponding to -100 cm of water drained soil samples for water in the macro-pores. In the box there is located a water recipient to ensure that the air is saturated with water, so that the samples and the clay do not dry out.



Figure B.5. Pressure gauge

The vacuum pump controls the amount of vacuum applied to the vacuum compartment. To control box with a vacuum gauge is used to adjust the vacuum needed. A vacuum of -100 cm water column is applied as seen in figure B.5. First vacuum pump is turned on

by turning the switch on the vacuum gauge. To put the retention box under vacuum to open / close mechanism of the front of the adult may be turned to the left.



Figure B.6. Water tank

The clay in vacuum box must be regularly saturated to ensure a proper vacuum and that cracks do not generate in the clay. This is done by turning off the vakummet and turning the opening / closing mechanism to the right. This offset the hydraulic pressure level between the water container and clay in the vacuum box. Therefore, it is necessary to add demineralized water to the container up to the green bar as indicated in figure B.6. If filling is more water than indicated by the score there is a risk that there is free water in the vacuum box. During waterlogging can vacuum pump drained by opening the top valve slowly. Next, the bottom valve is opened.

After drainage of soil samples in the vacuum box at -100 cm water column is the left term of the amount of water bound in the micropores, whereby the effective porosity is similar to the air-filled voids in the soil sample. Thereby, the effective porosity is determined by difference between the total porosity and the volumetric water content

Preparation of soil samples and apparatus operation

- Each 100 cm³ metal cylinder is weighed and the weight is noted.
- The unsaturated saturated samples are weighed. The weight is recorded.
- Pre-weighed plastic caps are mounted on the end of each cylinder. The tapered end of the cylinder is covered with a pre-weighed piece of filter material kept in place by a rubber O-ring with known weight.

- The samples are placed in a wetting box and saturated slowly. The saturated samples are weighed again.
- The kaolin surface is moistened lightly with a wet sponge.
- The samples are placed in the sand/kaolin box with the filter end placed downwards. Each cylinder is pressed lightly into the kaolin to create a maximum level of contact between kaolin and sample.
- A lid is placed on the box to prevent unnecessary evaporation.
- Weigh the samples every day until the weight of each sample changes less than 0.2 grams between two successive weighings. Equilibrium is now established and the resulting weight is recorded.

B.4 Constant head

The constant head method is used to determine the saturated hydraulic conductivity, based on Darcy's law.

The constant head experiment was conducted with the use of the constant head apparatus. It consists of:

- Constant head permeability cell
- Stand panel
- Constant level tank
- Pump
- Balance

The intact samples collected from the site were placed inside the constant head permeability cell. Firstly the metal ring was placed sharp end into one part of the permeability cell, making sure that the filters and rubber rings are placed, making it a tight fit to avoid any leakages and stop air entry from the outside. Next the second part of the permeability cell was placed on the opposite side of the metal ring. The top and bottom parts of the permeability cell were fastened tightly with screws. The samples were then placed in a stand panel, and the plastic tubes were connected to the top and bottom of the sample. Before every experiment, the water level was refilled in the constant level tank, and the temperature of the water was measured. The tank was then placed at the desired height. The next step was to saturate the soil sample. Firstly, the glass beaker was filled with water and the metal pipe of the constant head apparatus was submerged. The pump was switched on and the valves going from the top of the panel stand were opened, making sure that the last valve was opened half way carefully, to control the pressure. After the processes started, the air leaving the sample was visible in the form of the air bubbles in the upper plastic tube. Once there was no air exiting the sample, the saturation was completed, and all the valves were closed and the pressure was released. Before the constant head experiment could start, it was necessary to open the top valves to remove extra air that has remained in the valves.

To start the Darcy velocity experiment, the valves in the panel stand were opened going

from the top to the bottom. The last valve was opened until the flow of water was constant. Once the flow was constant, the time was measured until 300 g of water was collected in the beaker. When it was completed, the valve was closed and the time and the temperature of water were noted.

The experiment was repeated three times on each sample.

Appendix C

Statistical Analysis on Soil Parameters

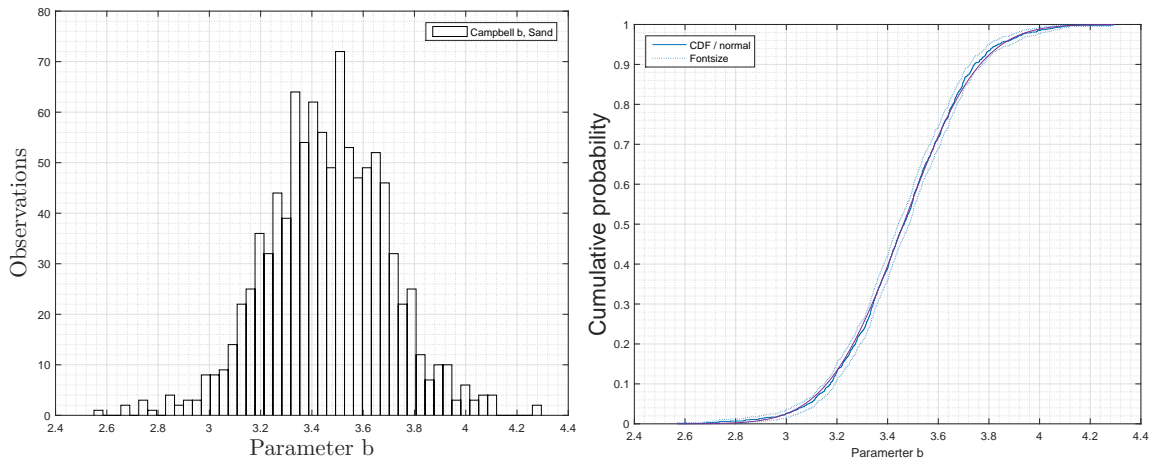


Figure C.1. Result of the bootstrapped regression of parameter b for sand

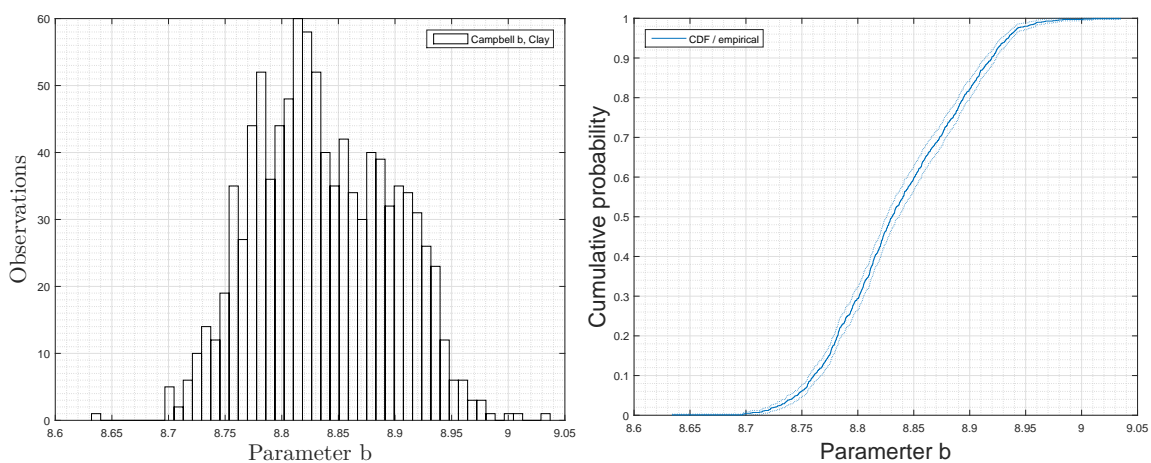


Figure C.2. Result of the bootstrapped regression of parameter b for clay

Appendix D

Penman-Monteith evapotranspiration

$$\lambda ET = \frac{\Delta(R_n - G) + \rho_a c_p \frac{(e_s - e_a)}{r_a}}{\Delta + \gamma \left(1 + \frac{r_s}{r_a}\right)} \quad (\text{D.1})$$

Where

λ	Latent heat of vaporization [MJ · kg ⁻¹]
Δ	Slope of the saturation vapor pressure curve [kPa · °C ⁻¹]
R_n	Net radiation [MJ · m ⁻² d ⁻¹]
ρ_a	Density of the air at constant pressure [kg · m ⁻³]
c_p	Specific heat of the air [MJ · kg ⁻¹ °C ⁻¹]
$e_s - e_a$	Vapor pressure deficit [kPa]
r_a	Aerodynamic resistance [m · s ⁻¹]
r_s	Surface resistance [m · s ⁻¹]
γ	Psychrometric constant [kPa · °C ⁻¹]

The net radiation R_n is the total radiative energy available, being the difference of incoming and outgoing radiation. The psychrometric constant relates the partial water pressure to the air temperature:

$$\gamma = \frac{c_p \cdot P}{\varepsilon \cdot \lambda} \quad (\text{D.2})$$

Where

P	Atmospheric pressure [kPa]
ε	Ratio of molecular weight of water vapor/dry air [-]

The air resistance r_a determines the energy transfer from the surface to the free air and

depends on the measurement set up, the wind speed and the zero displacement plane:

$$r_a = \frac{\ln \left[\frac{z_m - d}{z_{om}} \right] \cdot \ln \left[\frac{z_h - d}{z_{oh}} \right]}{k^2 u_z} \quad (\text{D.3})$$

Where

z_m	Height of wind measurements [m]
z_h	Height of humidity measurements [m]
d	Zero plane displacement height [m]
z_{om}	Roughness length for momentum transfer [m]
z_{oh}	Roughness length for transfer of heat and vapor [m]
k	Von Karman's constant [-]
u_z	Wind speed at height z [$\text{m} \cdot \text{s}^{-1}$]

The zero displacement plane is the plane above ground, in which the wind speed becomes zero, due to friction and thus energy dissipation and momentum consumption between the air and the surface.

The surface resistance r_s accounts for the land use. While the roughness of vegetated surfaces is more or less homogeneous for relatively large areas, the situation in urban areas is different. However, most of the precipitation in urban areas is collected and immediately drained to open waters, like rivers or lakes, after (ideally) being treated in wastewater plants and thus, does not contribute to the groundwater recharge by surface infiltration.

Different surface coverages generate different evapotranspiration rates and based on the degree of surface sealing a coefficient of contributing to the groundwater recharge can be estimated.

The soil heat flux is small compared to the net radiation and can be simplified to:

$$G = c_s \cdot \frac{\Delta T}{\Delta t} \cdot \Delta z \quad (\text{D.4})$$

Where

c_s	Soil heat capacity [$\text{MJ} \cdot \text{m}^{-3} \cdot {}^\circ\text{C}^{-1}$]
ΔT	Air temperature [${}^\circ\text{C}$]
Δt	Duration [d]
z	Effective soil depth [m]

Having calculated the total infiltration rate for the vadose zone, there is another process decreasing the groundwater recharge rate, the subsurface runoff. This can be important for the situation in Hvorup, where the aquifer is separated by an low-permeable layer.

The IPCC reports predict increasing average precipitation and increasing average temperatures. Both processes could neutralize each other when accounting for the groundwater recharge, but also the distribution of precipitation events will change, resulting in more frequent extreme precipitation events. This however can have a major impact on the recharge rate, because surface runoff is more likely to occur during extreme rainfall events and thus, excluding a large amount of water from the groundwater recharge.

As shown above, the net precipitation depends on a large number of parameters. They are all fraught with a high uncertainty, due to the lag of meteorological measurements in a sufficiently high spatial and temporal resolution. Meteorological models however provide a relatively good estimate of these parameters which can be used to calculate the net-precipitation.

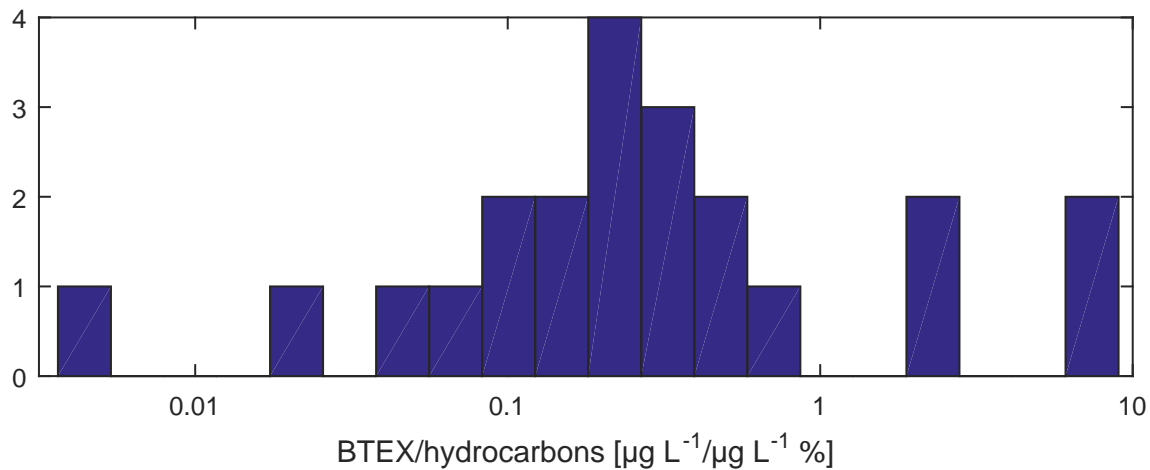
Appendix E

Determining BTEX-concentration with other samples as reference

The following are two attempts at determining the BTEX-concentration using other water samples in Hvorup barracks as reference. The other samples are from Niras' initial study, supplemental study as well the study of the heating central.

E.1 Method 1: Same fraction BTEX

A histogram of the concentration of BTEX compared with the concentration of hydrocarbons for water samples in Hvorup barracks is shown in figure E.1. In total 22 water samples have measured a concentration of BTEX and hydrocarbons. In measurements where one or more of the BTEXs haven't been detected the concentration is assumed to be equal to the detection limit.



For over 60% of the samples the measured concentration of BTEX is in between 0.1 % and 1 % of the measured concentration of BTEX. However for two of the water samples the fraction of BTEX is about 9 %. Xylene is the biggest contributor to the high BTEX-concentration, where the concentration in the samples are 106 and $115 \mu\text{g} \cdot \text{L}^{-1}$ respectively. The solubility of Xylene is between $160 \mu\text{g} \cdot \text{L}^{-1}$ to $200 \mu\text{g} \cdot \text{L}^{-1}$ [Loll and Moldrup, 2000], so concentrations as high as this are surprising. However as shown in table E.1 Xylene is expected to be the most prominent of the BTEXs, and it also has a lower biodegradation rate compared to benzene, toluene and ethylbenzene [Loll and Moldrup, 2000], which can explain the high concentration. The very high disparity between the BTEXs in these two samples indicate that the biodegradation would be the greatest factor in this. It is hence evaluated that this method is not useful for estimating BTEX concentration at the pollution site.

The mean of $m_{\text{BTEX}}/m_{\text{hydrocarbons}} \cdot 100$ is 0.07 %, so if the highest measured pollution were to follow this distribution, then the concentration of benzene would be $44 \text{ mg} \cdot \text{L}^{-1} \cdot 0.07 \cdot 10^{-2} = 0.0308 \text{ mg} \cdot \text{L}^{-1}$.

E.2 Method 2: PID

An alternative method is to use Photoionization detector (PID) measurements paired with the BTEX measurements. As the PID detects VOCs and the BTEXs make up a significant part of the VOCs in gasoline and diesel, it is expected that the PID is more sensitive to the BTEXs than the other hydrocarbons. As a measurement of PID is available for the pollution with a hydrocarbon concentration of $44 \text{ mg} \cdot \text{L}^{-1}$, it's possible to 'calibrate' the PID with the other samples as a reference to get the BTEX content for the pollution with high hydrocarbon content. Samples of water are used for the calibration. The BTEX content in relation to the PID-value for all the samples is shown in figure E.2.

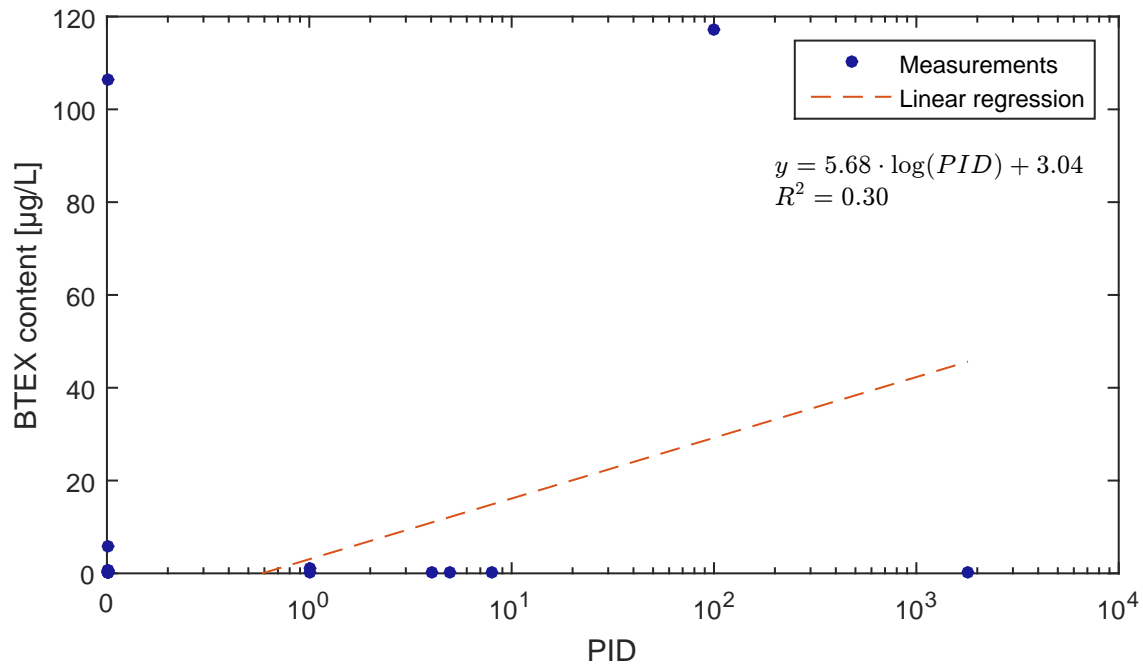


Figure E.2. BTEX content in samples of water in Hvorup barracks in relation to the measured PID-value for the same samples.

It's noted that two samples show high BTEX content but a PID-value of 0. As PID-tests measure the concentration of VOCs in the gas phase and these are samples of water, it's reasonable to assume that false negatives can occur. The points with a PID-value of 0 but a high BTEX content are hence excluded from the regression. As figure E.2 shows the regression is very poor. It is thus evaluated that the PID-measurements are a poor way of estimating the BTEX-content in Hvorup barracks.

Appendix F

Biodegradation Appendix

F.1 Physicochemical factors

Biodegradation in soil depends upon several parameters. The following section gives a short description of these parameters.

Temperature:

All microorganisms have a minimum temperature to allow for growth. Below this temperature, they are inactive. In the same way, there is a maximum temperature beyond which growth is no longer possible. The temperature also has a huge impact on the bacteria growth rates. Indeed, there is an optimum temperature corresponding to best growth rate. Some bacteria can grow below 0°C (cryophiles microorganism) or above 100°C (thermophile microorganism) but typically, the ideal temperature range is 20-30°C, near the maximum temperature supported by the microorganism. As such temperature is a very important factor in biodegradation.

Soil profile:

Another important factor is the soil profile. Typically bacteria and fungi grow in places with enough water and organic compounds to allow life. The biodegradation rate is hence closely related to the water content and the organic content. Water is essential for life microorganisms: it delivers nutrients to the microorganism and evacuate waste by diffusion.

pH:

Some bacteria can experience growth only with specific conditions of pH. The pH is a measurement of the acidity and varies usually between 4.0 and 9.0 in soil. Most of the microorganisms have an optimum pH between 5.0 and 9.0 where they can grow. Usually, fungi are more tolerant to acidic conditions (pH<5) than bacteria (pH between 6 and 8). The pH also changes the solubility of some important molecules for microorganisms. For

instance, the solubility of CO₂ is in part chosen by pH. If the acidity is too high, some parts of the cells can be denatured.

Redox potential:

A lot of chemical reactions inside microorganisms are reduction-oxidation reaction (redox). The redox potential is an indication of available potential electron donors and acceptors. It gives a good indication of the breathing process: a redox potential positive show an environment where oxidation are favored (presence of O₂). As for pH, the solubility of some nutrients can changes with the redox potential. For instance, for high redox potential, iron is present in soil as Fe³⁺ which is not soluble in water.

O₂ availability:

Another important part is the presence of oxygen. If the acceptor of electron inside the microorganism is O₂ the breathing is aerobic. If the acceptor is a mineral, such as NO₃⁻, NO₂, Mn⁴⁺, Fe³⁺, SO₄²⁻ or CO₂ then the breathing is anaerobic (and if the substrate is organic the process is called fermentation). It has been shown that degradation of common pollutants is faster in aerobic conditions than in anaerobic. However some bacteria can use both breathing process, depending of the conditions.

Nutrient availability:

The nutrients presents in soil also play a role in the growth rate of bacteria. Some inorganic compound are essential for microorganism and others can be toxic. The essential nutrients are carbon (used in all organic molecule), nitrogen (used in proteins) and phosphorus (mainly used in ATP). Nitrogen is available in organic form (such as amino acid) or in inorganic form (such as nitrate, nitrite or ammonium).

Pollutant:

If the bacteria and fungi that can degrade pollutants grow enough to allow for biodegradation, the next important factor to take into account is structure of pollutant. Indeed, the structure of the pollutants plays a role in the biodegradation rate. Some pollutants have a structure involving bond between atoms that can be easily cut in order to reduce the molecule. In another way, there are some pollutants that can act like poison for bacteria. That involves a more or less faster kinetic.

F.2 Description of experiment

F.2.1 Preparations of samples

After a day of pumping the air out of the sample (to eliminate interference from volatile oil compounds and ensure that the samples were free of pollutants and the oxygen concentration is at its maximum), the soils (10 g) and the water sample (20 mL) were put in contact with 4 different stock solutions:

- Stock solution 1, Benzene ($C = 0.5 \text{ mg} \cdot \text{mL}^{-1}$): 0.064 ml concentrated benzene in 110 ml of autoclaved and demineralized water.
- Stock solution 2, Benzene ($C = 1 \text{ mg} \cdot \text{mL}^{-1}$): 0.038 ml concentrated benzene in 10 ml of autoclaved and demineralized water.
- Stock solution 3, MTBE ($C = 1 \text{ mg} \cdot \text{mL}^{-1}$): 0.145 ml concentrated MTBE in 110 mL of autoclaved and demineralized water.
- Stock solution 4, MTBE ($C = 10 \text{ mg} \cdot \text{mL}^{-1}$): 0.161 ml concentrated MTBE in 10 mL of autoclaved and demineralized water.

Stock solutions 1 and 3 were used for the groundwater sample and 2 and 4 were used for soil samples. The MTBE solution was only used as an internal standard. All stock solutions were prepared in 117 mL bottles, sealed and placed on a shaking table for 24 hours to allow chemicals to reach equilibrium between the liquid and the gas phases. Furthermore, as a nutrient stock solution, a regular fertilizer is used, which contains 6% nitrogen, 1.3% phosphorous, and 5% potassium and various micronutrients.

In all prepared samples, 2 mL of air is added with stirring to cause a small pressure inside the bottles. Then, the samples were shaken for 3 hours to ensure equilibrium between the water phase and the gas phase. The conditions of the samples are shown in table F.1.

Table F.1. Samples for the biodegradation experiment. GW: Groundwater, S: Soil, C: Autoclaved and N: Nutrients

Wells name	GW502	GW512	GW516	GW502N	S502C	S502	S510	S514
Groundwater	+	+	+	+	-	-	-	-
Soil	-	-	-	-	+	+	+	+
Nutrients	after 20 days	-	-	+	-	-	-	-
Autoclaved	-	-	-	-	+	-	-	-

Notice that for GW502, nutrients were not added initially, but since no decrease in concentration was visible after 20 days, they choose to add nutrients.

In total, eight different experiments have been conducted at room temperature from samples taken from soils and waters samples. Each experiment was duplicate (or quadruplicate for the nutrient experiment).

One of the samples was autoclaved to the extent that all the bacteria and fungi in the sample were killed. This was to check if there exist any other degradation process such as chemical degradation.

In addition, one of the experiments was conducted with and without the addition of nutrients in the Carbon/Nitrogen/Phosphorus ratio 100:10:1 to investigate if the

biodegradation was optimizable in this way.

F.2.2 Measurement of benzene concentration

The concentration of benzene and MTBE are measured in the gas phase by Gas Chromatography (GC). Basically, GC is a thin column of 30 m long where the chemicals move inside carried by a vector phase (helium). Due to the phenomenon of retention, some chemicals move faster than other. For one type of column, with fixed conditions (temperature of oven, injection temperature, pressure), after the injection the chemical will reach the end of the column at a specific time (each time the same): the retention time. That allows differentiating MTBE from benzene and water.

At the outlet of the column, chemicals reach a FID detector which gives a signal as a function of the concentration of the chemical. To determine an unknown concentration, the first step is to make a calibration curve. Several samples with different known concentration of benzene and MTBE are used and the area of the peaks obtained are measured. The different parameter of the column are show in appendix F.2.3.

The concentration is measured each day until benzene are totally removed by biodegradation. The GC analysis shows only the concentration in air. The total benzene concentration can then be calculated with Henry's law, see equation (F.2), which gives the partition between air phase and water phase for a chemical.

$$C_{total} = C_{gas} + C_{water} \quad (\text{F.1})$$

$$C_{gas} = K_{henry} \cdot C_{water} \quad (\text{F.2})$$

$$C_{total} = C_{gas} \cdot \left(1 + \frac{1}{K_{henry}} \right) \quad (\text{F.3})$$

Where

C_{total}	Concentration total in pollutants [$\mu\text{g} \cdot \text{L}^{-1}$]
C_{gas}	Concentration in gas phase [$\mu\text{g} \cdot \text{L}^{-1}$]
C_{water}	Concentration in water [$\mu\text{g} \cdot \text{L}^{-1}$]
K_{henry}	Coefficient of partition between gas and water phase, [-]

F.2.3 Description of the Gas chromatography

Table F.2. Description of the different parameter for the Gas Chromatography
Gas Chromatograph (Agilent Technologies 7890A)

Detector	FID
Carrier Gas	Helium
Column Flow	0.9879 mL · min ⁻¹
Makeup Flow	25 mL · min ⁻¹
Oven temperature	80.0 °C
Detector Temperature	250.0 °C
Injection temperature	325.0 °C
Injection volume	0.3 mL · min ⁻¹
Pressure	6.016 psi
Column 1	Length: 30 m ID: 0.320 mm Film: 0.25 µm
Column 2	Length: 30 m ID: 0.530 mm Film: 30.25 µm

F.3 Presentation of different models of kinetics

Biodegradation rate can be modeled by several different equations. After a usual lag phase (in which the bacteria population adapt to the new chemical condition), the concentration of pollution starts to decrease. The most common model is the first order rate and the Michaelis-Menten model.

Power rate model, zero and first order:

It is the most basic model and in many cases it is enough to calculate the kinetics of biodegradation. The order of reaction, n , usually varies between 0 and 2. When the order is known, it becomes possible to integrate the kinetic equation F.4 with respect to time to give the concentration.

$$v = -\frac{d(C)}{dt} = K \cdot C^n \quad (\text{F.4})$$

Where

v	Biodegradation rate [$\mu\text{g} \cdot \text{L}^{-1} \cdot \text{s}^{-1}$]
K	Degradation rate constant [$\mu\text{g}^{(1-n)} \cdot \text{L}^{(n-1)} \cdot \text{s}^{-1}$]
n	Order of the kinetic [-]
C	Concentration [$\mu\text{g} \cdot \text{L}^{-1}$]
t	Time [s]

For a first order, n is equal to 1. The equation (F.4) can be integrated and gives:

$$C(t) = C_0 \cdot e^{(-K_1 \cdot t)} \quad (\text{F.5})$$

Where

C_0	Initial concentration [$\mu\text{g} \cdot \text{L}^{-1}$]
K_1	First order degradation rate [s^{-1}]

At the half-life, when half the concentration is already gone, equation (F.5) can be rewritten as follows:

$$\frac{C_0}{2} = C_0 \cdot e^{(-K_1 \cdot t_{1/2})} \implies K_1 = \frac{\ln(2)}{t_{1/2}} \quad (\text{F.6})$$

Where

$t_{1/2}$	Half-life time [s]
-----------	--------------------

For a zero order, n is equal to 0. The equation (F.4) can be integrated and gives:

$$C(t) = C_0 - K_0 \cdot t \quad (\text{F.7})$$

Where:

K_0	Zero order degradation rate [s^{-1}]
-------	---

Michaelis-Menten model:

For this model, it is assumed that the biodegradation is done with a constant amount of microbe (no growth). The relationship between pollutants concentration and the degradation rate is described by the Michaelis-Menten equation:

$$v = \frac{v_{max} \cdot C}{(K_m + C)} \quad (\text{F.8})$$

Where

v_{max}	maximum specific degradation rate [s^{-1}]
K_m	Michaelis-Menten constant [$\mu\text{g} \cdot \text{L}^{-1}$]

F.4 Biodegradation results and data

The results from the biodegradation experiments are shown in the following figures by assuming a first-order and a zero-order biodegradation.

F.4.1 First order biodegradation rate:

Groundwater samples:

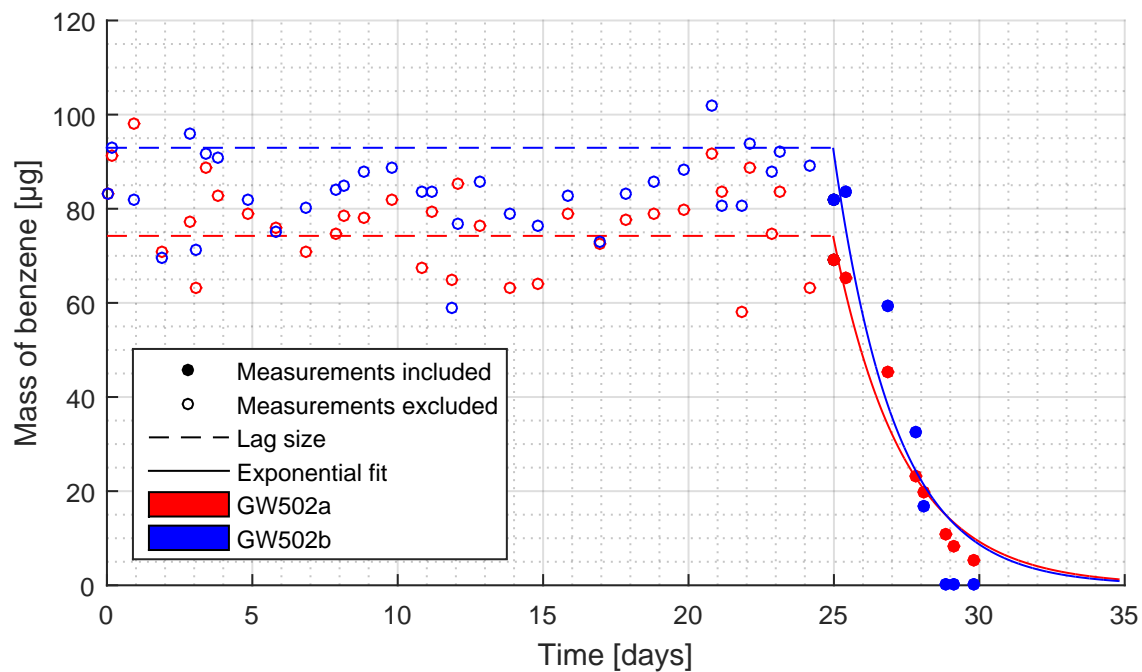


Figure F.1. Total mass of benzene measured over time in groundwater sample from well B502 and the modeled mass assuming a first-order biodegradation.

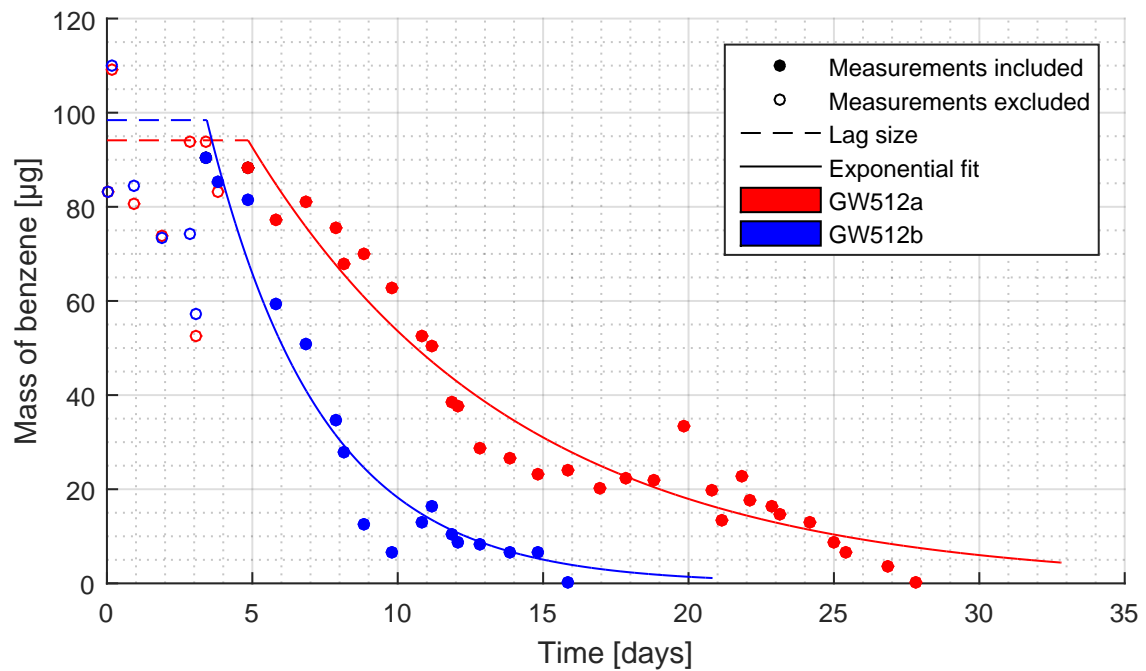


Figure F.2. Total mass of benzene measured over time in groundwater for sample from well B512 and the modeled mass assuming a first-order biodegradation.

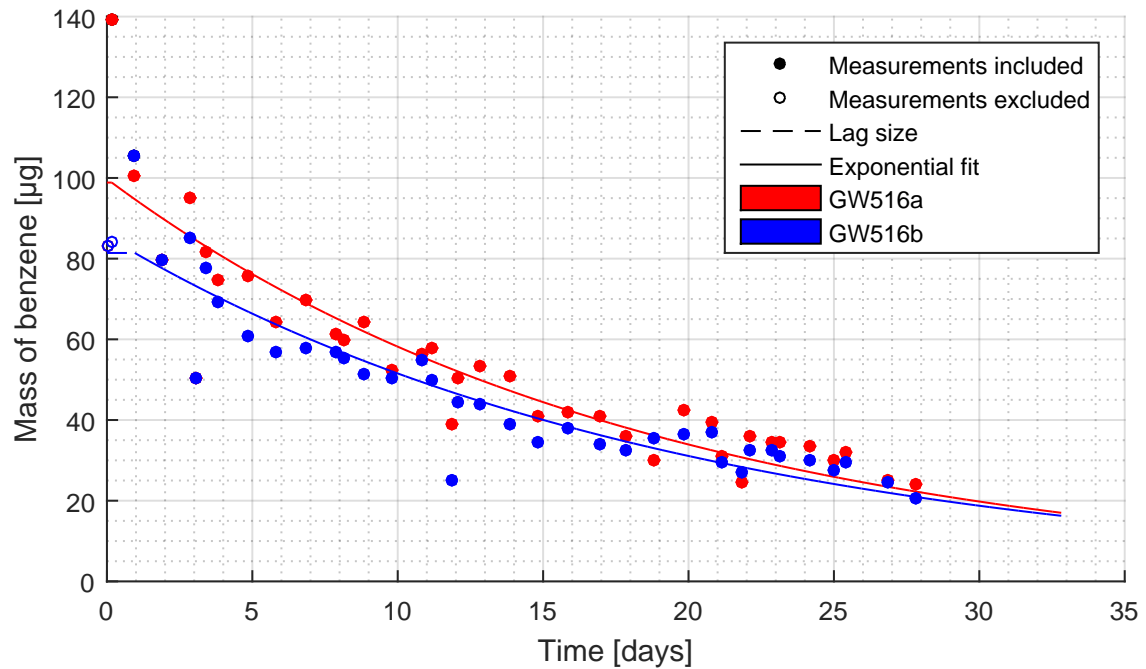


Figure F.3. Total mass of benzene measured over time in groundwater for sample from well B516 and the modeled mass assuming a first-order biodegradation.

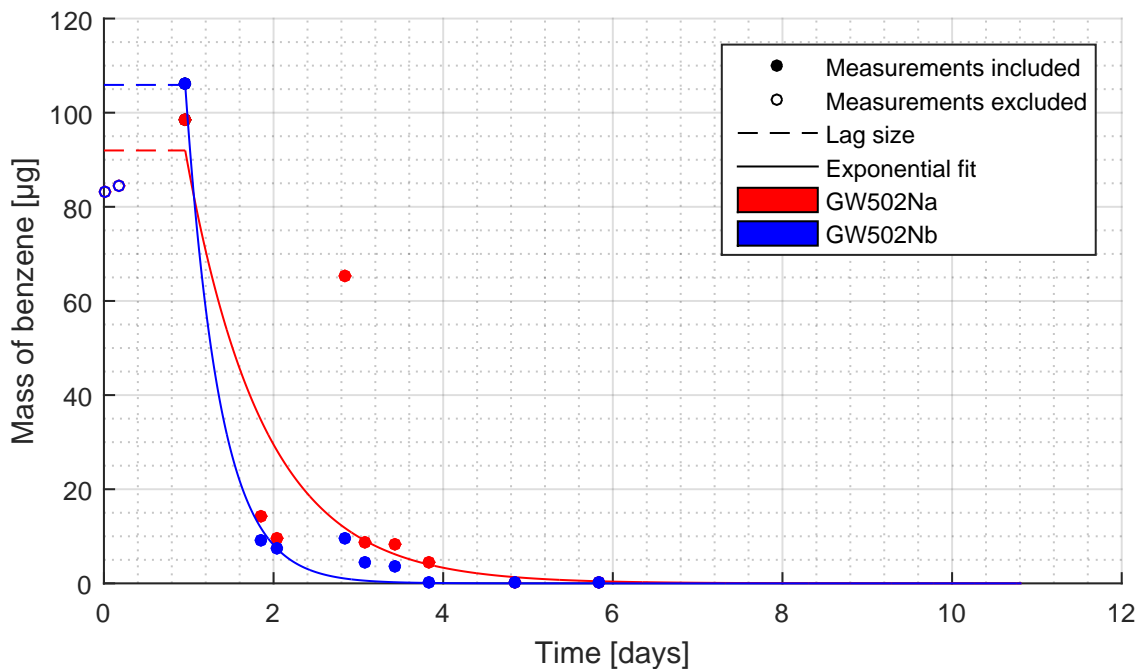


Figure F.4. Total mass of benzene measured over time in groundwater for sample from well B502 where nutrients was added and the modeled mass assuming a first-order biodegradation.

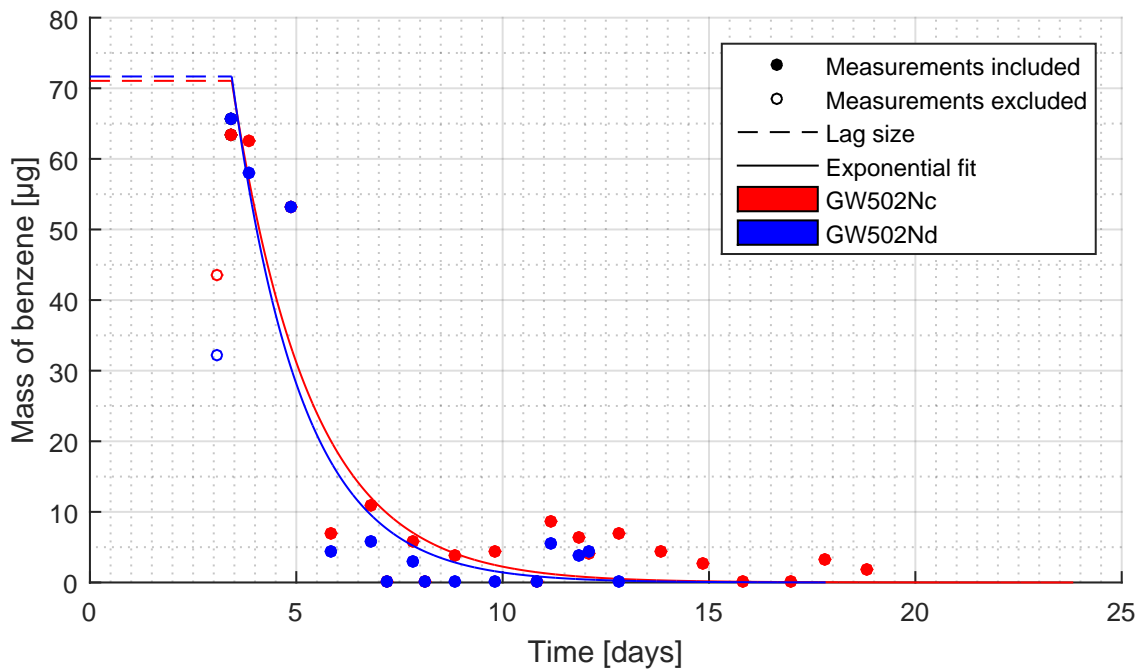


Figure F.5. Total mass of benzene measured over time in groundwater for sample from well B502 where nutrients was added and the modeled mass assuming a first-order biodegradation.

Soil samples:

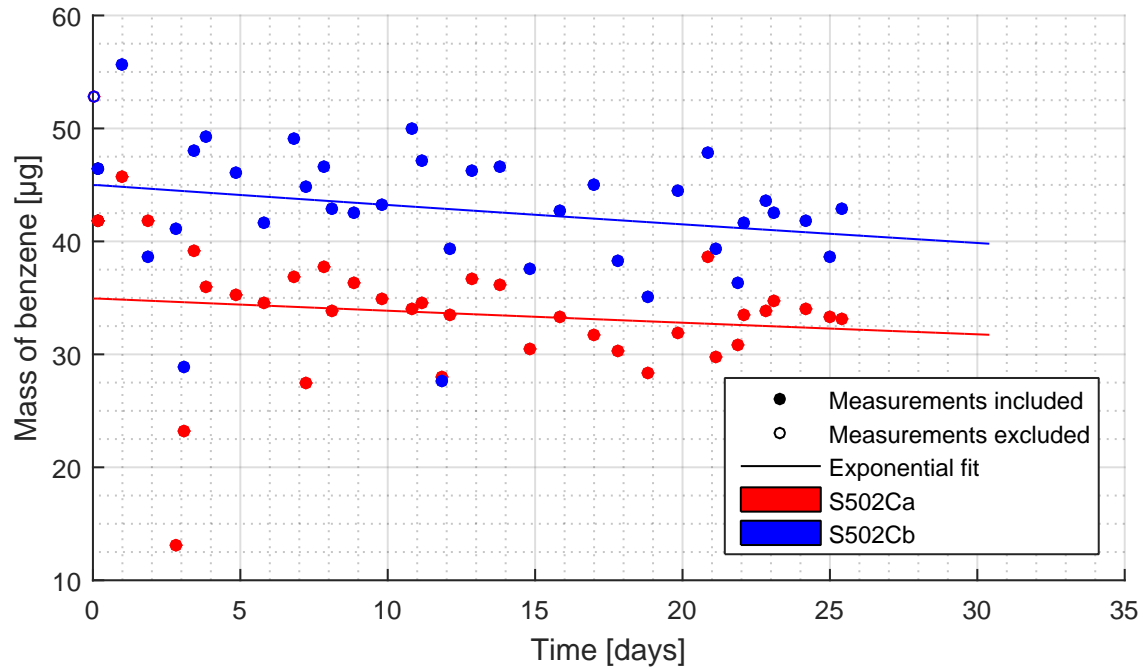


Figure F.6. Total mass of benzene measured over time in soil sample autoclaved taken near well B502 and the modeled mass assuming a first-order biodegradation.

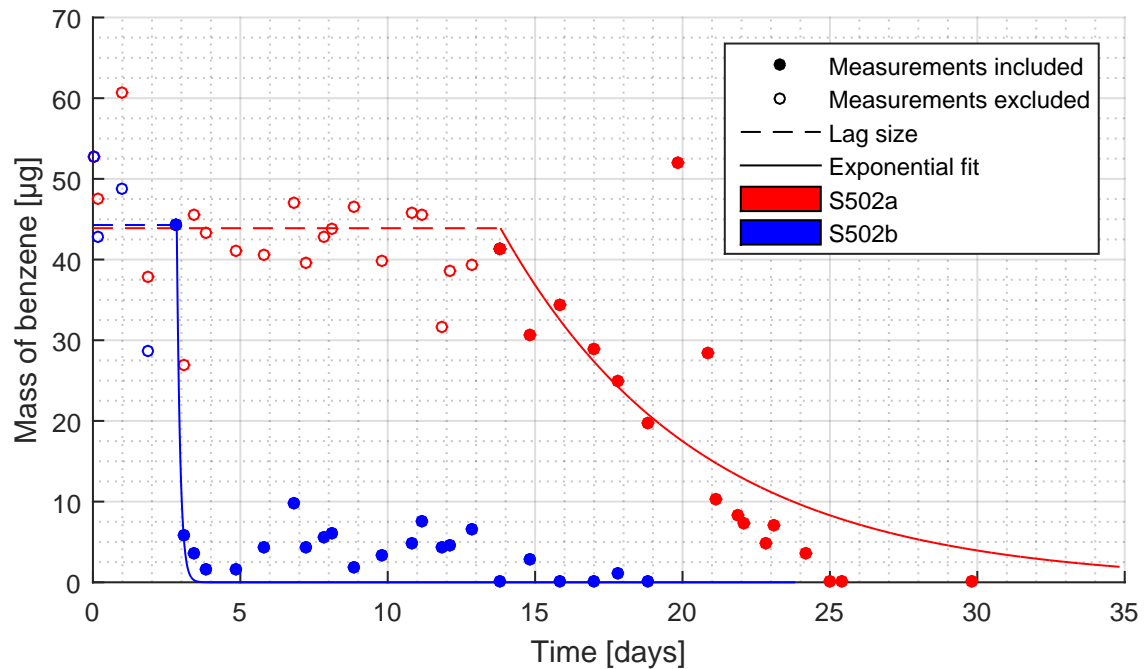


Figure F.7. Total mass of benzene measured over time in soil samples taken near well B502 and the modeled mass assuming a first-order biodegradation.

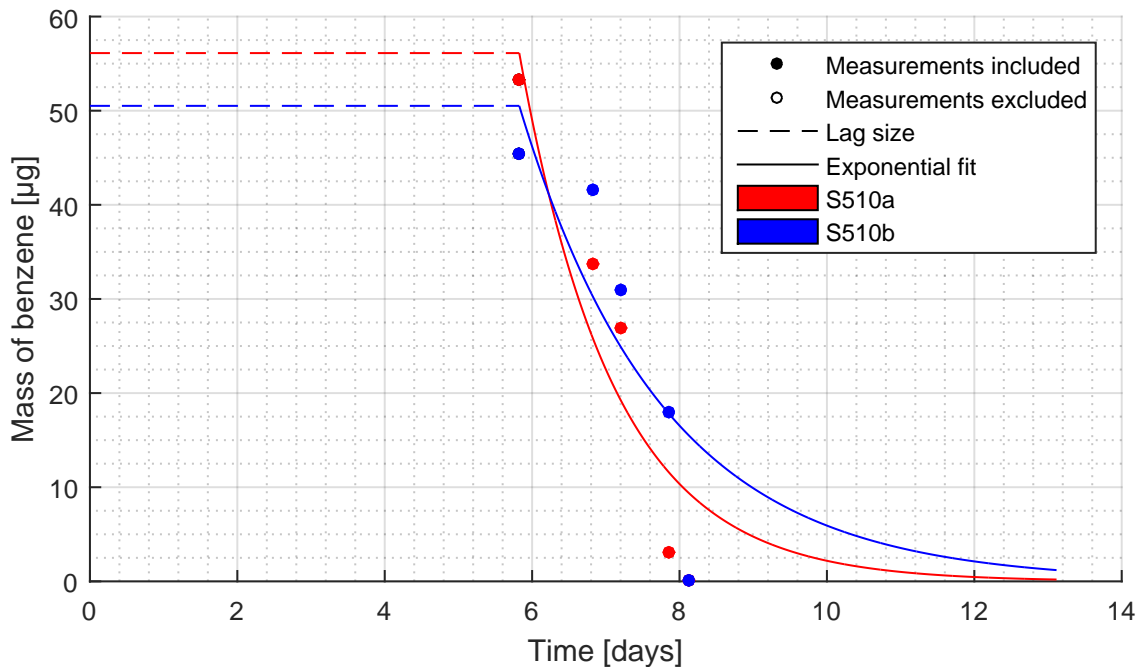


Figure F.8. Total mass of benzene measured over time in soil sample taken near well B510 and the modeled mass assuming a first-order biodegradation.

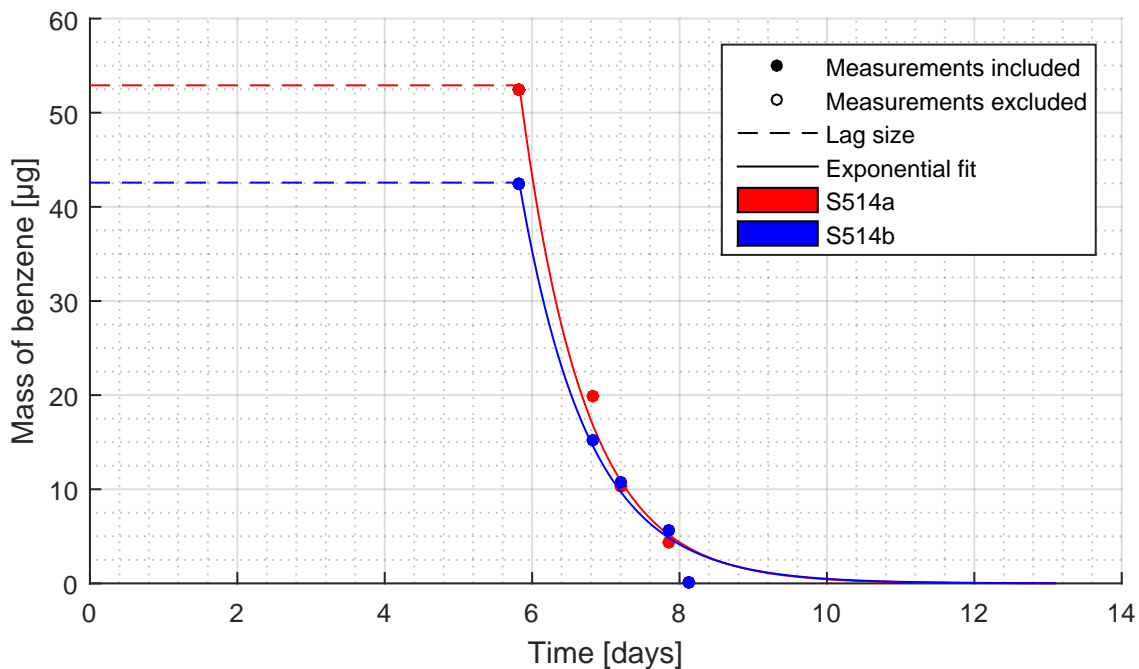


Figure F.9. Total mass of benzene measured over time in soil sample taken near well B514 and the modeled mass assuming a first-order biodegradation.

F.4.2 Zero order biodegradation rate

Groundwater samples:

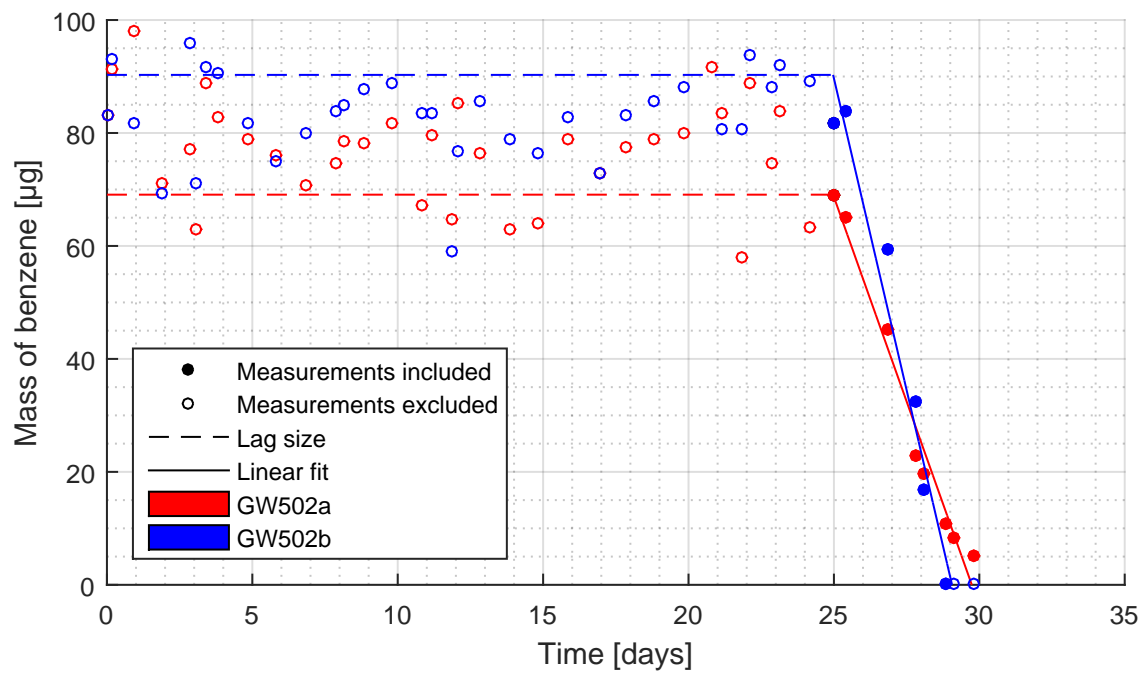


Figure F.10. Total mass of benzene measured over time in groundwater sample from well B502 and the modeled mass assuming a zero-order biodegradation. Nutrient were added on day 20.

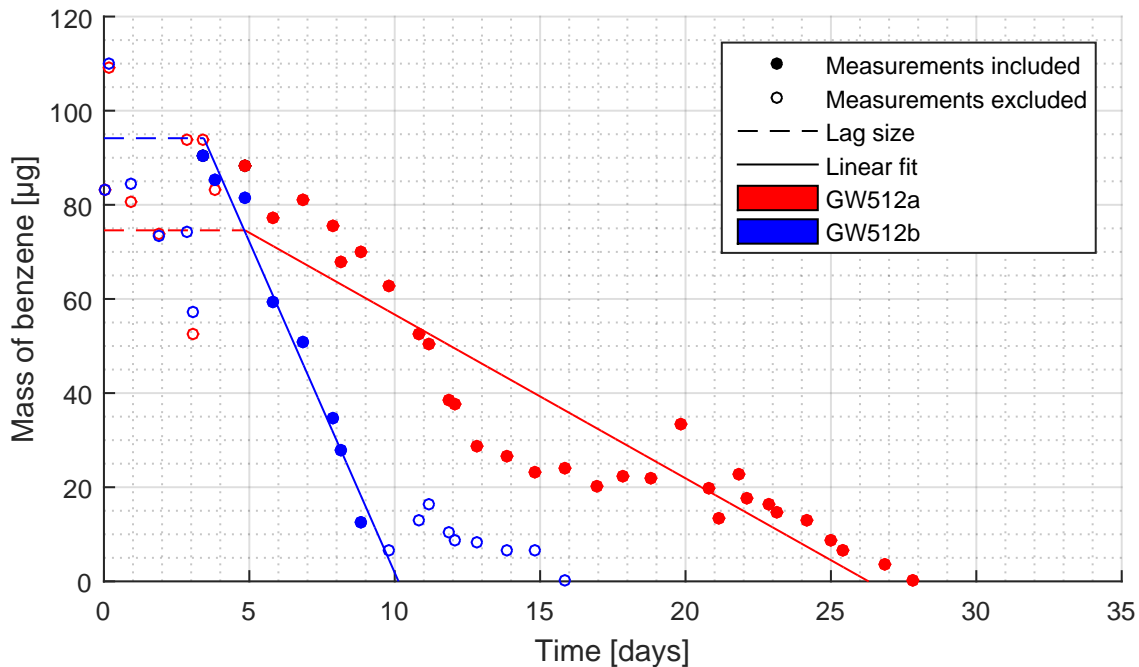


Figure F.11. Total mass of benzene measured over time in groundwater for sample from well B512 and the modeled mass assuming a zero-order biodegradation.

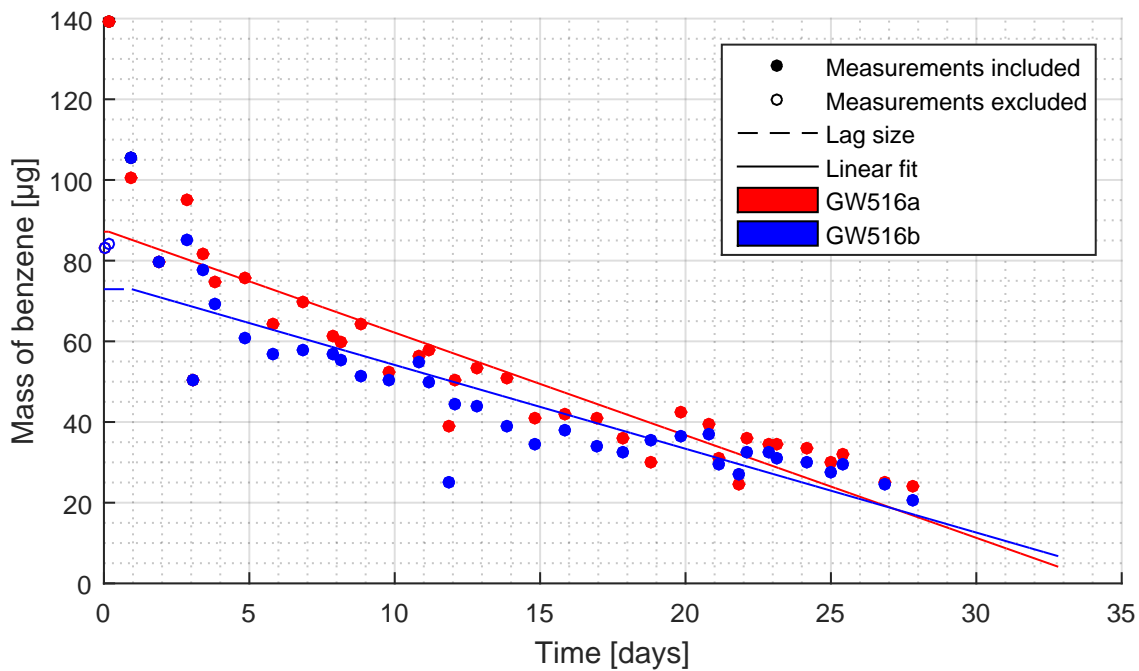


Figure F.12. Total mass of benzene measured over time in groundwater for sample from well B516 and the modeled mass assuming a zero-order biodegradation.

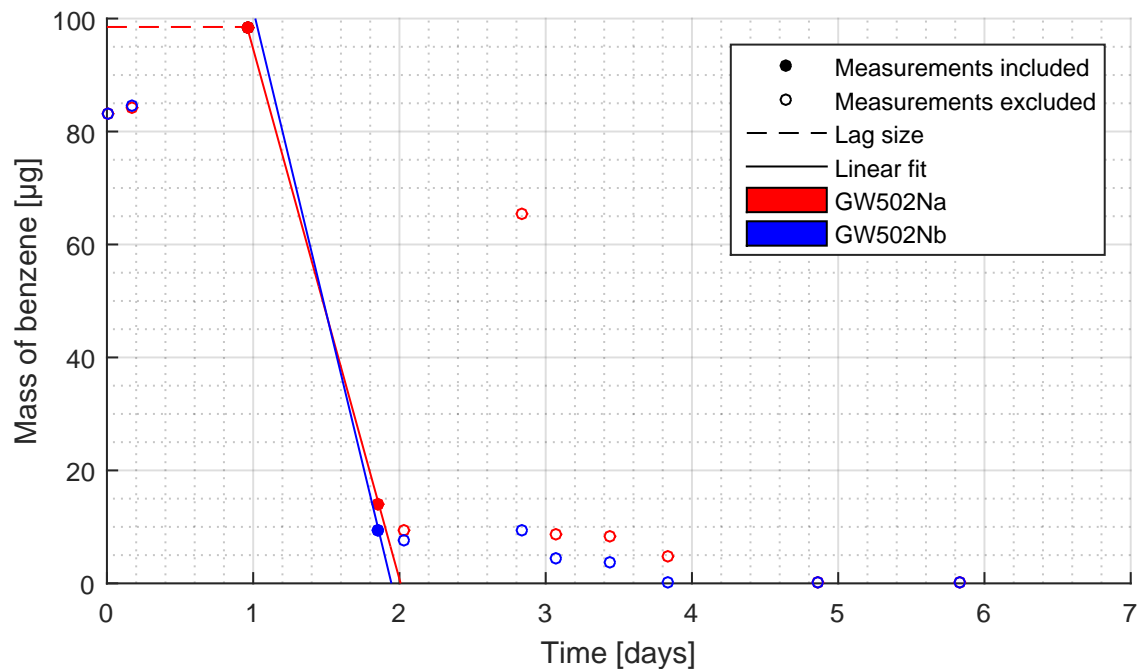


Figure F.13. Total mass of benzene measured over time in groundwater for sample from well B502 where nutrients was added and the modeled mass assuming a zero-order biodegradation.

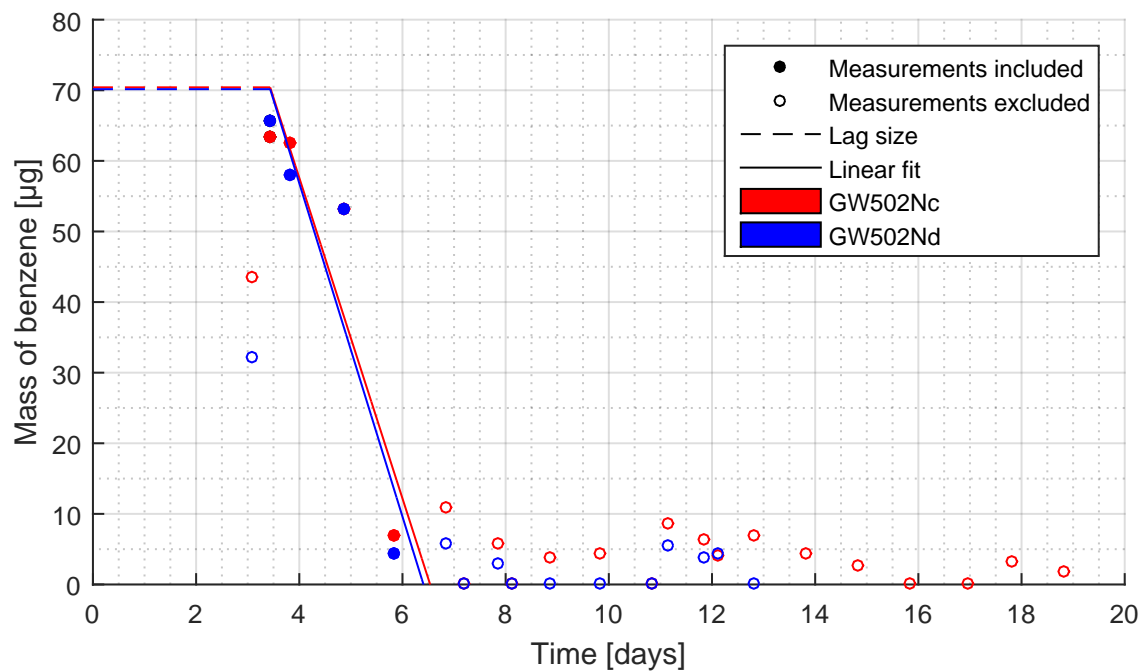


Figure F.14. Total mass of benzene measured over time in groundwater for sample from well B502 where nutrients was added and the modeled mass assuming a zero-order biodegradation.

Soil samples:

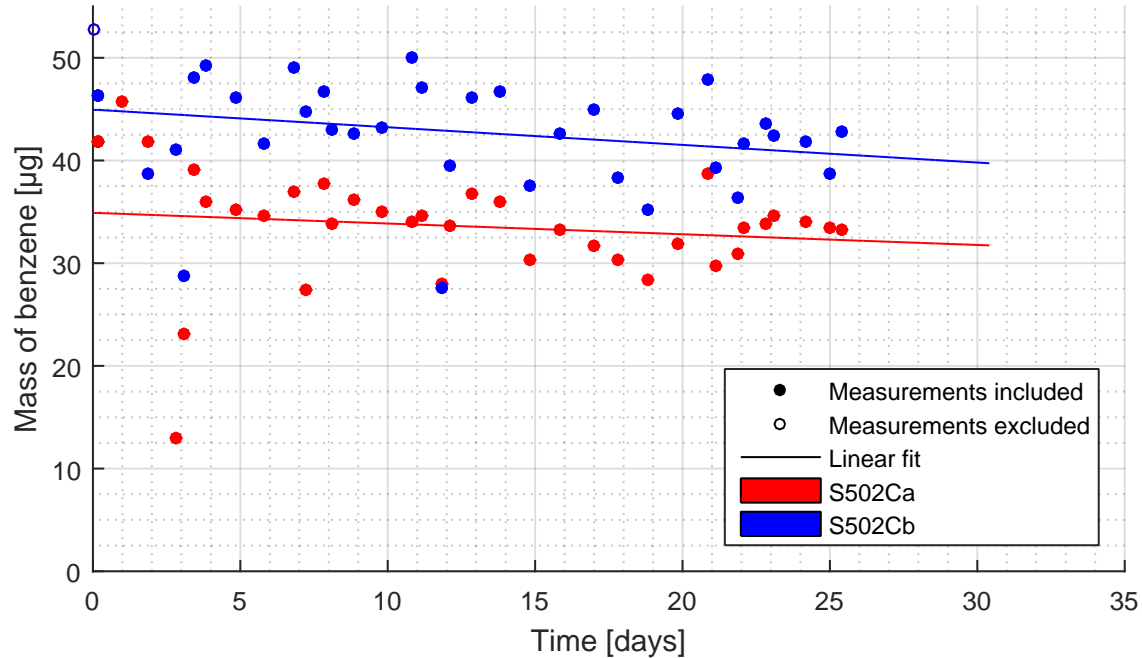


Figure F.15. Total mass of benzene measured over time in soil sample autoclaved taken near well B502 and the modeled mass assuming a zero-order biodegradation.

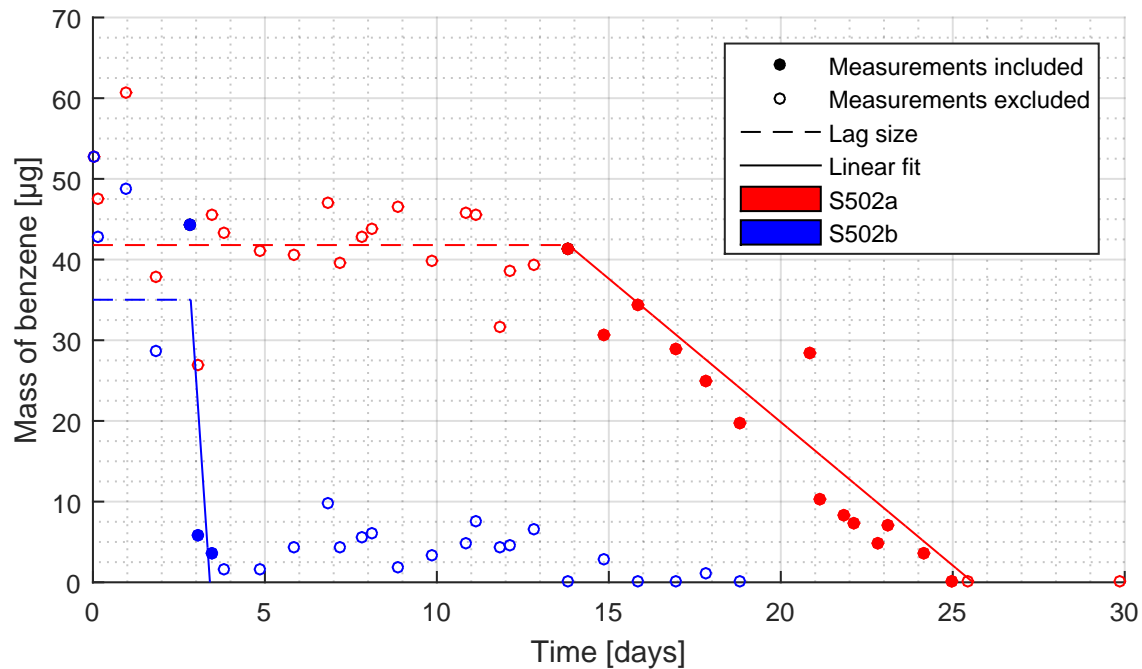


Figure F.16. Total mass of benzene measured over time in soil samples taken near well B502 and the modeled mass assuming a zero-order biodegradation.

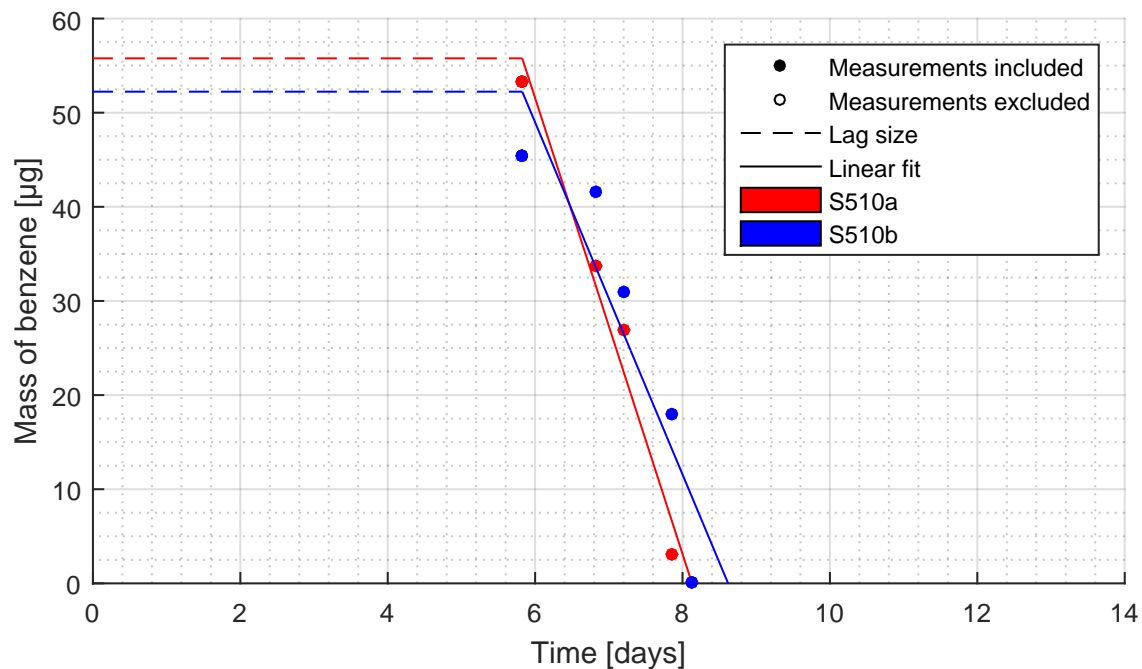


Figure F.17. Total mass of benzene measured over time in soil sample taken near well B510 and the modeled mass assuming a zero-order biodegradation.

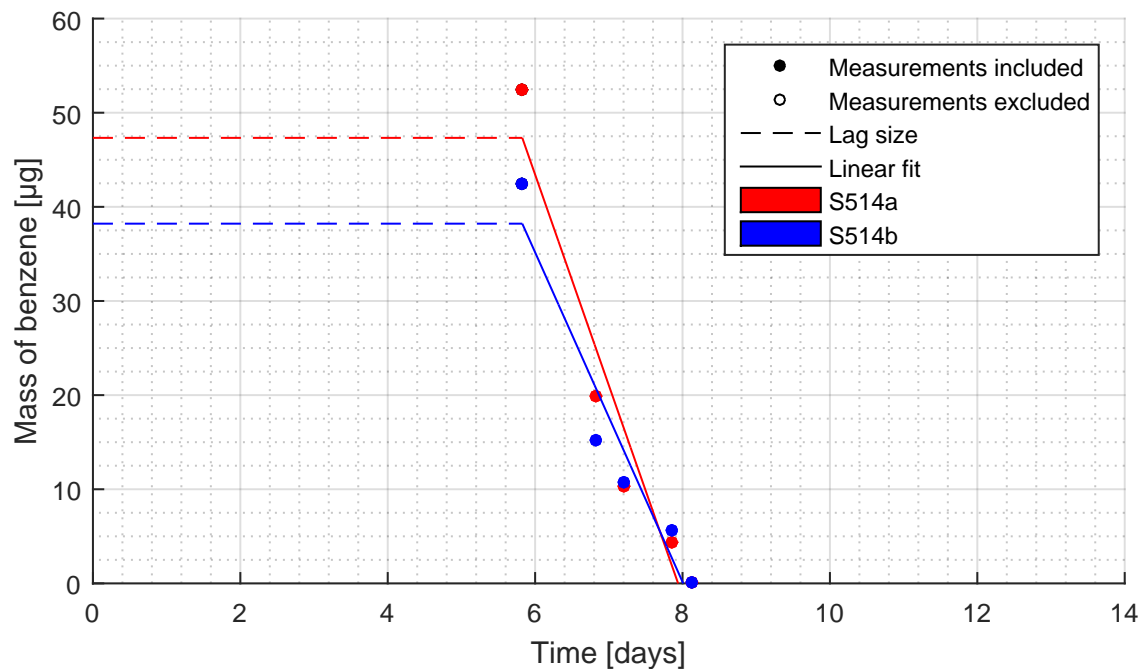


Figure F.18. Total mass of benzene measured over time in soil sample taken near well B512 and the modeled mass assuming a zero-order biodegradation.

F.5 Discussion

F.5.1 Autoclaved samples

The autoclaved samples show very small degradation rates. They are shown in figure F.19. By assuming a first-order biodegradation rate, K_1 is between 0.003 and $0.004\text{ }d^{-1}$. Applying equation (F.6), to calculate the half-life, i.e. the time needed to degrade half of the total initial concentration of benzene, it will take 231 days to reduce the initial concentration by half. There are two possible explanations for the small degradation rate. First, the autoclaving did not remove all the microorganisms and the remaining bacteria started to grow again after the autoclaving. A second possibility is, that sorption of benzene to soil particles caused a small decrease in the air benzene concentration. It could also be caused by a small leakage in the microcosm or because of the pollutant that is removed during sampling.

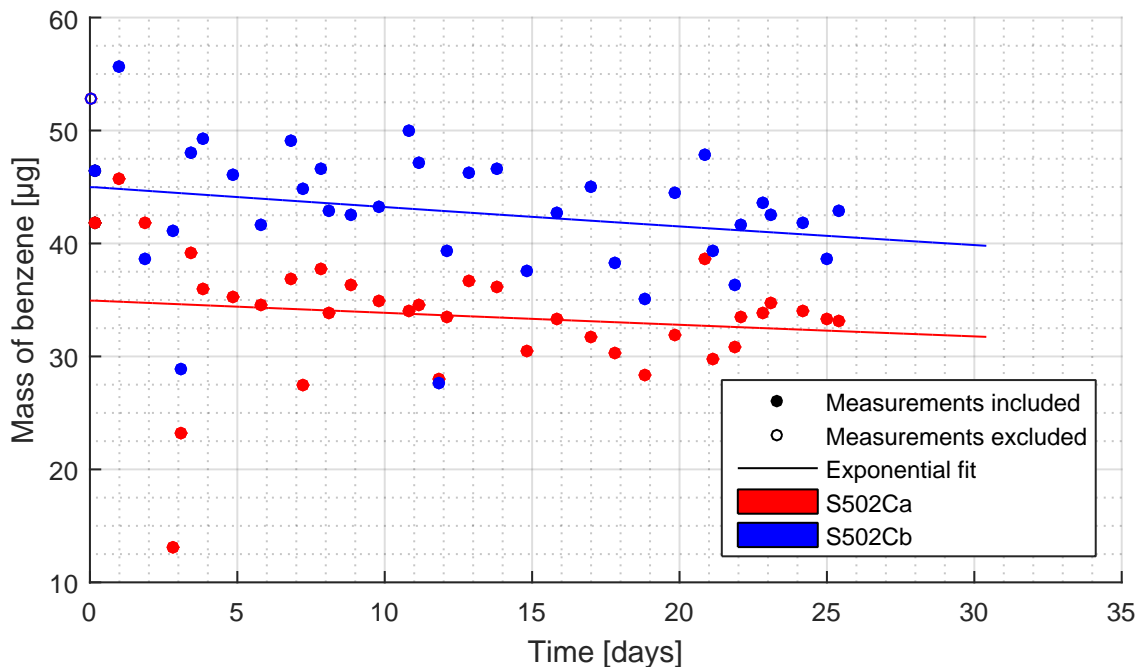


Figure F.19. Total mass of benzene measured over time in soil sample autoclaved taken near well B502 and the modeled mass assuming a first-order biodegradation.

F.5.2 Lag-phase and fluctuation

For almost all the samples, a lag-phase is observed. It is usually the time that the microorganism need to adapt to the new conditions in the microcosm, see figure F.20.

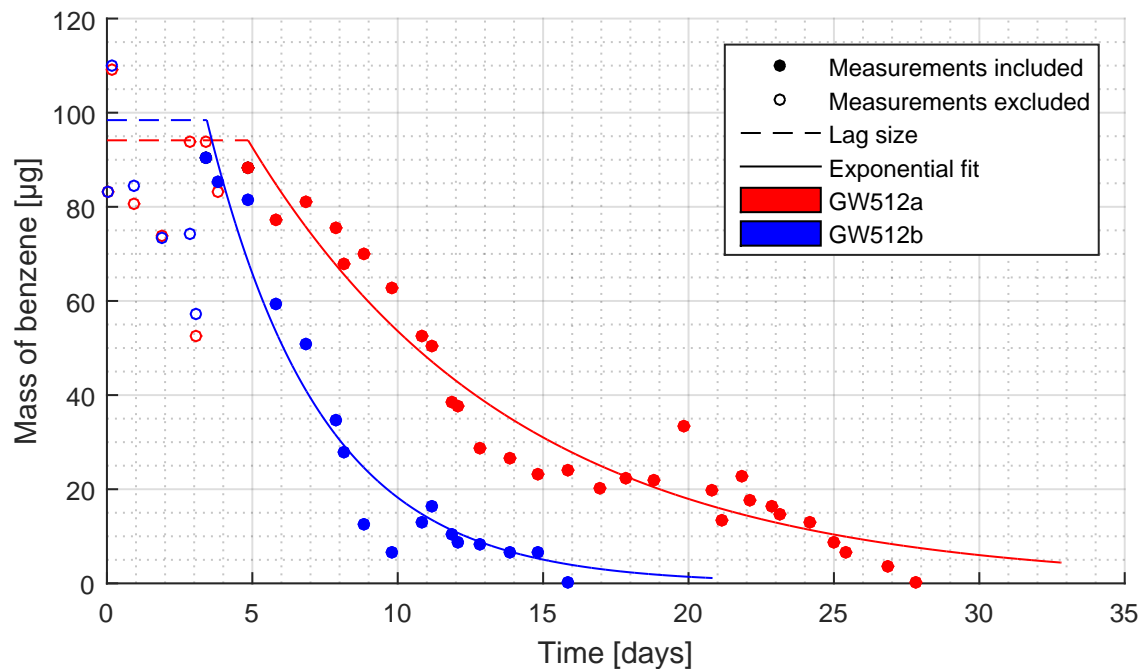


Figure F.20. Total mass of benzene measured over time in groundwater for sample from well B512 and the modeled mass assuming a first-order biodegradation.

Some fluctuations from day to day can also be observed. They are due to uncertainties concerning the assumption that benzene reaches an equilibrium between water phase and gas phase.

For the soil samples taken in close proximity to well B510 and B512 the majority of the benzene is degraded fast (3 days), but the soil sample from well B502 shows variations between the two duplicates. This can be due to an insufficient homogenization of the soil before the experiment, see figure F.21.

F.5.3 First-order versus zeroth-order

For the zero-order model, the measurements during the lag-phase and after total biodegradation were excluded. This can lead to major uncertainties, like for the soil sample from well 502, because the linear regression is only done with two points. See figure F.21.

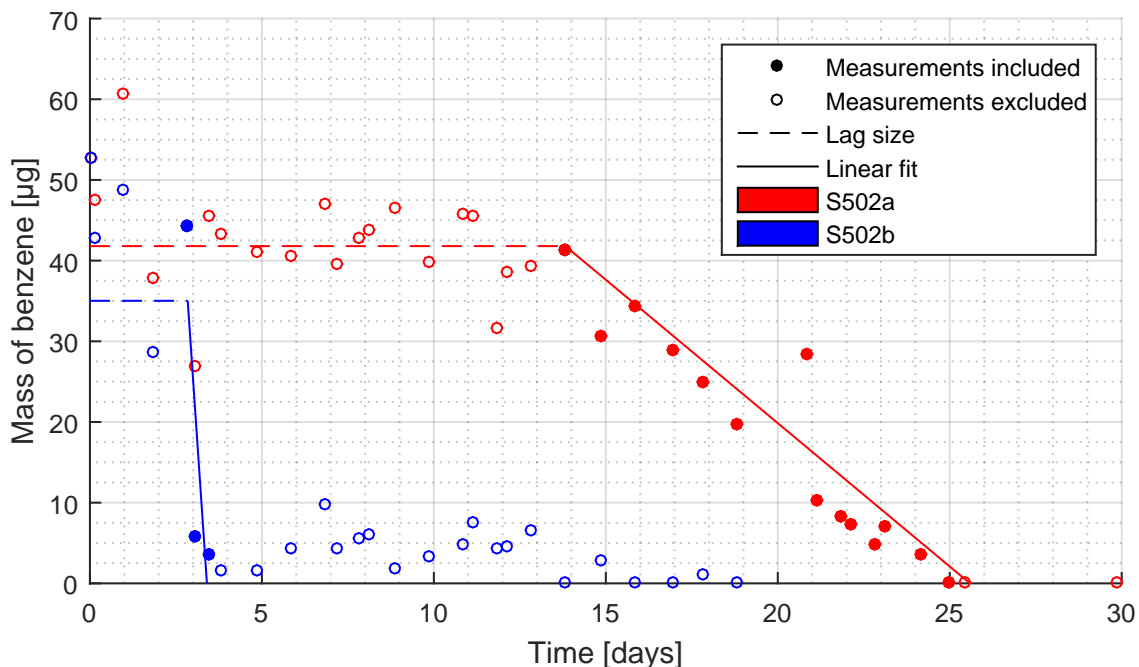


Figure F.21. Total mass of benzene measured over time in soil samples taken near well B502 and the modeled mass assuming a zero-order biodegradation.

For some samples, the first order model fits better than the zero-order one. The best model is chosen by comparing the different *RMSE*. It can be concluded that the biodegradation follows a first-order biodegradation kinetic best.

F.5.4 Nutriment and inhibitions

For the groundwater sample from well 502, an inhibition was observed, probably caused by the lack of nutriment, see figure F.22. Since benzene was detected by GC, it can be assumed that the biodegradation was inhibited. Therefore, nutrients were added to the pure groundwater samples on day 20 after the beginning of the experiment.

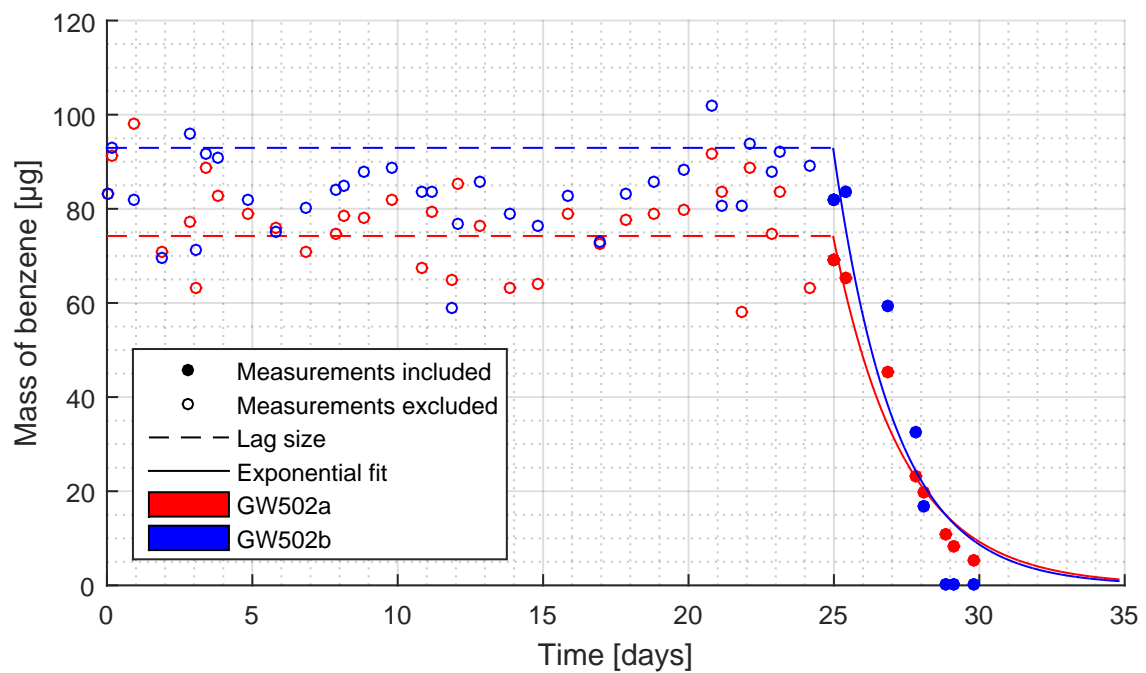


Figure F.22. Total mass of benzene measured over time in groundwater sample from well B502 and the modeled mass assuming a first-order biodegradation.

Appendix G

Abstraction amount

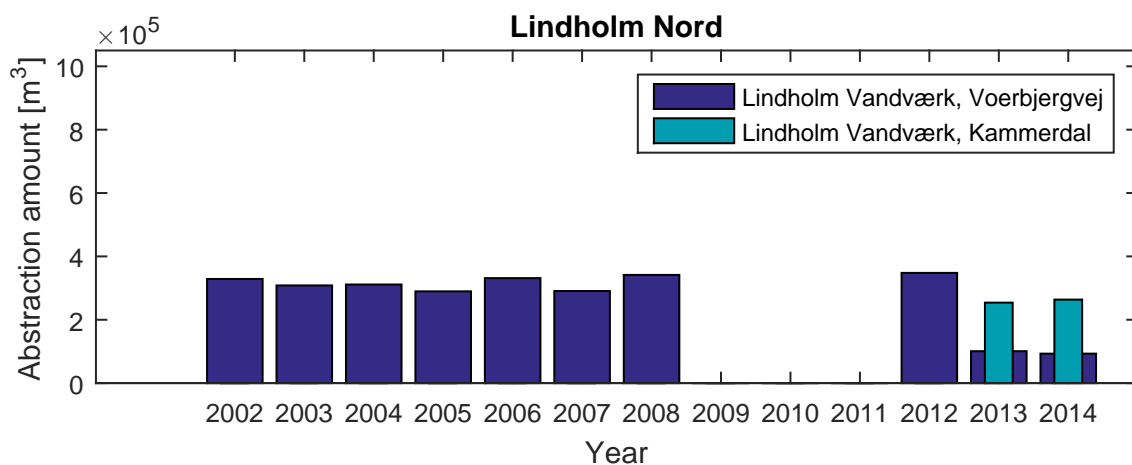


Figure G.1. The abstraction at the northern Lindholm well field.

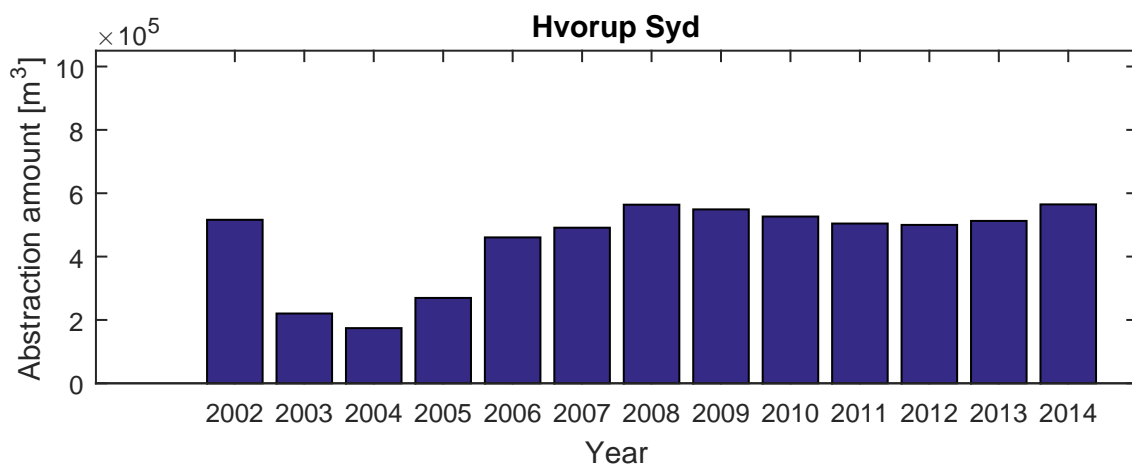


Figure G.2. The abstraction at Hvorup Syd well field.

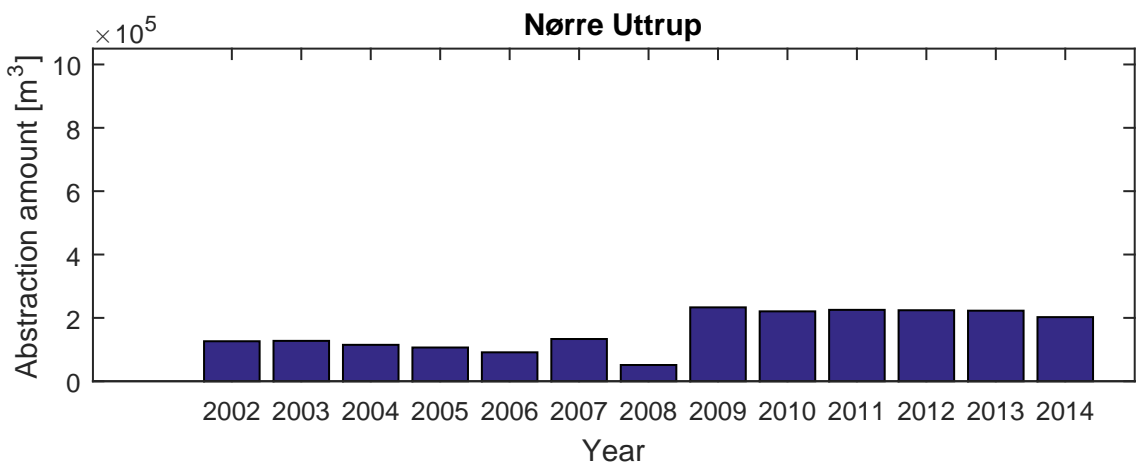


Figure G.3. The abstraction at Nørre Uttrup well field.

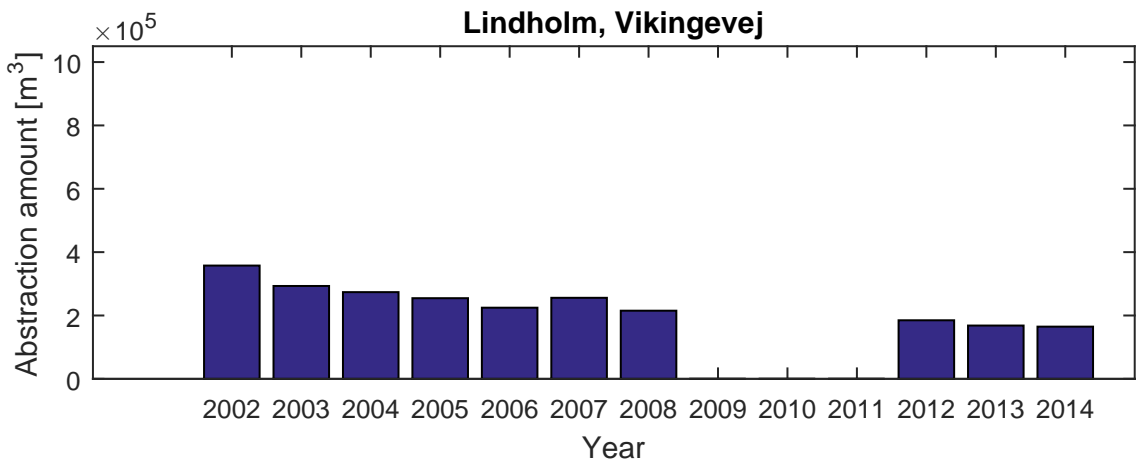


Figure G.4. The abstraction at the southern Lindholm well field.

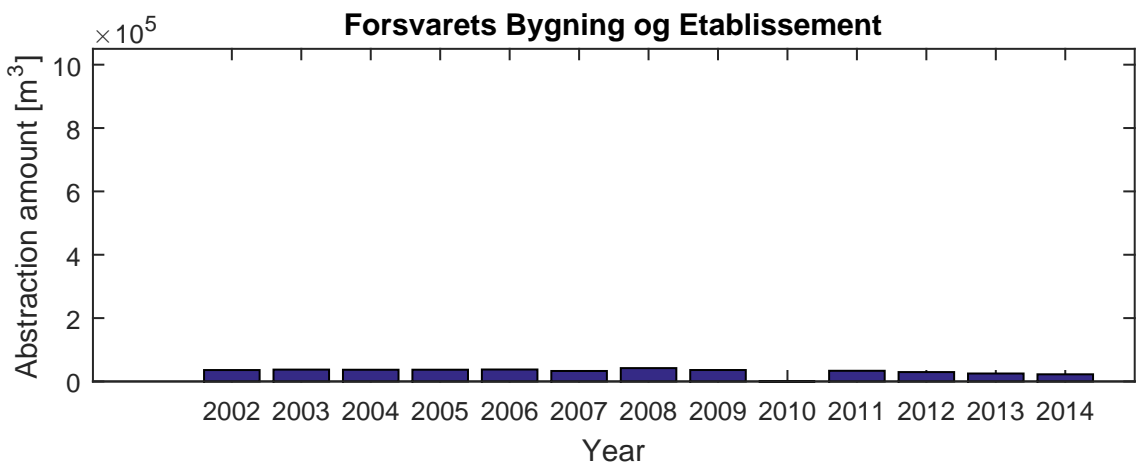


Figure G.5. The abstraction at Hvorup barracks.

Appendix H

Observed head compared to calculated head before calibration

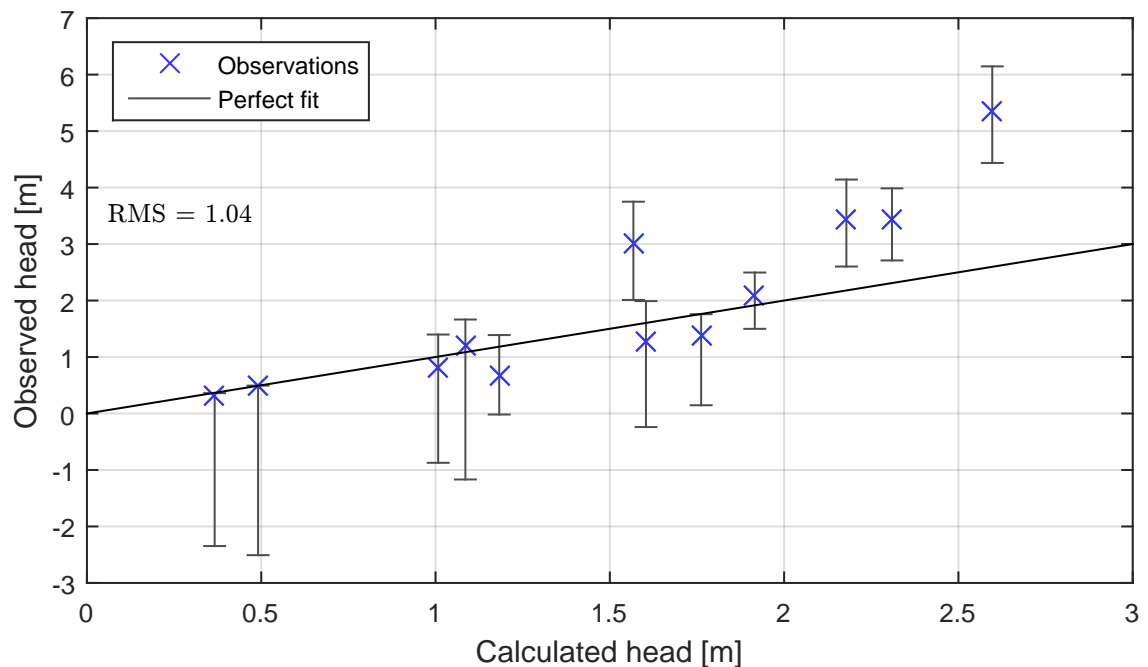


Figure H.1. Observed head compared to calculated head before calibration.